# EXPERIMENTAL EVALUATION OF IMMERSION-COOLED STRATEGIES FOR HIGH-POWERED SERVER MODULES

by

Aravind Sridhar

A thesis submitted to the Graduate Faculty of
Auburn University
in partial fulfillment of the
requirements for the Degree of
Master of Science

Auburn, Alabama
August 4, 2012

Keywords: High-performance computing, microporous surfaces, finned structures, enhanced nucleate boiling, electronics cooling



Approved by

Sushil H. Bhavnani, Chair, Professor of Mechanical Engineering
Roy W. Knight, Assistant Professor of Mechanical Engineering
Daniel Harris, Associate Professor of Mechanical Engineering

## Abstract

Cooling of server-level high-performance computing equipment is an ongoing challenge. Early approaches, based almost entirely on forced air cooling, resulted in unsustainably high energy usage in the air-conditioning units. Subsequently, several other schemes including a hybrid air-cooling/liquid-cooling concept, natural convection cooling for data centers located in cold climates, and provisioned liquid cooling have been attempted. This study explores the direct liquid immersion cooled option first implemented in the Cray supercomputing platforms of the 1980s.

Heat removal via pool boiling in FC-72 was tested. Tests were conducted on a multi-chip module using 1.8 cm × 1.8 cm test die with multiple thermal test cells with temperature sensing capability. Measurements with the bare silicon die in direct contact with the fluid are reported. Additionally testing includes the test die directly indium-attached to copper heat spreaders with surface enhancements. A screen-printed sintered boiling-enhanced surface (4 cm × 4 cm) was evaluated. This was followed by testing on surfaces that feature grooved (shallow-finned) surface enhancements.

Tests have been conducted on an array of five die. Parameters tested include heat flux levels, dielectric liquid pool conditions (saturated or subcooled), and effect of neighboring die. Information was gathered on surface temperatures for a range of heat flux values up to 12 W/cm2. The highest heat dissipated from a circuit board with five bare die was 195 W (39 W per die). Addition of the heat spreader allows heat dissipation

of up to 160 W per die.  High-speed imaging was also acquired to help examine detailed information on the boiling process.

## ACKNOWLEDGENTS

The author would like to thank Dr. Sushil H. Bhavnani, Dr. Roy W. Knight, and Dr. Daniel Harris for their guidance and support during this study. Many thanks are extended to Department of Defense for sponsoring the research. Thanks are extended to 3M Corporation for providing the microporous coatings used for this study. The support given by Alabama Microelectronics Science and Technology Center for fabricating the test chips is greatly appreciated. Much gratitude is extended to Charles Ellis, Mike Palmer and Dr. Michael Hamilton for their support and guidance during this study. Many thanks are extended to his colleagues Christopher Duron and Sarah Styslinger for their contribution and support over the period of this study. Special thanks are extended to his friends, Rahul Gupta and Naveenan Thiagarajan for their support. The author would like to express his thanks to his parents, extended family members and friends for their moral support and encouragement. Above all, the author would like to specially thank his brother, Rangesh Sridhar, for being an inspiration and driving him to accomplish his goal.

**TABLE OF CONTENTS**

## LIST OF FIGURES

## LIST OF TABLES

## NOMENCLATURE

| | |
|---|---|
| PUE | Power Usage Effectiveness |
| ONB | Onset of Nucleate Boiling |
| CHF | Critical Heat Flux, $W/cm^2$ |
| q” | surface heat flux, $W/cm^2$ |
| $T_w$ | wall temperature, ℃ |
| $T_{sat}$ | saturation Temperature, ℃ |
| $T_{pool}$ | pool temperature, ℃ |
| Bo | Bond number |
| $c_p$ | specific heat capacity of liquid |
| f | Frequency of bubble departure, Hz |
| g | Acceleration due to gravity, $m/s^2$ |
| $d_d$, D | departure diameter, mm |
| h | heat transfer coefficient, $W/m^2K$ |
| Ja | Jakob number |
| $T_w$-$T_{sat}$ | wall superheat, °C |
| ρ | Density, $kg/m^3$ |
| σ | surface tension, N/m |

**Subscripts**

| | |
|---|---|
| l | liquid phase |
| v | vapor phase |

# CHAPTER 1: INTRODUCTION

In the past few decades, the computational speed of microprocessor chips has increased drastically with decrease in size. Improvement in fabrication processes have made it possible to pack millions of transistors into a chip that is of size of a fingernail. This increase in number of transistors per chip was first predicted by Intel founder Gordon E. Moore in 1965; a prediction that is now termed Moore's Law. According to Moore's Law, the number of transistors on a microprocessor doubles every 18 months. Although, this exponential growth cannot continue forever due to the restrictions imposed by the laws of physics, modern technologies used in fabrication technology are delaying the end to the validity of Moore's Law. The power dissipated by a microprocessor is a function of the number of transistors. Moore [1] reported that the heat dissipation from the wafer would be a hindrance to populate more circuits in smaller area although the fabrication process itself would not be a point of concern. Hence, thermal management has become a debating issue in the field of electronics.

For the past five decades, various thermal management strategies have been explored in the field of electronics which can be categorized based on how effectively they can remove heat from the surface. Figure 1 shows a plot of temperature difference versus heat flux for different heat transfer modes and various coolants. It tells us that for a typical temperature difference of 60 °C between the component and the ambient, the heat flux that can be dissipated by free convection with air cooling is close to 0.05 W/cm$^2$. Forced

air convection cooling can dissipate around 0.5 W/cm$^2$ while single phase liquid cooling

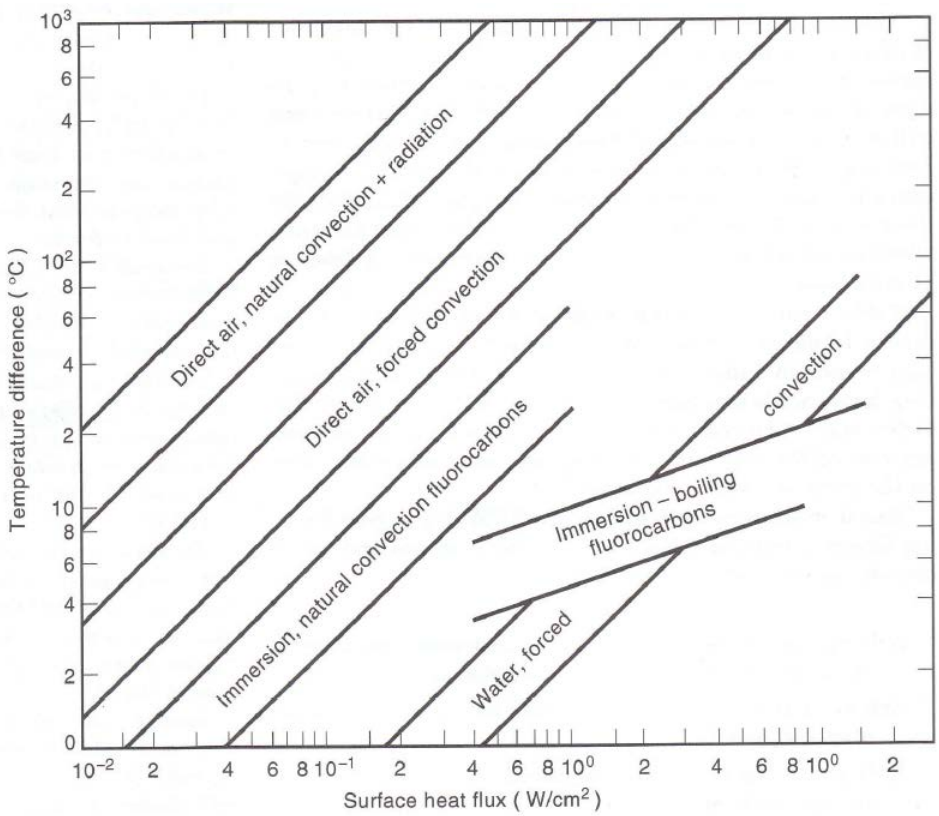


**Figure 1 Thermal management options (Bar-Cohen and Kraus [2])**

can operate for heat fluxes not more than 0.8-1 W/cm$^2$. In spite of low heat transfer capability, air cooling is still the most popular thermal management strategy in the electronics industry. Several other heat removal techniques such as thermoelectric cooling have been tried by different electronic companies but are not popularly used due to its high operating cost and low efficiency. Liquid cooling is considered a very good alternative since most liquids have better heat transfer properties than air. Several liquid cooling techniques such as heat pipes, microchannels, pool boiling, jet impingement

cooling and spray cooling are considered to be the best available alternative to traditional air cooling scheme.

Cooling of server-level high-performance computing equipment is an ongoing challenge. Early approaches, based almost entirely on forced air cooling, have resulted in unsustainably high energy usage in the air-conditioning units. Koomey [3] reported that the annual power consumption of data centers is 1.7-2.2% of the total power consumption in the United States in 2010. The performance of data centers is characterized by the Power Usage Effectiveness (PUE).

$$\text{PUE} = \frac{\text{Total facility power}}{\text{Total server power}} \qquad (1)$$

The ideal value for PUE is 1.0 indicating that all the energy consumption is used for computing. A 2007 US EPA report [4], indicated PUE values as high as 1.36 to 3.6, suggesting very high energy consumption in auxiliary equipment used for cooling and other infrastructure needs. It was reported that the energy consumption by data centers was 61 billion kWh enough to power 71 million homes in the USA and was expected to double every five years. However, the statistical data provided by Koomey [3] suggested that the power consumed by the data centers has increased by 36 % by 2010 and has not doubled as expected. This is due to the fact that the increase in number of data centers reported by EPA was not achieved. Salim and Torez [5] recently assessed the energy consumed by 40 data centers. It was reported that the average annual PUE for 40 data centers was 2.19. This shows that the 56% of the total power supplied to the data center is

used for cooling and electrical distribution. It was also reported the refrigeration system used in these data centers consumed 48% of the total power. Lui[6] attributes the reason for high power consumption to be unavailability of sufficient models to account for the dynamic behavior of the system. Iyengar et al [7] explained the thermal cycle of a typical data centers. It was reported that the heat from the servers are carried by the Computer Room Air Conditioning and reject to refrigerated water through a heat exchanger. The refrigerated water works on the vapor compression cycle. The heat is then transferred to another chilled water heat exchanger which rejects the heat to cooling towers that uses forced convection air to reject the heat. Every data center tries to utilize more than one chiller units which need lot of power to run. Many companies have attempted to address this issue by moving the datacenter location to cold climates such as above the Arctic Circle, Sweden, and Oregon. Liquid immersion cooling may prove to be an attractive option in cases in which moving to colder climates is not feasible.

### 1.1 Introduction to Pool Boiling

Pool boiling is the phenomenon of boiling at the surface of a body immersed in a motionless liquid. Boiling occurs in various applications such as boilers, heat exchanger tubes and quenching of metals. Pool boiling follows Newton's Law of Cooling which can be expressed as,

$$q'' = h \, \Delta T \qquad (2)$$

From Eqn. 2 it is understood that the heat flux is a function of the wall superheat. A pool boiling experiment can be conducted by either, holding the heat flux constant and

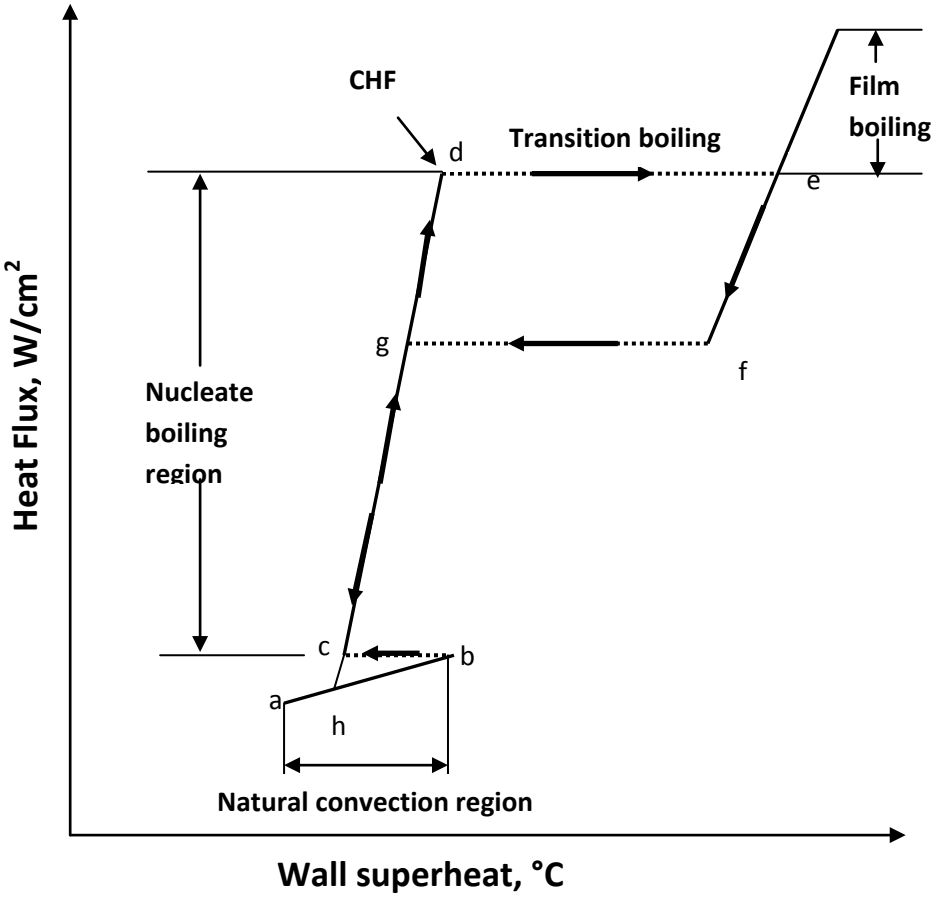


**Figure 2 Pool boiling curve for a heat flux controlled experiment**

measuring the wall superheat, or vice versa. The heat flux was plotted against the wall super heat on log-log coordinates to get a curve typically called the boiling curve. A boiling curve for a heat flux controlled experiment is shown in Figure 2. The first region a-b is called the natural convection region. At this region, the heat flux is too low to activate the nucleation sites and hence, heat is transferred by natural convection. As heat flux is increased, nucleation is initiated and there is sudden drop in wall temperature from b-c. The point at which nucleation is initiated, denoted by b, is called Onset of Nucleate Boiling (ONB). This sudden drop in wall temperature from point b to point c is called temperature overshoot. The wall superheat and the heat flux at ONB are termed the incipience superheat and incipience heat flux, respectively. Once ONB has occurred, the heat transfer mode shifts from natural convection to the nucleate boiling. The nucleate boiling region is shown in the figure from point c to point d. The slope of the curve in the nucleate boiling region is much steeper than in the natural convection region, i.e., nucleate boiling dissipates heat with lower wall superheat rise than does natural convection. The maximum heat dissipated by the nucleate boiling regime is called critical heat flux (CHF) and is denoted by point d. Any further increase in heat flux causes the vapor bubbles to agglomerate to form a vapor blanket thereby increasing the wall superheat drastically by shifting the curve from point ‘d to point e, leading to film boiling. The region between point d and point e is called transition boiling. Since, the wall superheat at this point is much higher than the melting point of most materials; the

surface is never allowed to reach the CHF in practice. Hence, the CHF is also known as the burnout heat flux.

A reduction in heat flux in the film boiling region, causes a reduction in the thickness of the vapor blanket, leading to a different set of states on the pool boiling curve. The curve traverses from ‘point e to point f. Further decrease in the heat flux shifts the curve from ‘point f to point g re-entering the nucleate boiling regime. This large-scale hysteresis can span hundreds of degrees Celsius. When the heat flux is further reduced, the curve doesn’t go back to point b but instead follows the path g-h, thereby yielding another hysteresis loop.. Hence, there are two hysteresis regions on the pool boiling curve.

As the need for heat flux levels is expected to rise above 100 $W/cm^2$, enhanced nucleate boiling is seen as one of the most effective processes to accomplish this with an acceptable temperature rise. Additionally, due to non-uniform heating of the processors in servers, there are localized hotspots being generated at locations which dissipate a higher heat flux than the average chip-level heat flux. Another relevant issue is the increased heat load on downstream chips in a multichip configuration due to neighboring microprocessors.

# CHAPTER 2: LITERATURE REVIEW

This section reviews the different pool boiling heat transfer augmentation techniques used, followed by a review of studies conducted by different researchers in order to understand bubble characteristics. The review will also discuss the research that has been carried out in studying the effects of neighboring dies.

## 2.1 Heat Transfer Augmentation

Due to high packaging densities and high processing speeds, high performance cooling has become a need of the day. Researchers have been studying two phase immersion cooling of electronics for the past two decades and still exploring various different aspects to enhance the boiling process. Use of enhanced surfaces is one such technique that is considered to be very effective and inexpensive. Recent developments in the creation of enhanced surfaces are primarily focused on methods to reduce the incipience of overshoot, increasing the critical heat flux, and improving the slope of boiling curve i.e. allowing for the increase in the heat flux with minimal increase in the wall superheat. Surfaces can be enhanced by applying microstructured materials that produce small-sized cavities thereby reducing the size of the departing bubble, delaying the formation of the vapor blanket, and resulting in the increase of critical heat flux. One technique used is the deposition of particles of specific sizes to form cavities of the desired size that increase the nucleation site density, thereby reducing the incipience overshoot.

### 2.1.1 Use of Microstructured Surfaces

Various researchers have created different microstructured structure using a variety of materials such as copper, aluminum, silver, etc. Each of these materials has different properties and cannot be deposited on a surface by the same technique. All these surfaces have different thermal characteristics and it is extremely valuable to discuss the enhancement of the boiling process due to microstructured surfaces.

You et al. [8] studied the effects of microstructure using a particle layering technique. A 0.1 μm thin film of alumina was sputtered on 10mm × 10 mm × 0.15 mm thick platinum heater. Then, alumina particles were attached to the 70% of the heater area. Two different heater configurations were made. Heater #1 and Heater #2 were layered with 0.3μm size alumina particles and 0.3-3μm size alumina particles respectively. A boiling curve was plotted for a heat flux controlled environment for all three surfaces (untreated surface, Heater #1 and Heater #2) and shown in Figure 4. It was found that the particle layering technique increased the CHF by 39% and 36% and decreased the wall superheat by 37% and 46% for Heater #1 and Heater #2 respectively. A painting technique was proposed by O'Connor and You [9] to create a microporous coating on the surface. This process resulted in the evaporation of alcohol and the adherence of silver flakes and epoxy on the surface. A microscopic view of the silver flakes is shown in Figure 5. The test specimen was immersed in a saturated pool of FC-72 and subjected to a pool boiling test. To study the performance of the microstructured coating, similar tests were run on a smooth aluminum foil surface. It was found that the painted surface

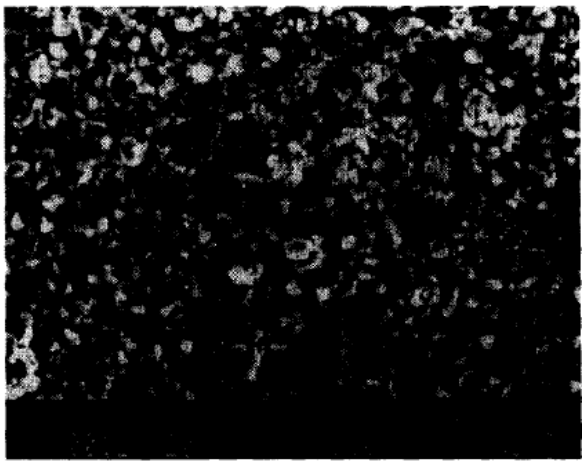

**Figure 3 Surface microgeometry taken by SEM (x 1000); 0.3 - 3µm-alumina (You et al.)**

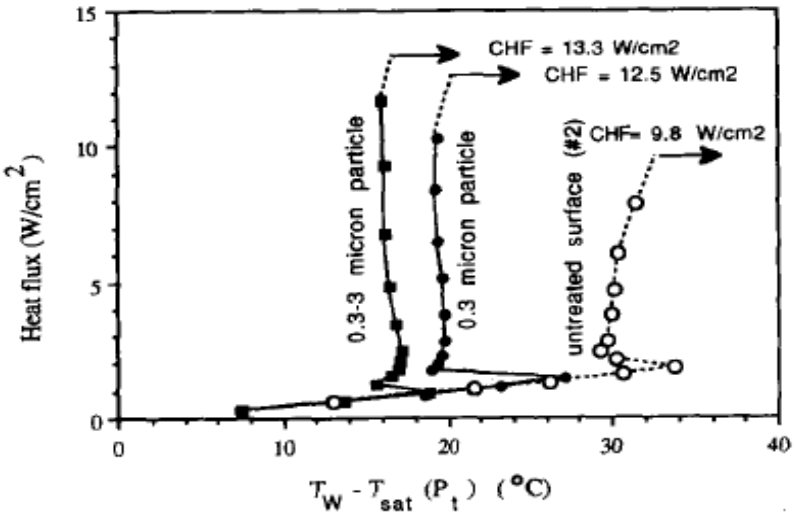


**Figure 4 Effects of particle layering on pool boiling curve ( You et al.)**

produced much smaller bubbles as compared to the smooth surface. This resulted in low superheats for the painted surface as compared to the smooth surface. The CHF levels of the painted surface were observed to be much higher than the smooth surface as shown in Figure 6. Chang and You [10] continued the work by using diamond particles as microporous coating with particles sizes of 2μm±1, 10μm±2, 20μm±3, 45μm±5, 70μm±10 bonded to a 10mm × 10mm copper surface. The tests were run on these surfaces and on a plain copper surface. A significant reduction in incipient superheat on the microporous coatings as compared to the bare copper surface was reported.

Other studies have also verified the efficacy of using microporous surface enhancements. Kim et al. [11] conducted an experiment on 390 μm microporous coated wire in a saturated pool of FC-72 at atmospheric pressure. The results confirmed that microporous coating enhances nucleate boiling due to increase in the nucleation site density. A microporous coating generates smaller bubbles compared to plain surfaces thereby increasing the bubble frequency. Normally inactive nucleation sites are activated at lower heat flux and reduce the formation of superheated liquid layer at higher heat flux. Honda et al. [12] conducted a pool boiling experiment to the study effects of submicron-scale roughness on a smooth silicon chip. RMS roughness of 25-32 nm was fabricated on a 10 × 10 × 0.5 $mm^3$ silicon chip and immersed in a pool of FC-72. The study involved both degassed and gas-dissolved pool. The study was carried out for different subcooled conditions. The major findings from the experiments were that submicron-scale roughness was very effective in enhancing the boiling process. It also

**Figure 5 Microscopic view of the silver flake surface (a) Top (b) Front (O'Connor and You)**

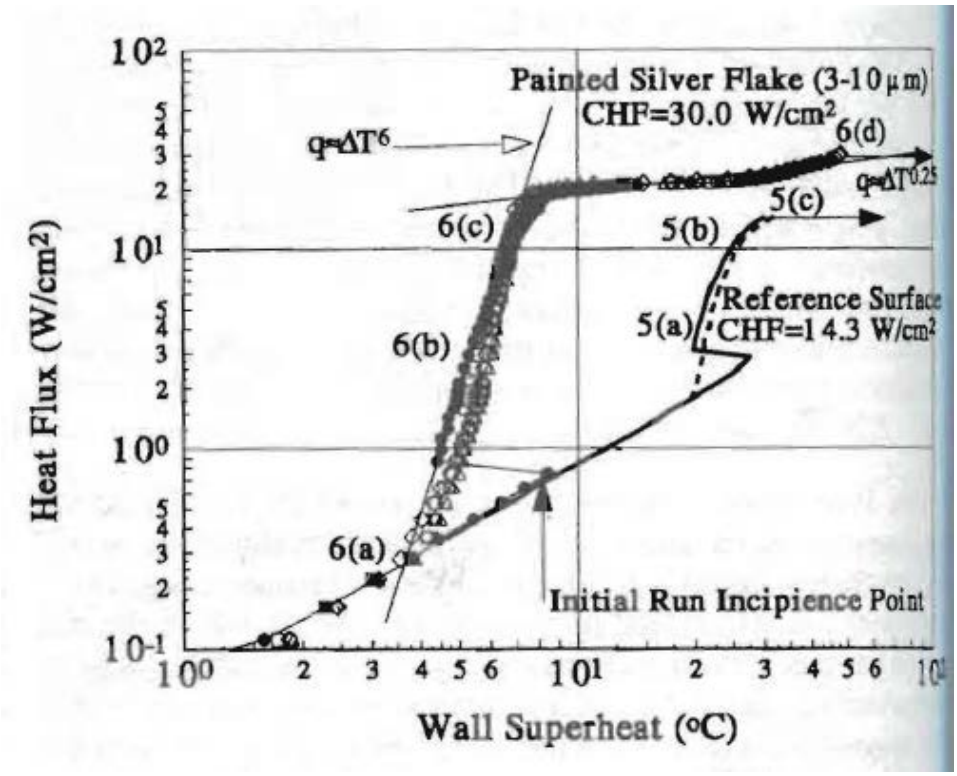


**Figure 6 Heat transfer enhancement (O'Connor and You)**

**Table 1 Summary of the enhancements for different microstructures**

| Name | Fluid | Specimen size | Microstructure Particles used | Size of the particles | Critical Heat Flux[Smooth surface] W/cm$^2$ | Incipience superheat [Smooth surface] °C |
|---|---|---|---|---|---|---|
| **You et al.** | FC-72 | 10 mm × 10 mm | Alumina | 0.3-3 µm,0.3 µm | 13.3,12.5 [9.8] | 27,18.4 [33.1] |
| **O'Connor and You** | FC-72 | 0.51 cm × 1.65 cm | Painted silver flakes | 3-10 µm | 30 [14.3] | 3-8.5 [20-27] |
| **Chang and You** | FC-72 | 10 mm × 10 mm | diamond | 2, 10, 20, 45 and 70 µm | 22-28 [15.0] approx. | - |
| **Kim et al.** | FC-72 | 390 µm diameter | DOM | 8-12 µm | 39.5[17.0] | - |
| **Honda et al.** | FC-72 | 10 mm × 10 mm | $Sio_2$ | 3 µm | 23 [12] | - |
| **Parker and El-Glenk** | FC-72 | 10 mm × 10 mm | Porous Graphite | NA | 27.3 [16.9] | <1 [5-9] |

increased the CHF with a considerable decrease in wall temperature. Parker and El-Genk [13] investigated a pool boiling experiment on a porous graphite block 10 mm × 10 mm in surface area and 3.0 mm thick. The pores and cavities in this structure varied from 1 micron to 100 microns in size. A copper block of 10 mm × 10 mm in surface area and 1.6 mm thick was used for comparative study. Both the chips were immersed in a pool of FC-72 and powered up using a heater glued to the block using epoxy. They reported that the CHF at saturated condition was 1.6 times the copper surface and further increased to 2.3 on subcooling. Table 1 shows the comparison between the CHF levels of the researchers reviewed above.

Li and Peterson[14] conducted a parametric study of pool boiling on highly conductive microporous coated surfaces. The test specimen was fabricated by placing an 8mm × 8mm sintered multilayered copper wire mesh on a copper bar of the same area separated by 0.03mm thick foil. Different test sections were prepared to study parameters such as volumetric porosity, thickness, mesh size, etc. In general, it was shown that microporous coating yielded better heat fluxes than plain surfaces. At low heat fluxes, coatings with high thermal conductivity performed better than those with low thermal conductivities. Boiling incipience can be greatly reduced by using porous coatings and can be controlled by varying the pore size or the thickness of the coating. Pool boiling experiments were performed by Vemuri and Kim [15] on nano particles of 50-250 nm in size and concluded that there was a decrease of 30% in incipience superheat as compared to the bare copper surface. Ali and El.Glenk [16] experimented 10 × 10 $mm^2$ microporous

copper (MPC) coated surface in a pool of PF-5060 dielectric liquid. The surface had a central hotspot of area 1 mm × 1 mm or 2 mm × 2 mm.

The heat transfer coefficient for the nucleate boiling region is plotted for MPC and plane copper surface. It was reported that the heat transfer coefficient of MPC was much higher than the plane copper surface with lower surface temperature. At higher surface temperatures, Nucleation sites in the central hotspot region coalesce together offering some thermal resistance which decreases the heat transfer coefficient. However, it was reported that the heat transfer coefficient was always higher than the plane copper surface with lower wall surface temperature and it was concluded that the microporous coating certainly enhanced the plain copper surface.

Enhancement of boiling using microstructures has been constantly in development and researchers have come up with lots of interesting results. Although, the materials used for the microstructure have been different in most cases, enhancement has always been reported. This is due the fact that, microstructures increase the number of active sites on a surface and also decrease the bubble size thereby decreasing the wall superheat and shifting the CHF to a higher value.

### 2.1.2 Use of finned surfaces

A finned structure is one of the primitive mechanisms in enhancing heat transfer. This passive component is used in cooling electronics due to simple construction and providing a larger area for the heat dissipating component to which it is attached. Two

popular types used in industry are rectangular fins and longitudinal fins. Fins can be constructed using almost all metals which make it compatible to any known fluid. They are used in Central Processing Units (CPUs), refrigeration units and automobiles. Due to all these merits, finned structures are sort out as an important technology in enhancing nucleate boiling.

Guglielmini et al. [17] investigated the effects of pool boiling on square finned surfaces immersed in a dielectric liquid (Galden HT-55) for vertical and horizontal orientations. The dielectric fluid has a boiling point of 55°C at atmospheric pressure. The test heater in the form of a 30 mm circular copper block attached with a heater and insulated at the lower side using alumina. The upper side serves as the boiling surface. A 3mm long finned surfaces were obtained by cutting perpendicularly through a copper bar by electrostatic discharge machining. The dimensions of the fin array are shown in Figure 7 and

**Table 2**. Tests were run for horizontal and vertical orientations. The pool boiling curves for finned and plain surfaces are compared for two different configurations as shown in Figure 8. It was concluded that the square finned surfaces performed better than the plain surface. The vertical configuration dissipated more heat flux than the horizontal configuration for a given wall superheat. Wie and Honda [18] studied the effects of fin

dimensions on pool boiling from silicon chips immersed in a pool of FC-72. Micro pin-fins were fabricated on a silicon chip of size 10 × 10 × 0.5 $mm^3$ by a chemical etching process. Six kinds of micro pin-fins of dimensions 30 × 60, 30 × 120, 30 × 200, 50 × 60, 50 × 200, 50 × 270 $\mu m^2$ (thickness × height) were fabricated and named PF30-60, PF30-

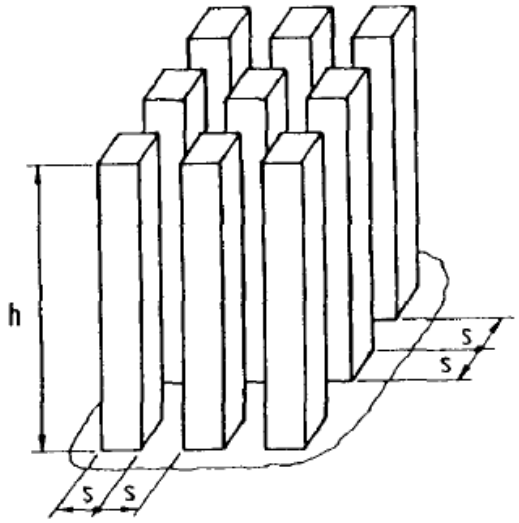


**Figure 7 Geometry of extended surfaces (Guglielmini et al.)**

**Table 2 Dimensions of the spines (Guglielmini et al.)**

| Surface | h (mm) | s (mm) | $A_r$ |
|---|---|---|---|
| 0.4 spines | 3 | 0.4 | 8.50 |
| 0.8 spines | 3 | 0.8 | 4.75 |

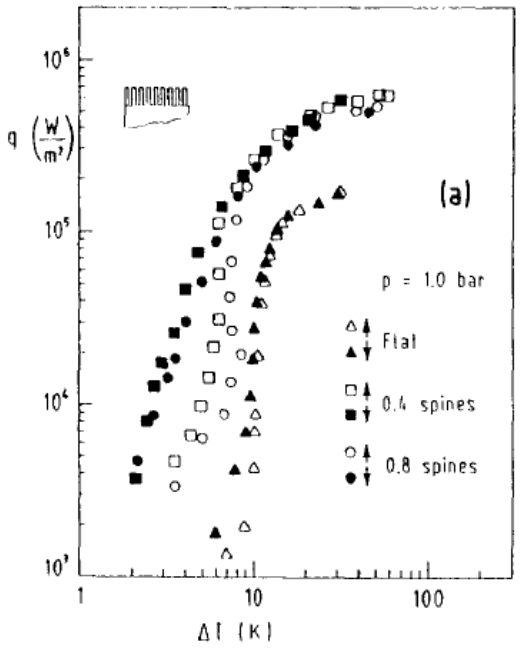

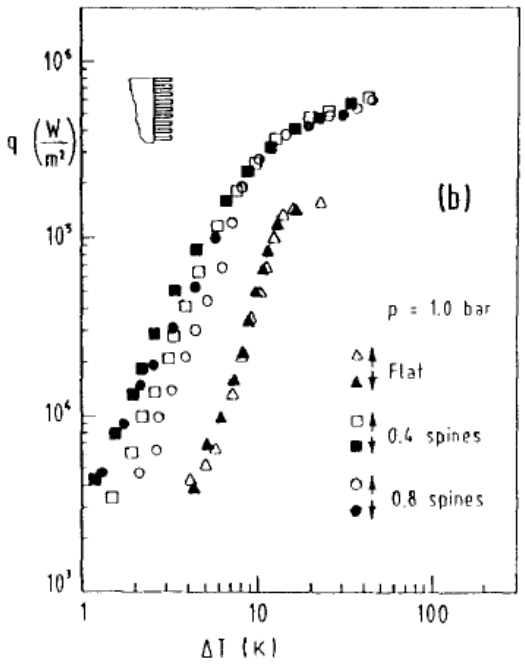


**Figure 8 Boiling curves for 0.4 spines and 0.8 spines compared with flat surface for (a) horizontal base surface (b) vertical base surface (Guglielmini et al.)**

120, PF30-200, PF50-60, PF50-200, PF50-270 respectively. Boiling curves for all the pin-fins structures at zero subcooling is shown in Figure 9. It was found that pin-fins enhanced the boiling process. All the pin-fins showed an increase in surface temperature with sharp increase in heat flux. However, the chips PF50-200 and PF50-270 showed a bend in the boiling curve after a heat flux of 26 W/cm$^2$ (based on the projected area) . This was assumed to be due to the partial dryout in the gap between two adjacent fins. All the micro pin-fins chips had higher CHF and lower wall superheat than the unfinned chip. Yu and Lu [19] produced an extensive study of the effect of fin dimensions on boiling heat transfer of a rectangular fin array. A test heater of dimension 10 mm × 10 mm was attached to copper heat sinks of different configurations. Two primary parameters, fin

spacing and fin length were varied. Fin spacing of 0.5 mm, 1 mm and 2mm and fin length of 0.5 mm, 1 mm, 2 mm and 4 mm were studied. The boiling curves for all these configurations are shown in Figure 10. Yu and Lu [19] reported that the incipience wall superheat decreased as the fin length increases and the fin spacing decreased. Temperature overshoot was eliminated for a fin spacing of 0.5 mm and length 4 mm. It was concluded that the heat transfer increased as fin spacing decreases and fin length increases. A heat transfer rate of 98.3 W was reported which was five times the heat transfer rate of an unfinned surface. Kim et al [20] studied pool boiling enhancements using pin-fins. Pin-finned surface was obtained by etching a copper block to a depth of 50 μm. Each pin-fin had dimensions of 100 μm × 100 μm and  spacing of 200 μm. The data was compared to the unfinned surface for studying the enhancements due to pin-fins. Pin-

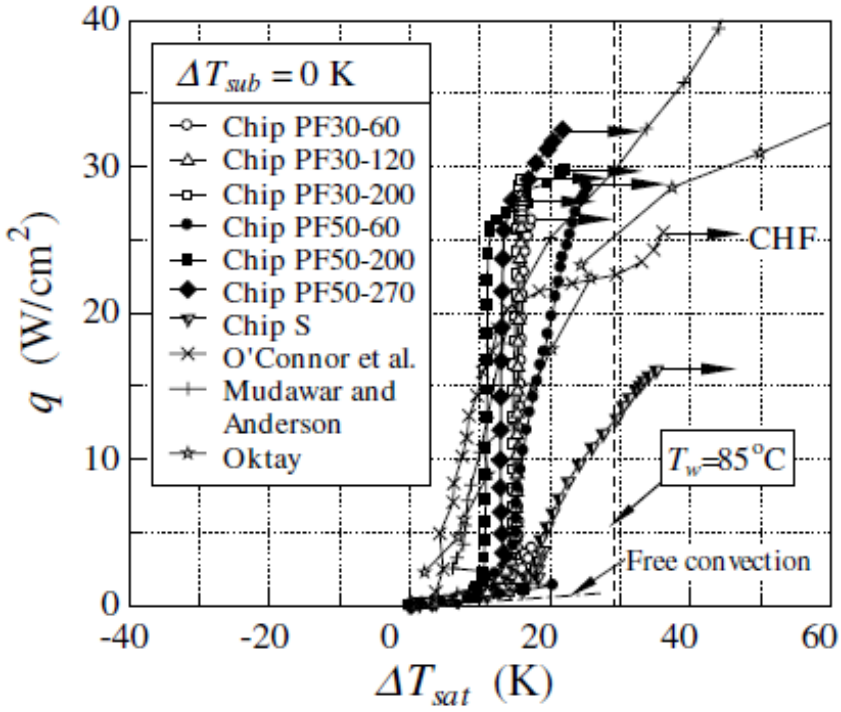


**Figure 9 Boiling curves for all the pin-fins structures at zero subcooling (Wie et al.)**

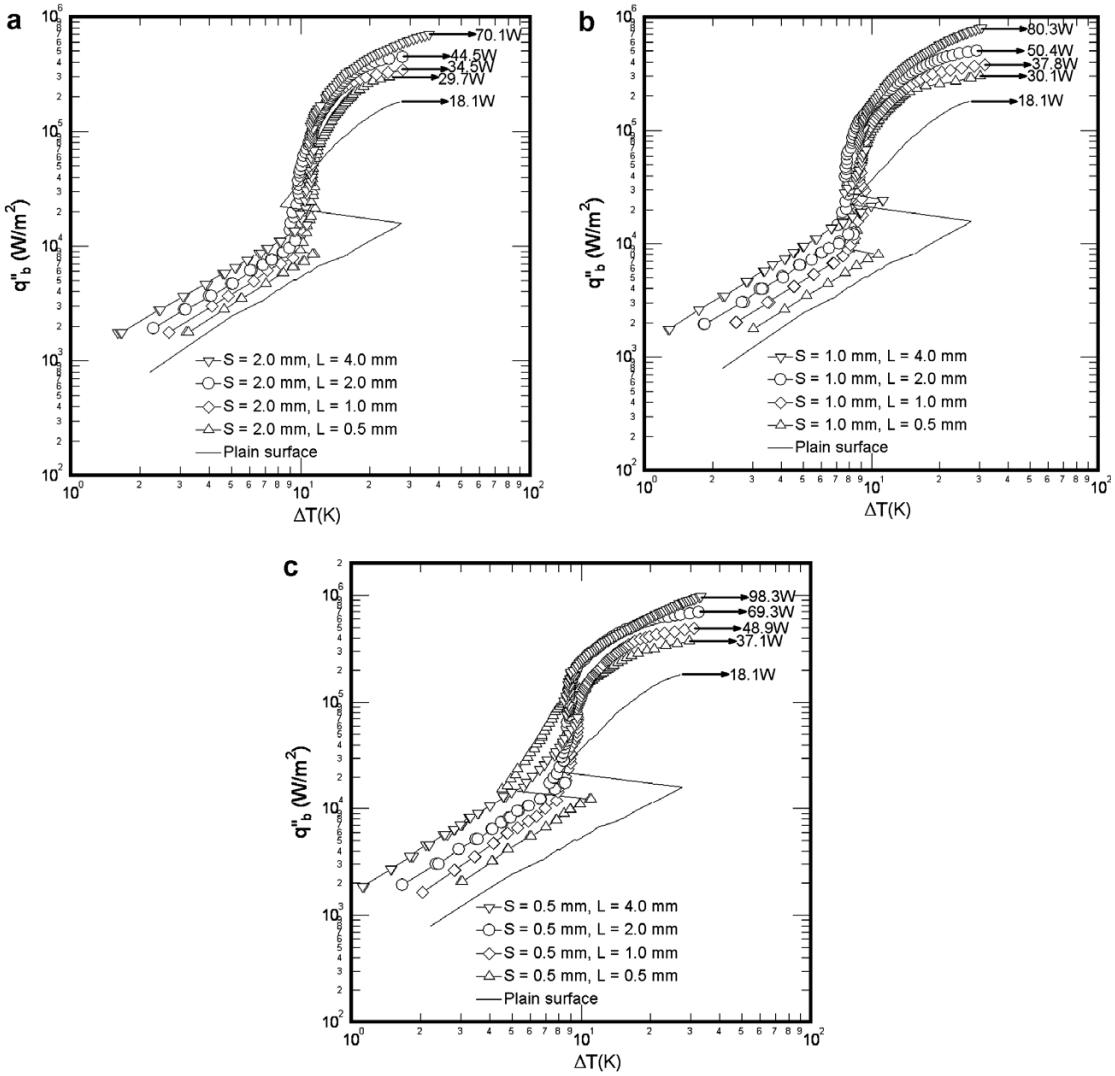


**Figure 10 Boiling curves of copper finned surface with increasing heat flux. (a) finned surfaces of 2 mm fin spacing, (b) finned surfaces of 1 mm fin spacing, (c) finned surfaces of 0.5 mm spacing (Yu and Lu [19] )**

fins showed 44.2% decrease in wall superheat compared to plain surface. It was reported that pin-fins had the advantage of increased surface area which resulted in more nucleation sites thereby decreasing the wall superheat. Also, bubbles generated from the fin base interact with the bubbles originating from the fin sides thereby detaching it from the surface. The use of finned structure provided a path way for the liquid trying to rewet the cavities which resulted in the enhancement of the boiling process. Ghiu and Joshi [21] designed an enhanced surface with microchannels on both the faces of the test heater, perpendicular to each other to form a mesh structure. The structure had an overall dimension of 10 × 10 $mm^2$ and 1 mm thick fabricated out of cooper. Pool boiling experiments were conducted on the enhanced surfaces with varied widths and pitches. It was reported that the enhanced surfaces showed a better heat transfer performance compared to the plain chip. It was also reported that the performance increased with increase in channel width and very prominent at the lower heat flux regions. Cooke and Kandlikar [22] conducted pool boiling experiments on six silicon chips with distilled water as the working fluid. Five of these silicon chips were etched to form a microchannel using deep reactive ion etching (DRIE) method. Each chip has an overall dimension of 20 mm × 20 mm and micromachined heater areas of 10 mm × 10 mm. five categories of chip were used. A plain chip, four microchannels and an offset strip fin design was used. Three microchannels out of four have notch on the sidewalls. Detailed dimensions of all six silicon chips are tabulated in

Table **3**. Surface heat flux was plotted against the wall superheat based on the projected surface area as shown in

**Table 3 Dimensions of all six test chips**

| Chip | Type | Channel ($\mu$m) | Fin ($\mu$m) | Depth ($\mu$m) | Notch | Area increase ($A_{chip}/A_p$ |
|---|---|---|---|---|---|---|
| A | Plain | N/A | N/A | 0 | No | 1.00 |
| B | Microchannel | 200 | 200 | 208 | No | 1.92 |
| C | Microchannel | 200 | 200 | 192 | Yes | 2.00 |
| D | Microchannel | 100 | 100 | 275 | Yes | 3.75 |
| E | Microchannel | 100 | 100 | 182 | Yes | 2.82 |
| F | OSF (fins 500 $\mu$m long) | 40 | 60 | 180 | No | 3.92 |

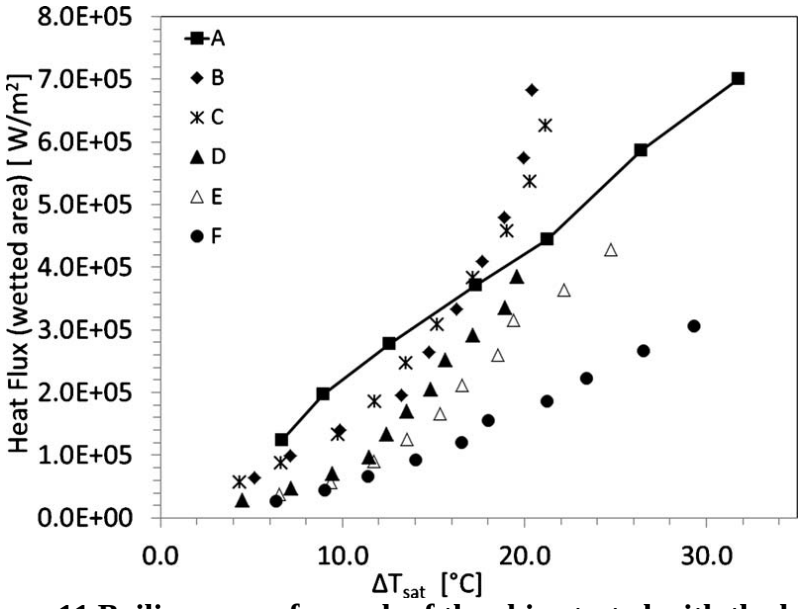


**Figure 11 Boiling curve for each of the chips tested with the heat flux normalized to the surface area**

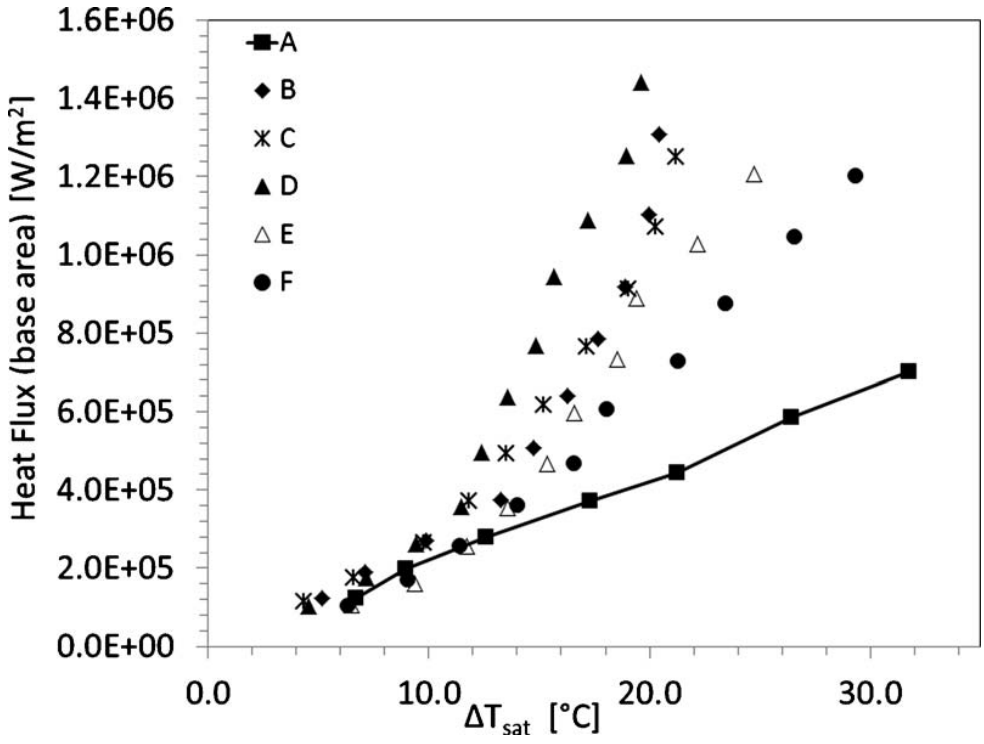


**Figure 12 Boiling curves for all six test chips based on projected base area**

Figure 12. It can be seen from the plot that all structured surfaces shown enhancements compared to the unstructured surface. However, it was reported that this might be either due to the increase in surface area or the structure of the surface affecting the bubble departing from the surface. In order to study the enhancement effects better, a normalized surface heat flux was calculated based on the wetted surface area and plotted against the wall superheat as shown in Figure 11. It can be seen that chip B, C and D performed better than chip A while chip E and F under performed. Cooke and Kandlikar [22] concluded that chip E and F showed enhancements due to the increase in surface area and not due to the surface characteristics. Other silicon chips showed enhancements due to the benefit of the structure of the surface.

From the above studies on finned surfaces, it can be inferred that fins enhances pool boiling effectively. Boiling in fins has a great dependence on the fin spacing and fin height. The wall superheat is decreased with increase in fin spacing and fin height. Also, the structure of the fins positively helped the flow of liquid entering the channel trying to rewet the cavities. Due to the above mentioned advantages, finned structures are being investigated in the current study.

**2.2 Interaction between different heat sources**

The issue of temperature overshoot, the phenomenon of hysteresis at nucleation incipience, is of significance in the field of electronics because of the low operating temperature of silicon chips. If left uncontrolled, the temperature attained due to the hysteresis might reach the operating temperature quickly and might lead to the failure of

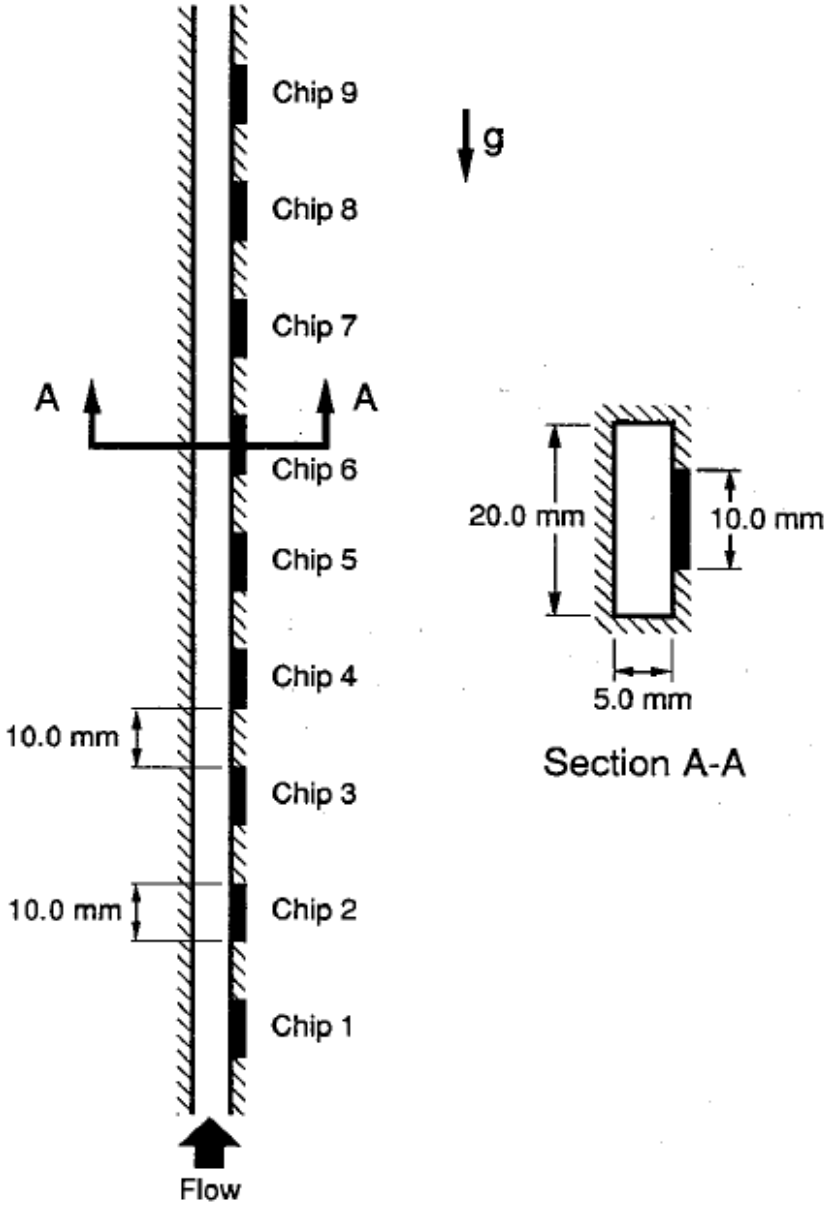


**Figure 13 Multichip array (Willingham and Mudawar)**

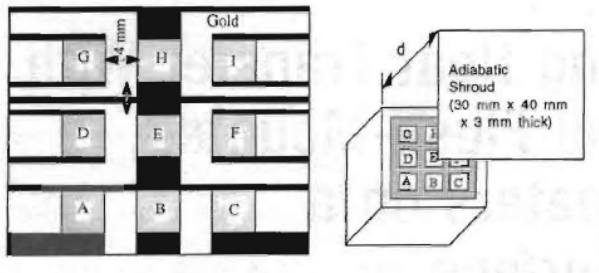


**Figure 14 3 × 3 array of 5 mm × 5 mm square heaters (You et al.)**

**Table 4 Description of the test cases (Tb = 35°C, P, = 1 atm., vertical 15, orientation, d = 2.3 mm)___**

| Case | # of independent run | $T_f$-$T_b$ (°C)* | Operating heaters | Incipient Superheat Range (°C) |
|---|---|---|---|---|
| SQ0410 | 10 | - | H only | 15-39 |
| SQ0419 | 3 | 4.0 | H,E boiling at 1.4 W/cm2 | 14-17 |
| SQ0413 | 3 | 3.9 | H.E boiling at 7.8 W/cm2 | 6.6-6.8 |
| SQ0413 | 3 | 3.9 | H.E boiling at 7.8 W/cm2 | 6.6-6.8 |
| SQ0414 | 3 | 0.9 | E,H boiling at 7.8 W/cm2 | 19-37 |
| SQ0424 | 6 | 0 | H,C boiling at 7.8 W/cm2 | 24-38 |
| SQ0419 | 3 | 4.0 | H,E boiling at 1.4 W/cm2 | 14-17 |
| SQ0420 | 6 | 7.0 | H,E in N.C. at 1.4 W/cm2 | 20-40 |

* $T_f$ is Temperature of the approaching fluid to the test heater and $T_b$ is temperature far from the test heater

the component. Several different approaches have been attempted to overcome this phenomenon, including the use of bubble generating sites that produce nucleation that serves to favorably impact the boundary layer at the location of the most critical components in an immersion-cooled phase-change cooling system. The following papers review the research work carried out by different researchers to account for this problem and the solutions proposed to reduce the hysteresis.

Several tests have been performed on multichip module to study the effects of convective interactions on thermal performance of the package. Willingham and Mudawar [23] examined the forced convection of FC-72 in a linear array of nine heaters (10 mm × 10mm) in a rectangular channel of 20mm × 5mm at different bulk fluid velocities as shown in Figure 13. The spacing between each heater was 10 mm. It was concluded that the downstream chip reached boiling incipience first followed by successive upstream chips. As a result, upstream chips experienced larger incipience superheats than the downstream chips. The effects of liquid subcooling were also examined. Subcooling increased both the CHF, and boiling incipience. There was an observed decrease in bubble size as the subcooling was increased.

You et al [24] studied the effects of boiling due to neighboring heaters on the test heater. A vertically oriented 3 × 3 array of flush mounted, 5 × 5 $mm^2$ square heaters arranged 4mm apart on a glass substrate were immersed in a pool of FC-72 (Figure 14). The heaters were constructed of platinum coated with alumina particles. The heaters were individually powered up using a power supply and monitored using a data acquisition

system to study the effects of convective interactions between different heaters. The different test cases are tabulated in Table 4 . It was found that there was a considerable reduction in the incipient superheat for a test heater with a heater boiling below it. There wasn't a significant effect on the boiling curve for the boiling at other locations. Bhavnani et al. [25] experimentally investigated the boiling curves for the interaction between two neighboring die. Five 0.7 × 0.7 $cm^2$ heaters with a spacing of 0.7 cm were used. It was shown that the temperature overshoot can be eliminated at lower wall superheats by having bubbles nucleating from a chip below the test chip. The boiling curves for the test heater with and without active heater below the test heater is shown in Figure 15.

Bergles and Kim [26] studied the effects on the temperature overshoot for a vertically oriented nichrome heater of dimensions 5 × 5 $mm^2$ submerged in a pool of refrigerant R-113. A bubble generator was placed at a distance of 10 mm below the heater. The power was supplied to the bubble generator such that only one site was nucleating at 5 bubbles per second (Figure 16). Tests were run for different horizontal distances of the bubble generator from the heater. For a distance of x=5 mm, the wall superheat for a plain surface and sintered surface was found to be 33 K and 22 K respectively. This superheat was same as the one with no bubble generator. The horizontal distance was so large that the bubbles emanating from the bubble generator didn't come in contact with the surface and hence, there wasn't any reduction in wall superheat. For a distance of 1-4 mm, wall superheat of 8-12 K and 7-10 K was observed for plain and sintered surfaces respectively

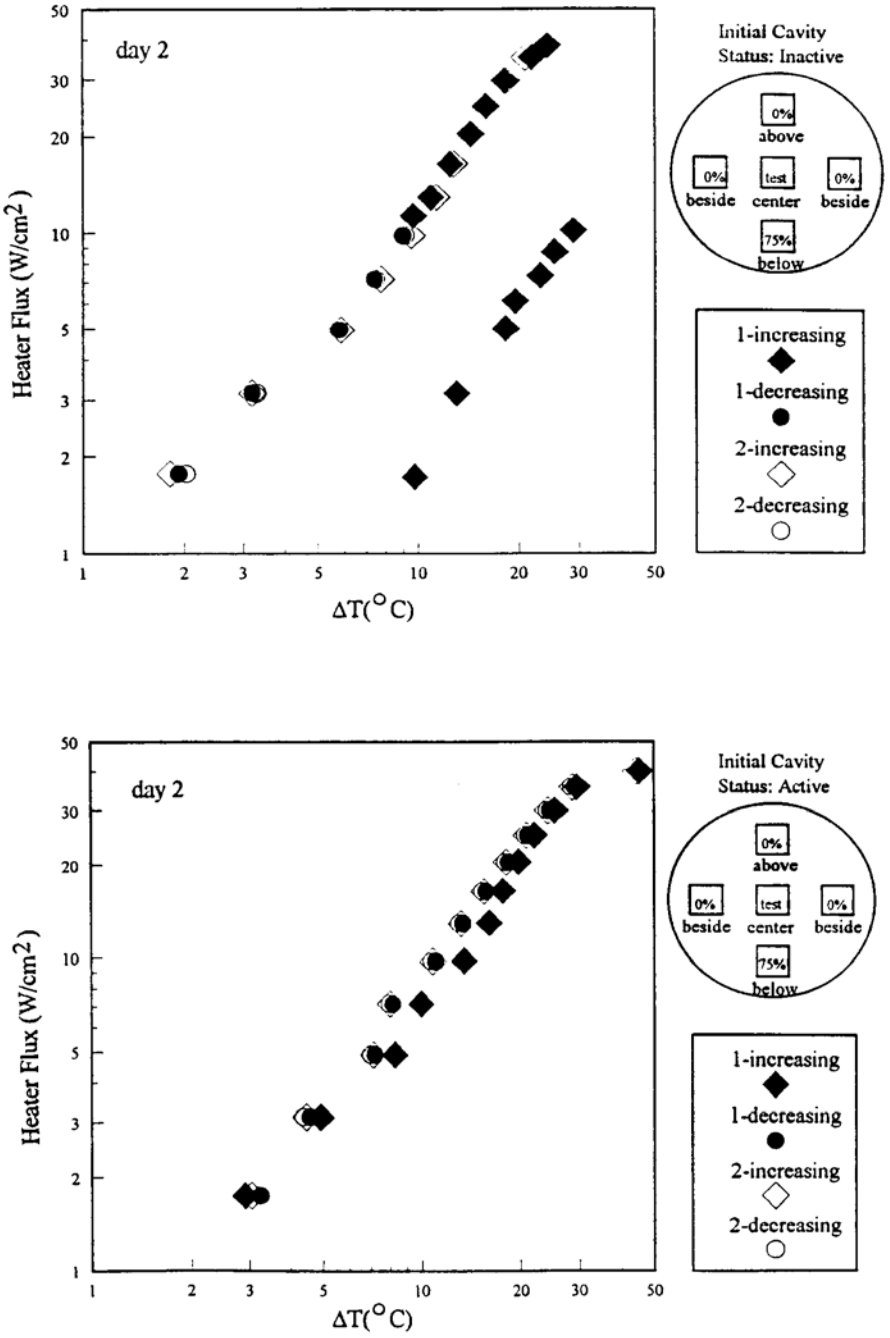


**Figure 15 Performance characteristics of the central test heater with 75% of the incipient heat flux dissipated below the test heater. (a) Below, Inactive and (b) Below, Active. (Bhavnani et al.)**

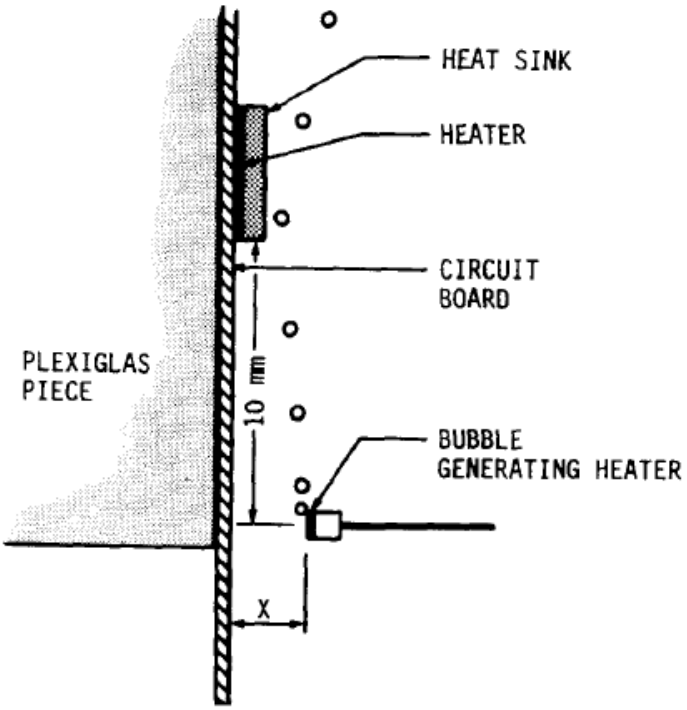


**Figure 16 Details of positioning of the bubble generating heater (Bergles and Kim)**

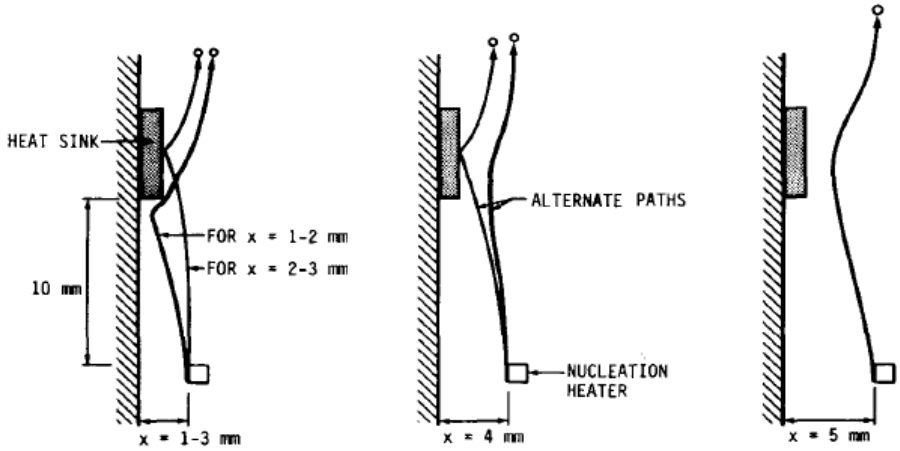


**Figure 17 Typical bubble paths for various spacings (Bergles and Kim)**

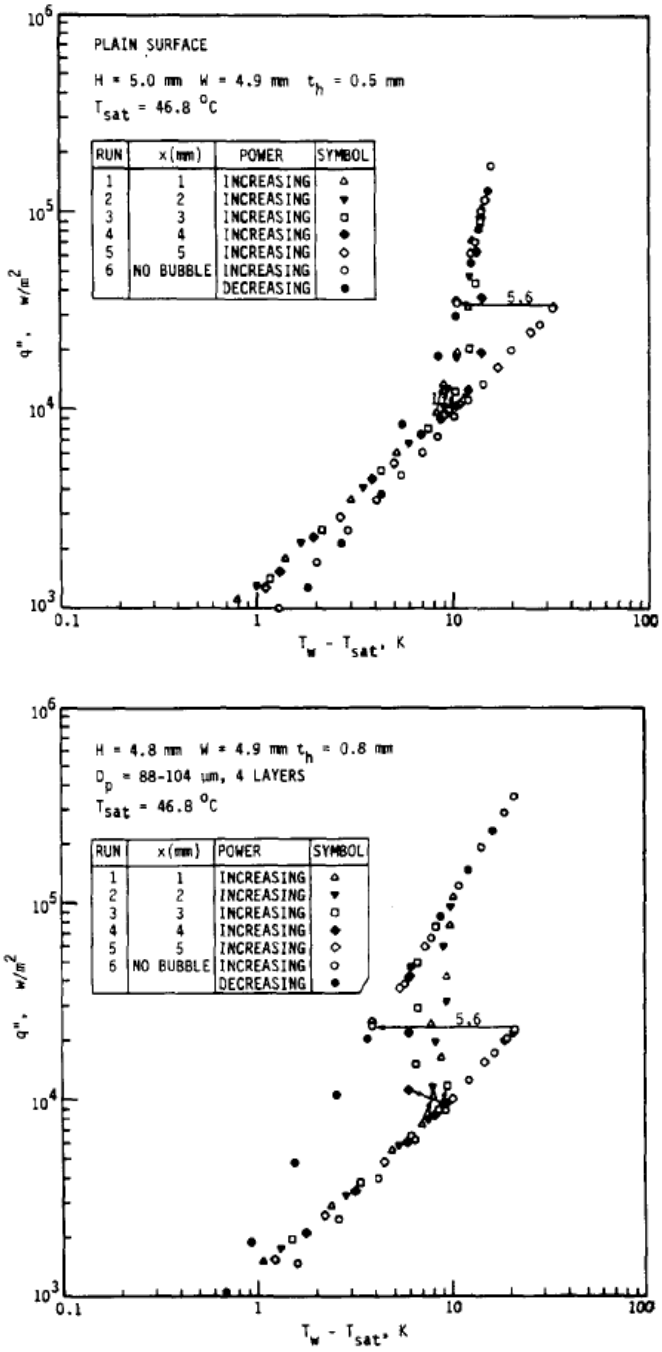


**Figure 18 Boiling curves showing the influence of bubble generation from below for the (a) plain heat sink (b) sintered heat sink (Bergles and Kim )**

as shown in (Figure 18).

Due to multiple hotspots being generated in modern computers, understanding the effects of neighboring interactions is important as well. Various studies have reported that bubbles emanating from the neighboring dies have certainly eliminated the temperature overshoot. This is due to the fact that the bubbles disrupt the boundary layer thereby eliminating the temperature overshoot.

## 2.3 Bubble characteristics

The process of heating of liquid, nucleation, bubble growth and release, collectively known as the ebullition cycle is a dominating factor in maintaining the remarkably high heat transfer coefficient for phase change as compared to natural convection. Hence, it is very important to learn the bubble characteristics to enhance the boiling process. A bubble departing from the surface is characterized by two important forces acting on it. One is the surface tension forces that prevent the bubble from departing, and buoyancy forces trying to lift the bubble away for a horizontal upward facing surface. Hence, the frequency of bubble departure is another key factor in determining bubble departure. Bubble frequency is the inverse of the total time elapsed for a bubble to form from a surface and depart. Hence, the longer the bubble takes to grow, the lower the frequency and the larger diameter. Hence, there lies a relationship between the bubble departure diameter and the bubble frequency. Though a direct relationship cannot be formed, a relationship can be derived by the use of force balances and other liquid properties. Most

of these relations are based on a dimensionless number called the Bond number. It is proportional to the buoyancy forces divided by surface tension. It is defined as follows,

$$Bo = \frac{g(\rho_l - \rho_v)d_d^2}{\sigma} \qquad (2)$$

A vast amount of research has been carried out to develop relationships between the bubble departure diameter and the bubble frequency. In the past, many researchers have come with different correlations for predicting the bubble departure diameter. Jensel and Memmel [27] came up with a comprehensive study on the available correlations for the bubble departure diameter of their times, and proposed a modified correlation for the bubble departure diameter. Jensel and Memmel [27] found out the theoretical value of the bubble departure diameter from the available correlations and compared it with the experimental data. It was found that the correlation proposed by Kutatladze and Gogonin [28] (Eqn. 3) was the most accurate followed by Cole and Shulman [28] (Eqn. 4) and Nishikawa [29] (Eqn. 5). Based on the results, Jensen and Memmel [27] proposed a correlation as stated in Eqn. 6.

$$Bo^{\frac{1}{2}} = 0.25(1 + 10^5 K_1)^{\frac{1}{2}} \qquad (3)$$

$$where\ K_1 = \left(\frac{Ja}{Pr_l}\right)^2 \left\{\left[\frac{g(\rho_l - \rho_v)}{\mu_l^2}\right]\left[\frac{\sigma}{g(\rho_l - \rho_v)}\right]^{\frac{3}{2}}\right\}^{-1}$$

$$Ja = \frac{\rho_l c_{pl}[T_w - T_{sat}]}{\rho_v h_{lv}}$$

$$Bo^{\frac{1}{2}} = 0.04\, Ja \qquad (4)$$

$$Bo^{\frac{1}{2}} = 0.12 + 0.08\, Ja^{\frac{2}{3}} \qquad (5)$$

$$Bo^{\frac{1}{2}} = 0.19(1.8 + 10^5 K_1)^{\frac{2}{3}} \quad (6)$$

Jakob [31] observed that the bubble departed from the surface at equal time interval and equal size. Jakob [31] presented that over a range of diameters, f.D can be assumed constant. Peebles and Garber [32] showed that the velocity of the bubbles rising from the surface can be expressed as,

$$u_\infty = 1.18\,[\frac{\sigma g(\rho_l - \rho_v)}{\rho_l^2}] \quad (7)$$

Based on this, Zuber [33] stated that the product of frequency and diameter was a function of fluid properties and assumed that $f.D \propto u_\infty$ and found that

$$f.D = 0.59\left[\frac{\sigma g(\rho_l - \rho_v)}{\rho_l^2}\right]^{\frac{1}{4}} \quad (8)$$

McFadden and Grassmann [34] proposed a correlation based on a dimensional analysis assuming that the product of bubble frequency and bubble diameter to be a function of surface tension, density of the liquid and density of the vapor. It was expressed as follows:

$$f.D^{\frac{1}{2}} \approx 0.56\left(\frac{g(\rho_l - \rho_v)}{\rho_l}\right)^{\frac{1}{2}} \quad (9)$$

Ivey [35] investigated the boiling process in water and stated that a single expression was not adequate to express the bubble frequency and bubble diameter for all bubble diameters. Hence, he proposed three different regions and gave three individual correlations separately.

1. Hydrodynamic region, in which

$$f.D^{\frac{1}{2}} = 0.90g^{\frac{1}{2}} \quad (10)$$

2. Transition region, in which

$$f.D^{\frac{1}{2}} = 0.44\, g^{\frac{1}{2}} \quad (11)$$

3. Thermodynamic region, in which

$$f.D^{\frac{1}{2}} = constant \quad (12)$$

In the recent past, Many researchers have been reported the influence of bubble departure diameter and frequency on the nucleate boiling process and CHF. Different trends for the bubble departure diameter and frequency has been observed for an increase in heat flux. Pascual et al [36] conducted a pool boiling experiment for R-123 on a rectangular heater. The bubble dynamics were visually study at five different heat fluxes using a high speed camera. It was found that the bubble frequency increased and then decreased with the increase in heat flux. Chatpun et al [37] conducted a pool boiling experiment for water at atmospheric pressure. Bubble dynamics were studied on a 20 mm × 20 mm silicon surface with 10 μm diameter and 80 μm depth cylindrical cavities. Two different cavity arrangement, inline and triangular were studied for 1 mm, 2 mm, 3 mm and 4 mm cavity spacing. It was reported that the bubble departure diameter increased with increase in heat flux. Also, the bubble departure diameter increased with increase in the cavity spacing. However, it was found that for higher heat fluxes, the bubble departure diameter for 4 mm spacing was smaller than the one for the 3 mm spacing. It was also reported that the cavities with inline pattern performed better than the triangular pattern.

Ramasamy et al [38] investigated pool boiling for FC-72 in microchannels. It was found that the bubble departure diameter increased with increase in wall superheat and the bubble frequency first decreased and then increased with increase in wall superheat. Nimkar et al [39] constructed micro-pyramidal re-entrant cavities on a silicon wafer as shown in Figure 19. Pool boiling experiment was conducted to study the active site densities on the test specimen, with and without a heater producing convection plumes from the neighboring heater below the test heater at the rate of 50% of incipient heat flux. Three surfaces were tested with cavity center-to-center spacing of 0.5 mm, 0.75 mm and 1 mm. It was found that the surface that had widely-spaced cavities performed better than the densely packed cavities. It was reported that the densely packed cavities had a repulsive interactions with each other thereby affecting the overall heat transfer coefficient. It was also reported that the bubble departure diameter and frequency increased with increase in heat flux. Recently, Hutter et al [40] conducted pool boiling experiment on artificial cavities etched on silicon. Three different cavity depths were fabricated and tested. It was found that the bubble frequency showed a trend of increase in bubble frequency with increase in heat flux. McHale and Garimella [41] conducted a visual study of pool boiling of FC-77 at atmospheric pressure on smooth and roughened aluminum surfaces. The smooth surface was obtained by mechanical polishing and rough surface was obtained by electrical discharge machining. The roughness value for the polished and roughened area was given to be 0.03 μm and 5.89μm respectively. The bubble dynamics were studied using a CCD camera at 8000 frames per second. The

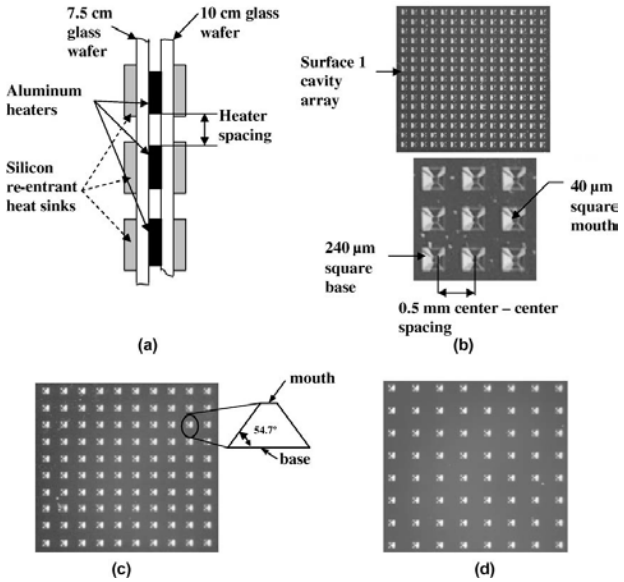


**Figure 19 (a) Symmetric arrangement on a glass substrate (not to scale); (b) surface 1 and surface1 details showing cavity characteristics, and inter-cavity spacing; (c) surface 2—0.75 mm inter-cavity spacing with a 2D schematic of the pyramidal cavity; (d) surface 3—1.0 mm inter-cavity spacing. (Nimkar et al.)**

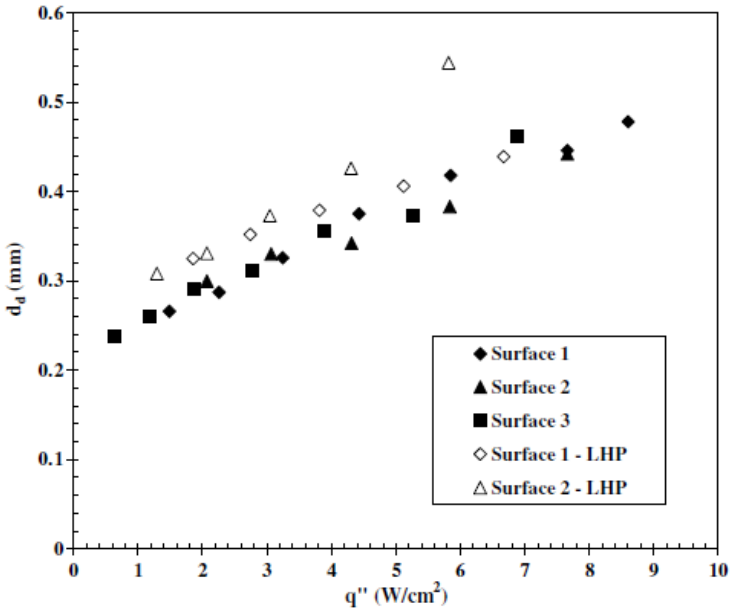


**Figure 20 Comparison of variation of departure diameter with heat flux for all cases. (Nimkar et al.)**

bubble departure diameter were experimentally determined and compared against the various correlations available. It was found that the bubble departure diameter showed an increase in departure diameter as in the case of previous studies of Nimkar et al. [39], Ramasamy et al. [38]. Also, the active site density increased with increase in heat flux. However, none of the available correlations were able to predict the correct bubble departure diameter for both the surfaces.

From the above literature, it can be inferred that the bubble departure diameter and frequency shows a varied trend and is dependent on more than one factor. Though numerous correlations exist, bubble departure diameter and bubble frequency is dependent on the liquid, the cavity size of the surface being used, the operating conditions and the spacing between the cavities.

**2.4 Objective of this study**

The objective of this study is an attempt to explore the various effects alluded to above in the literature review, using thermal test die to evaluate both the limits of heat dissipation using nucleate pool boiling, and the effect of neighboring heat sources. In addition, fundamental primary variables such as pool temperature, surface enhancement and bubble departure diameter are examined. These data can be used to develop a practical dielectric fluid immersion cooling system for server applications that is an alternative to the current air-cooled model.

# CHAPTER 3: EXPERIMENTAL SETUP AND PROCEDURE

This chapter will explore in detail the experimental setup and procedure used in conducting the study. It will start with a brief description of the experimental loop, followed by detailing the steps employed in using individual components, such as the power supply, DAS system and other auxiliary equipment used in the setup. It will also describe the calibration process for temperature sensing. The characteristics of the enhanced surfaces used will also be described.

## 3.1 Experimental Setup

A robust self-contained experimental rig was designed that could be used for experiments beyond the scope of this study. Hence, a 3 feet × 5 feet × 2.4 feet structure was build using strut channels that can accommodate more than 1000 pounds of weight.

### 3.1.1 Test Rig Construction

The key components of the pool boiling test rig are: a pair of polycarbonate (Lexan) tanks fitted with quartz viewing windows, supported on a metal structure (Unistrut), a condenser/chiller, power supplies (American Reliance), a data acquisition system (National Instruments/LabView), a high-speed camera with associated lens (Vision Research/Infinity), and a PC/monitor. A schematic diagram of the test rig is shown in Figure 21. Lexan tanks were supported on a metal structure with one tank enclosed within the other. Lexan tanks were constructed from a 4 feet × 4 feet × 8 feet lexan sheet of 0.5 inch thickness. The dimensions of the outer test tank were 25’’ × 25” × 18.5”

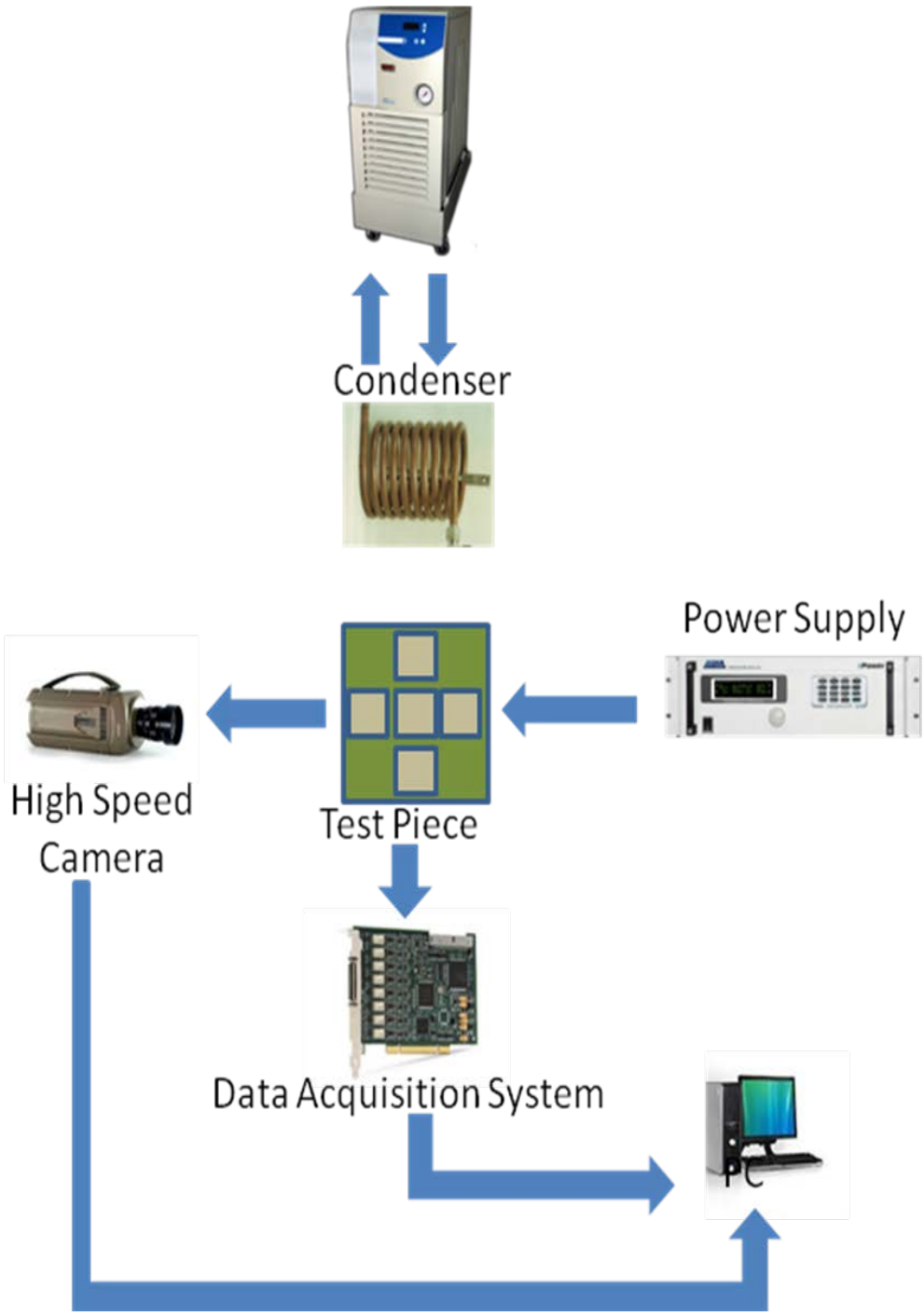


**Figure 21 A schematic diagram of the pool boiling test rig**

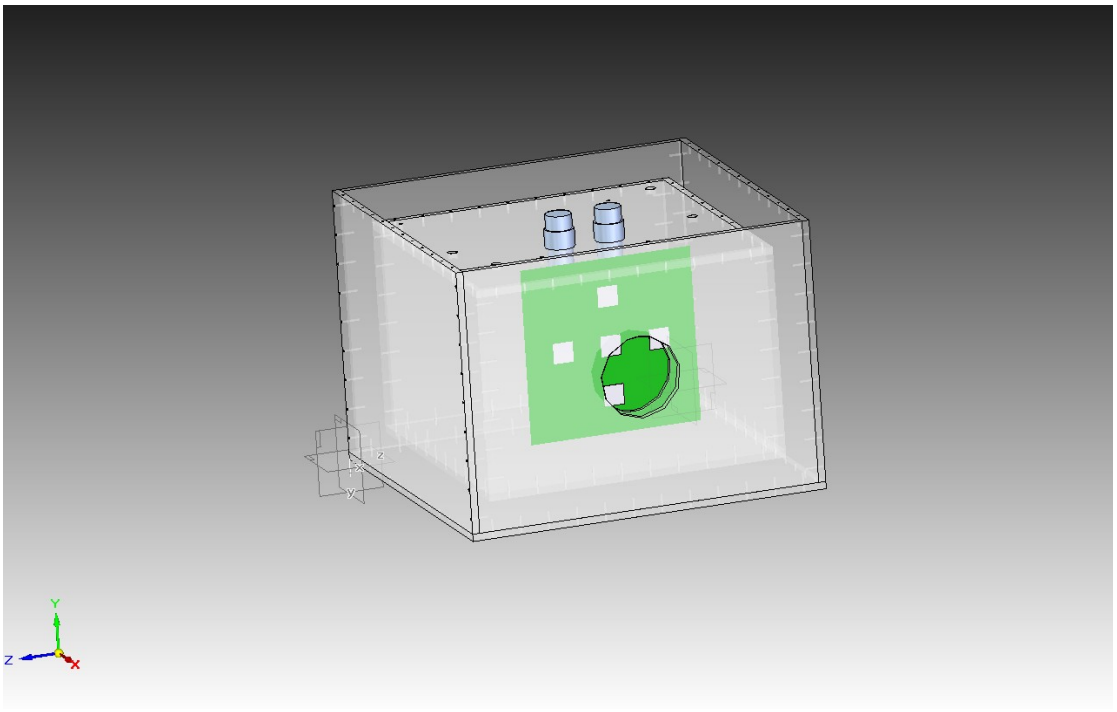


**Figure 22 A sketch of the pool boiling test tank**

(length × breadth × height). The size of the inner tank was 21'' × 21" × 14.5" that can hold 26.78 gallons of FC-72. Although, the amount of liquid needed for the study was not more than 5 gallons. Lexan tanks consist of 6 inches quartz window for visualizing the boiling process and recording the bubble dynamics using a high speed camera. A CAD drawing of test tanks are shown in Figure 22. The test board was immersed in the inner tank containing the dielectric working fluid (FC-72). The working fluid in the inner tank was maintained at a constant temperature by circulating de-ionized water at a set temperature in the outer tank using a circulating heater. The working fluid in the inner tank was maintained at atmospheric pressure using a Graham condenser to minimize the fluid loss. FC-72 was chosen because of a larger set of existing data available for this commonly used fluid. A Thermo-Scientific chiller was used to augment the condensation capacity. 50% water-ethylene-glycol mixture was used as the working fluid in the chiller. The inlet and outlet of the circulation chiller were connected to a copper coil condenser immersed in FC-72 inside the inner tank. The copper coil was designed to exchange 3 kW heat from the system which was well above the maximum heat dissipated in this study. The power supplies provide DC power to the die, the data acquisition system records power and local temperatures, and the Phantom V-310 high-speed camera captures the nucleation activity. The support structure is mounted on castors.

**DC Power Supply**

The experiments were equipped to run at high power levels ranging from 1 to 3 KW. Hence, 3KW American Reliance SPS 150-20 DC power supply was needed to power the

boards that contained the test dies. Details on the test die used in this study will be explained in the subsequent chapters. The power supply has two terminals which can be operated in both series and parallel mode. The power supply had the capability of manual and computer controlled operation. The power supply can be connected to computer using Ethernet, GPIB or RS-232 port. RS-232 port was chosen as it was very common and readily available. LabView drivers were available with the software package to control the power supply. A program was written in LabView to control the power supply through the computer.

**Data Acquisition System**

Data Acquisition System (DAS) is necessary to record the temperature and current values obtained from the experiment. NI 9205 (voltage module) and NI 9227 (current module) were assemble in a NI cDAQ 9178 chassis which was internet connected to the computer using a USB cable. LabView drivers were installed for the DAS. The measurement capability of NI 9205 is -10 to 10 V and NI 9227 is 0 to 5 A.

**High Speed Camera**

High speed imaging helps us understanding the bubble characteristics better due to its small size and high velocity. A Phantom V310 high speed camera was used to the capture high speed images of the bubbles emanating from the test surface due to boiling. As the sizes of the bubbles were in the order of microns, a microscopic lens was needed. A K2/Sc microscopic lens by Infinity Photo-Optical Company was bought. Three different objectives were used based on the size of the chip. The camera can operate from 200 fps

to 120000 fps. 3200 fps were typically used in recording most of the videos in the current study.

### 3.1.2 Test Board

A schematic layout of the PCB and thermal die is shown in Figure 23 (a) and (b). A test board typically consisted of five die, each of which has nine thermal test cells equipped with temperature sensing capability. Figure 23 (b) describes the pin layout of one single die. The thermal test die has four leads for supplying power and eight leads for temperature measurements. Pin 1, 7, 6 and 12 are used for power supply. Each thermal test cell was incorporated with either a Wheatstone bridge type network or a five-diode series string for local temperature measurement. Pins 2, 3, 8, 9 are used for five-series diode and Pins 4, 5, 10, 11 are used for Wheatstone bridge type network. The sensitivity of the five-diode series string is 10mV/°C and the Wheatstone bridge network has a sensitivity of 2mV/°C. The five-diode string scheme was used for temperature measurement in the present study. Each five-diode string has four leads, two for supplying the excitation current and two for measuring the voltage across the circuit. A total of nine sensors for each test die and 45 temperature sensors were used on the PCB. Each test die had three heaters broken into six circuits that could carry 0.5 A each. Six heater circuits needed twelve leads to connect to the power supply. Hence, there were totally one hundred and eighty leads for temperature sensors and sixty leads for the power circuit. Robust hermetically sealed connectors were used as shown in Figure 24 to

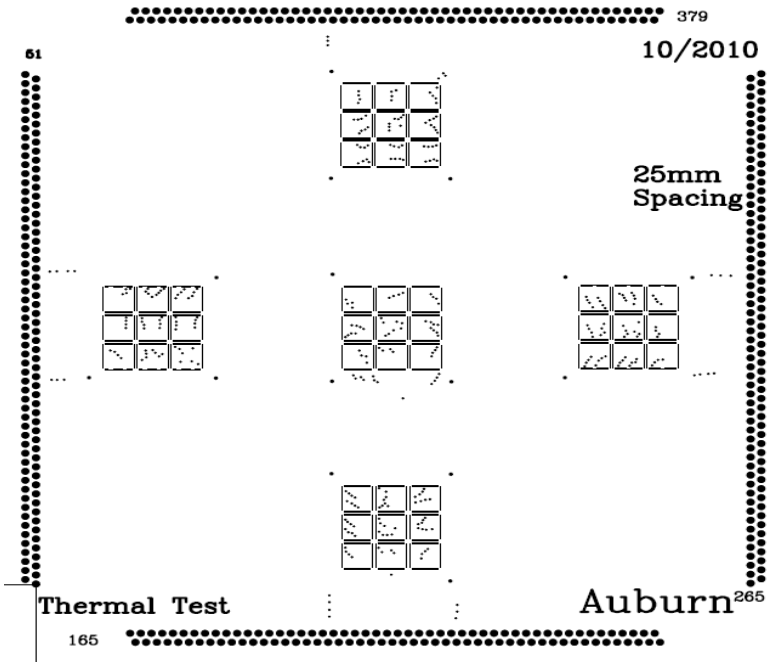


**Figure 23 (a) A schematic layout of the PCB**

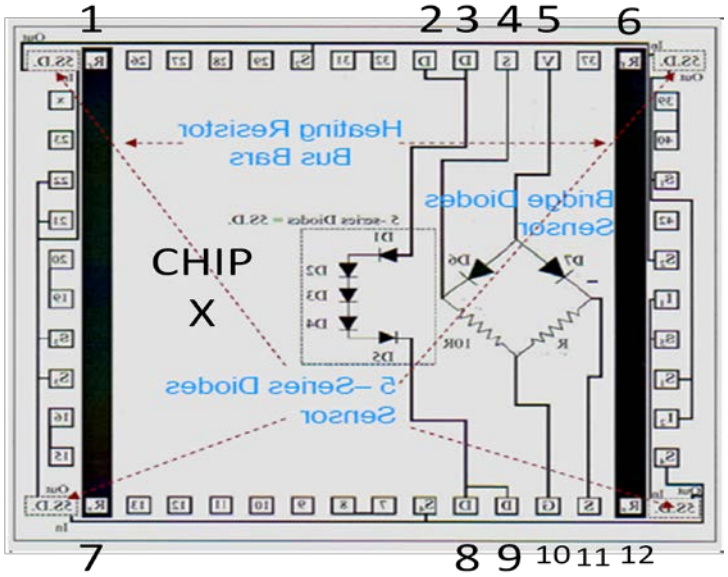


**Figure 2 (b) Pin layout for a single thermal test die**

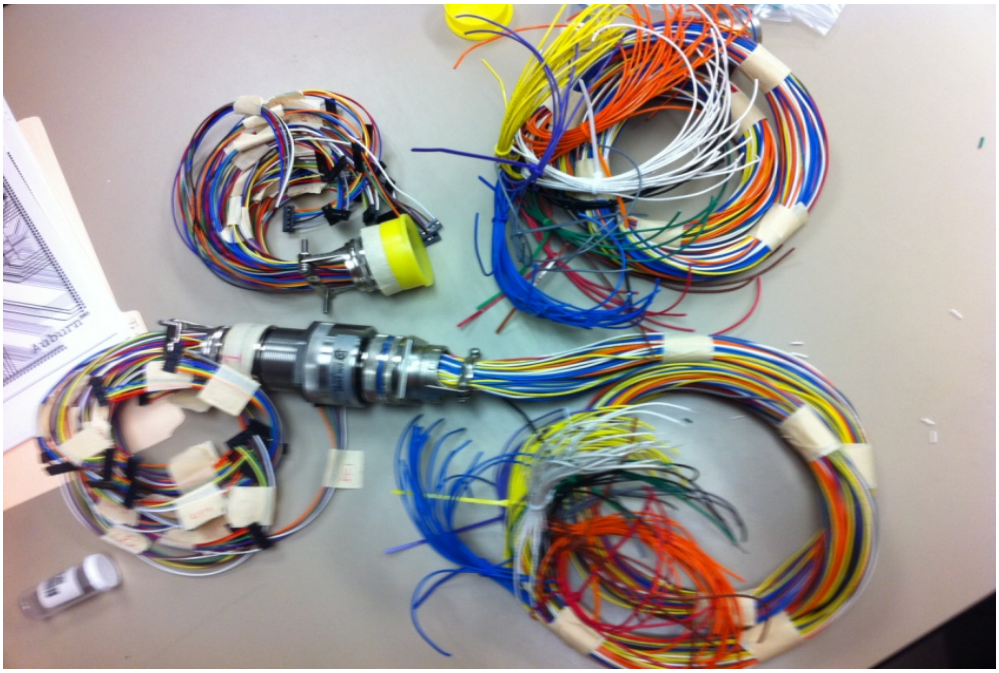

**Figure 24 Wiring harnesses with quick disconnect**

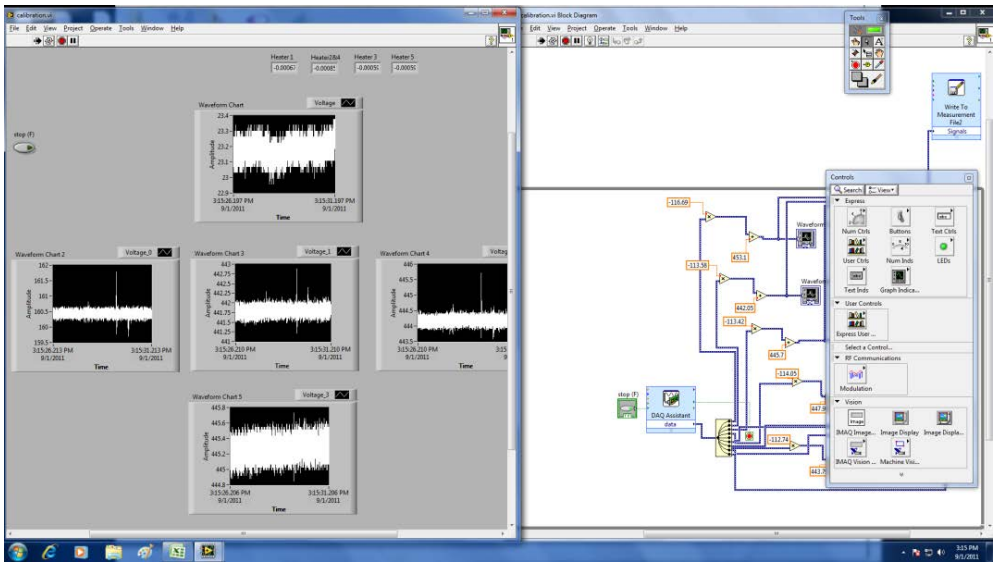

**Figure 25 Sample LabView Screen**

manage two hundred and 40 wires coming out of the test board. The hermetically sealed connector was bought from Douglas Electrical connectors and the model number was 24060. Additional hardware was incorporated to facilitate the excitation of all the temperature sensors. This additional hardware, in the form of a relay output board, was integrated in the data acquisition to excite all the sensors using single power supply. A microcontroller level program was written to control the relays via the data acquisition program. A Keithley 2401 SourceMeter was used to supply the excitation current of 100mA to the diodes. The positive terminal of the SourceMeter was connected to the anode of the diodes using a breadboard. The cathode of each diode was connected to the each NO (Normally Open) terminal of the relay circuit board. The CM (common) terminals of the relay circuit board were connected in series on the breadboard which in turn was connected in series to the negative terminal of the SourceMeter. The other two terminals of the diode were connected to the voltage module of the DAS. After the circuit connection was completed and tested, calibration for the temperature sensor was performed.

### 3.1.3 Temperature Calibration

Prior to data collection, the temperature-sensing diodes were calibrated against a NIST-traceable thermistor (±0.01°C) in a constant temperature bath of DI water. In order to avoid short-circuit in the test board; the chip was covered with two layers of sealed bags. The test board was immersed in the water bath and the voltages of the diode were recorded using the DAS (NI 9205) for temperatures from 25 °C to 85 °C and a calibration

curve was plotted between thermistor temperature and the diode voltage. A linear equation was obtained from the plot and the equation was programmed in LabView to convert the diode voltages into surface temperature. A screenshot of the LabView screen is shown in the Figure 25.

### 3.1.4 Test Procedure

After the sensors were calibrated, the test specimen was assembled into the inner tank containing the working fluid. The working fluid in the inner tank was heated to the saturation temperature using a cartridge heater to degas the liquid. The saturation temperature of FC-72 is 56.6 °C at atmospheric pressure. The fluid was degassed to obtain accurate boiling data without the confounding effects of dissolved non-condensables that mimic the boiling process and alter the partial pressure. The pool boiling experiment was conducted by supplying DC current to the heater circuit behind the test die using 3KW AMREL power supply. The current was measured using the DAS module (NI 9227) and the voltage drop across the heater circuit was measured using HP34401A multimeter. The product of the measured current and the voltage drop gave the power supplied in watts. The supplied power was divided by the die area and the heat flux dissipated from the die surface was calculated. The temperature was recorded using the LabView program and the boiling curve was plotted between the heat flux and the wall superheat on log-log coordinates. The power was increased until a vapor blanket formation was observed on the test die. After the vapor blanket formation was observed,

the heat flux was reduced in small steps to zero. The experiment was repeated for one more cycle to check for repeatability of the results obtained and record hysteresis effects.

# CHAPTER 4: RESULTS AND DISCUSSION

The present study enumerates the enhancement in pool boiling by using structured surfaces. The study also focuses on the effect of a neighboring chip below the test chip operating at various heat fluxes. Tests were conducted on a multi-chip module using 1.8 cm × 1.8 cm test die with multiple thermal test cells with temperature sensing capability. The different surfaces evaluated were as follows :

- Bare silicon chip
- silicon chip directly indium-attached to copper micro-porous heat spreaders
- Silicon chip directly indium-attached to copper pin fins.
- silicon chip directly indium-attached to copper straight fins

Parameters tested include heat flux levels, dielectric liquid pool conditions (saturated or subcooled), and effect of neighboring die. To understand the effects of neighboring die better, two different effects were studied. The first effect produced a natural convection plume that passed over the surface of the test chip. The second effect was producing bubbles from the entire surface of the neighboring die that passed over the test chip. In order to understand the boiling process, a baseline study was carried out on a single-chip module. The next section describes the procedure for the baseline study and also the key results

obtained.

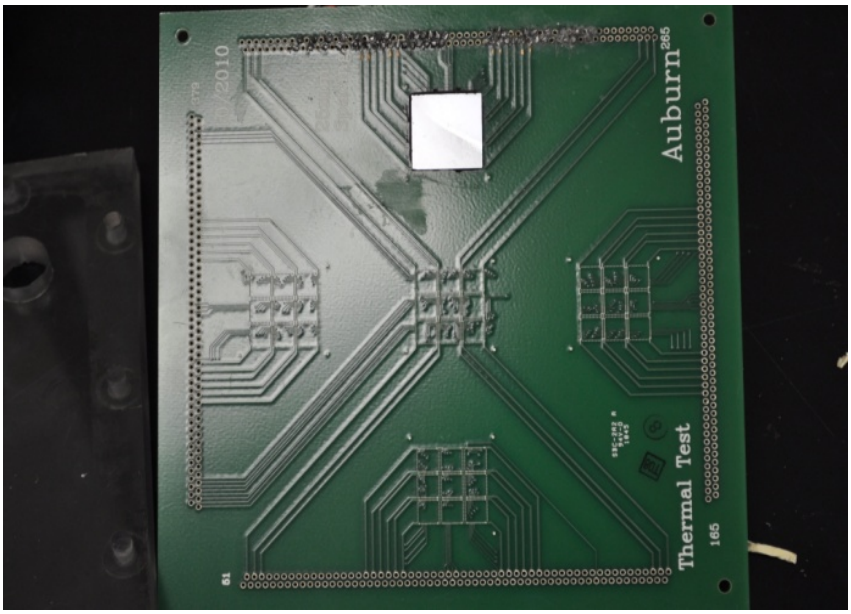


**Figure 26 Test board with single die**

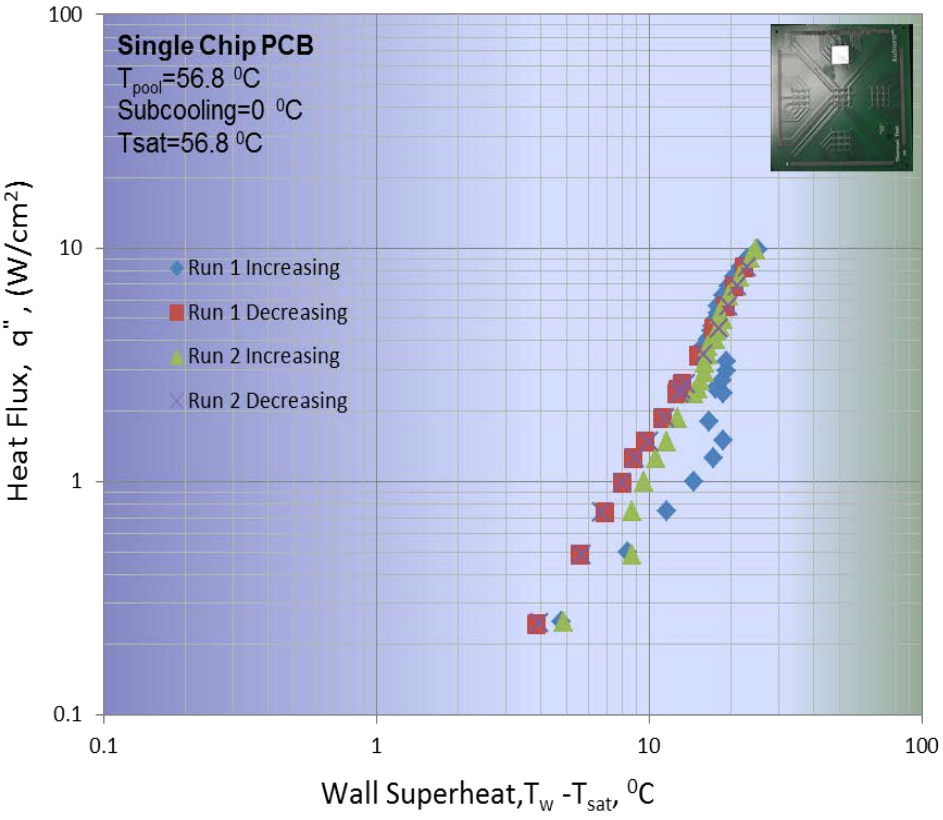


**Figure 27 Pool boiling curve for the baseline study**

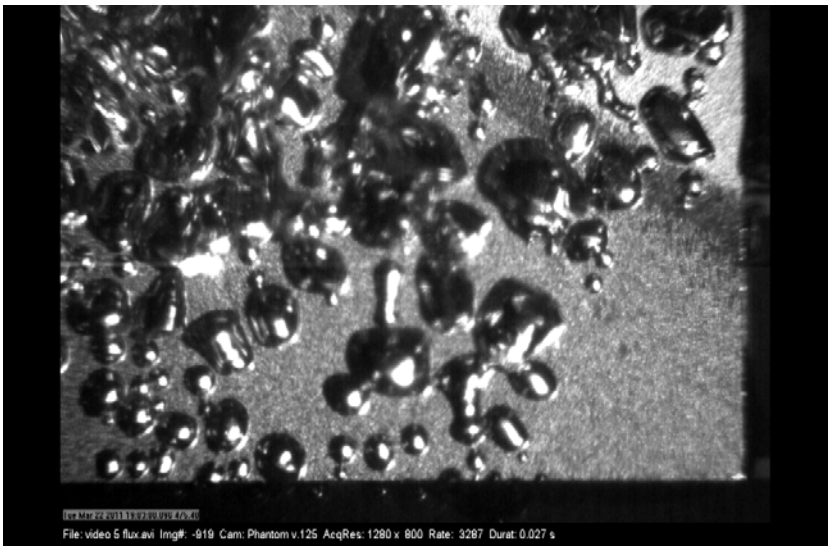


**Figure 28 Nucleation image of single die board at 5 W/cm$^2$**

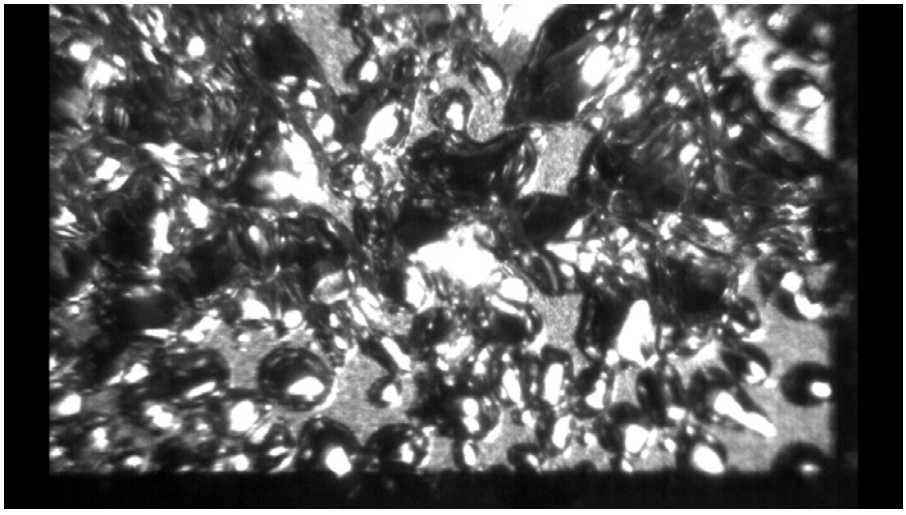

**Figure 29 Nucleation image of single die board at 10 W/cm$^2$**

## 3.1 Single Die Board – Baseline Study

Initial testing focused on collecting surface temperature measurements from a single die, as a function of the heat flux. Figure 26 shows the board with one test die comprised of nine thermal test cells. The total surface area of the heated surface is 1.8 cm X 1.8 cm. Figure 28 and Figure 29 are screen capture shots of high-speed video clips of the bottom two-thirds of the die at 5 W/cm$^2$ showing nucleation sites distributed over most of the surface; and 10 W/cm$^2$, the highest flux recorded where some coalescence between bubbles is apparent. The total heat dissipated at 10 W/cm$^2$, is 32 W. The plot shown in Figure 27 is processed temperature and heat flux data for two increasing/decreasing heat flux cycles. The data show the typical hysteresis between increasing and decreasing flux and the typical differences between the first cycle from a subcooled starting condition on the first cycle and a saturated starting condition when the surface defects have entrapped vapor present. The overshoot (sudden drop in temp) as the mechanism changes from natural convection at very low heat flux, to pool boiling as bubbles start to nucleate at higher heat flux [Carey [42])] , occurred in three-four steps instead of all at once since nucleation did not appear all over at once as it might on a surface with manufactured uniform surface roughness. Note that a typical surface has a range of randomly distributed surface roughness features.

## 3.2 Multiple Test Dies

The primary objective of this study include the effects of surface enhancements, the effect of changes in pool temperature, and the effect of heat dissipation from neighboring heat sources in pool boiling of FC-72. Three types of boards were used to study the effects of surface enhancements. They are listed as follows:

- Board A: Bare silicon dies of dimension 1.8 cm × 1.8 cm(Figure 30).
- Board B: Sintered copper heat spreaders of dimensions 4 cm × 4 cm (Figure 31).
- Board C: finned copper surfaces of base area 1.8 cm × 1.8 cm (Figure 32).

A sequence of four tests was conducted on each of the test boards as follows:

a) One silicon die was powered up from zero to a value of the heat flux at which the surface temperature was not exceeding 85℃ with all others turned off.

b) One silicon die was powered up from zero to a value of the heat flux at which the surface temperature was not exceeding 85℃ with the die immediately below it generating natural convection plumes which crossed the die above it.

c) One silicon die was powered up from zero to a value of the heat flux at which the surface temperature was not exceeding 85℃ with the die immediately below it generating vapor bubbles.

d) All five die powered up together from zero to a value of the heat flux at which the surface temperature was not exceeding 85℃.

This set of tests was conducted in a saturated pool and repeated in a subcooled pool at a subcooling of 15°C (pool temperature maintained at 41°C, which is 15°C below the saturation temperature of 56°C for FC-72 at atmospheric pressure). All tests were conducted in FC-72. The sequence of four tests conducted under both saturated and subcooled conditions is described below, with identifiers A through D.

A) The center die was powered up from zero to a value of the heat flux at which the surface temperature did not exceed 85℃ with other die turned off. The die surface temperature at various heat fluxes was recorded and a boiling curve was generated showing heat flux as a function of wall superheat (temperature difference between the center thermal test cell in the die and the fluid in the pool). Recognizing that the surface temperature of the entire die was uniform allowed use of just the center thermal test cell surface temperature to be representative of all nine in the die. However, tests involving heat spreaders needed recording of all nine temperatures due to the non-uniformity from the larger footprint of the spreader.

B) The center die was powered up from zero to a value of the heat flux at which the surface temperature did not exceed 85℃ with the die immediately below it (all tests with board oriented vertically) maintained at a constant heat flux such that a natural convection current generated at the lower die passes over the center die. This test is the first of two conducted to study the effects of neighboring heat sources.

The third set of tests was conducted to study the effects of boiling emanating from a neighboring die. For this data run, the center die was once again powered up from zero

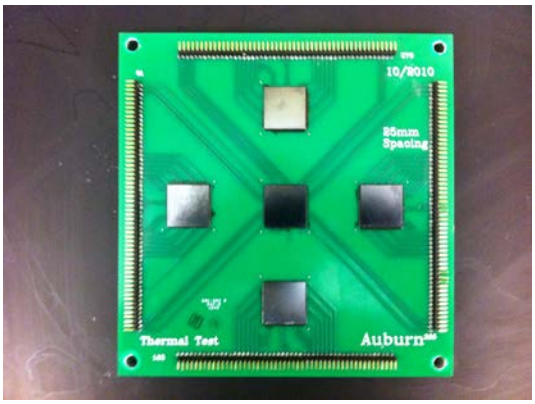


**Figure 30 Test board A**

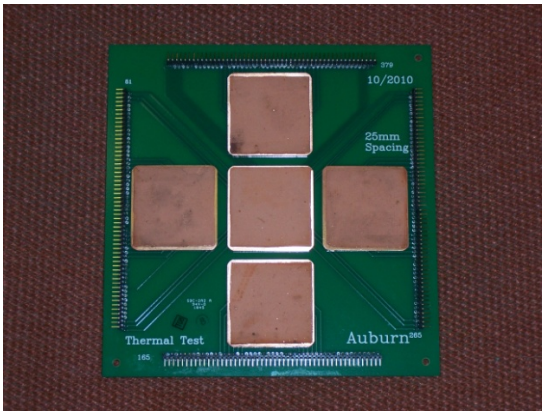


**Figure 31 Test board B**

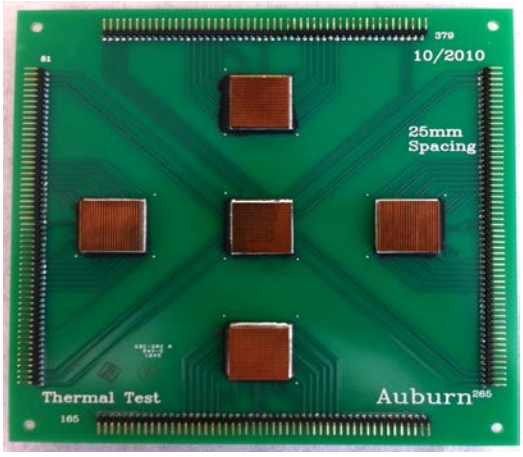


**Figure 32 Test board C**

C) to a value of the heat flux at which the surface temperature did not exceed 85℃ while the lower die was powered at a constant heat flux such that the bubbles were emanating from the entire surface.

D) The fourth test was conducted with all five die powered simulatneously from zero to a value of the heat flux at which the surface temperature did not exceed 85℃.

## 3.3 Surface Enhancements

Single heater pool boiling experiments for bare silicon die were conducted in a saturated pool of FC-72. The die surface temperature at various heat fluxes was recorded and a boiling curve was generated showing heat flux as a function of wall superheat (temperature difference between the center thermal test cell in the die and the fluid in the pool). The boiling curve is shown in Figure 33. The center die of board A was powered up from 0 to 10 W/cm$^2$ and denoted as “Run 1 Increasing” in Figure 33. The heat flux was slowly reduced from 10 W/cm$^2$ to zero W/cm$^2$ and was denoted as “Run 1 decreasing”. One more cycle of increasing and decreasing heat fluxes was carried out to check the repeatability of the boiling process and were denoted as Run 2 Increasing and Run 2 Decreasing respectively. Note that these results are slightly different from those for an ostensibly similar surface shown in Figure 27. Some differences are to be expected since boiling is very sensitive to microscopic surface characteristics. A prominent surface artifact running diagonally across the surface of the single-die board, visible in

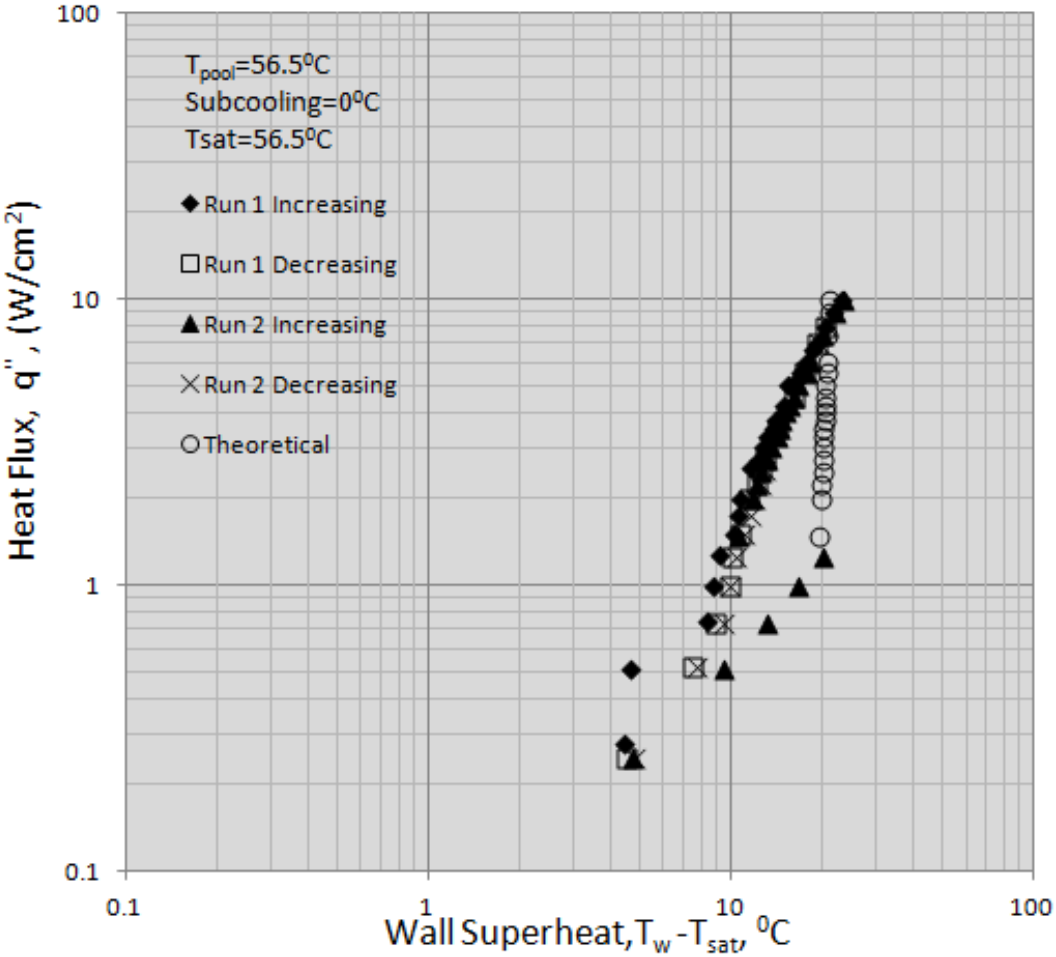


**Figure 33 Boiling curve for the bare silicon die with the other four die not powered**

Figure 28 and Figure 29, led to the triggering of partial nucleation on that surface, leading to a series of steps in the increasing heat flux portion of the curve; a result that was different from that shown in Figure 33. The key result, the superheat at a heat flux of 10 $W/cm^2$ (and other heat flux values) does still remain the same. You et al [43] conducted pool boiling experiment of FC-72 on different surfaces and found the constants used in the Rohsenow correlation. These constants were used in determining the theoritical value of the wall superheat for different heat fluxes in the nucleate boiling regime. The theoritical values were plotted in the boiling curve along with the experimental values. The values of the wall superheat were higher than the experimental results for the lower heat fluxes but fitted well for the higher heat fluxes in the nucleate boiling regime. This difference would be due to the surface roughness of the silicon chip used as boiling process is strongly influenced by the surface characteristics of the material.

### 3.3.1 Sintered copper heat spreaders

A similar test of two runs were conducted on board B in a saturated pool of FC-72. The center die was powered up from 0-10 $W/cm^2$ and the temperature was measured at all the thermal test cells of the test die. The heat fluxes for a bare silicon die and with surface enhancements for saturated conditions for Run 1 are shown in Figure 34. As the increasing heat flux conditions had temperature overshoot associated with it, the decreasing heat fluxes for Run 1 are plotted. Although the silicon die with sintered copper heat spreader was subjected to a heat flux of 10 $W/cm^2$, some fluctuations in the

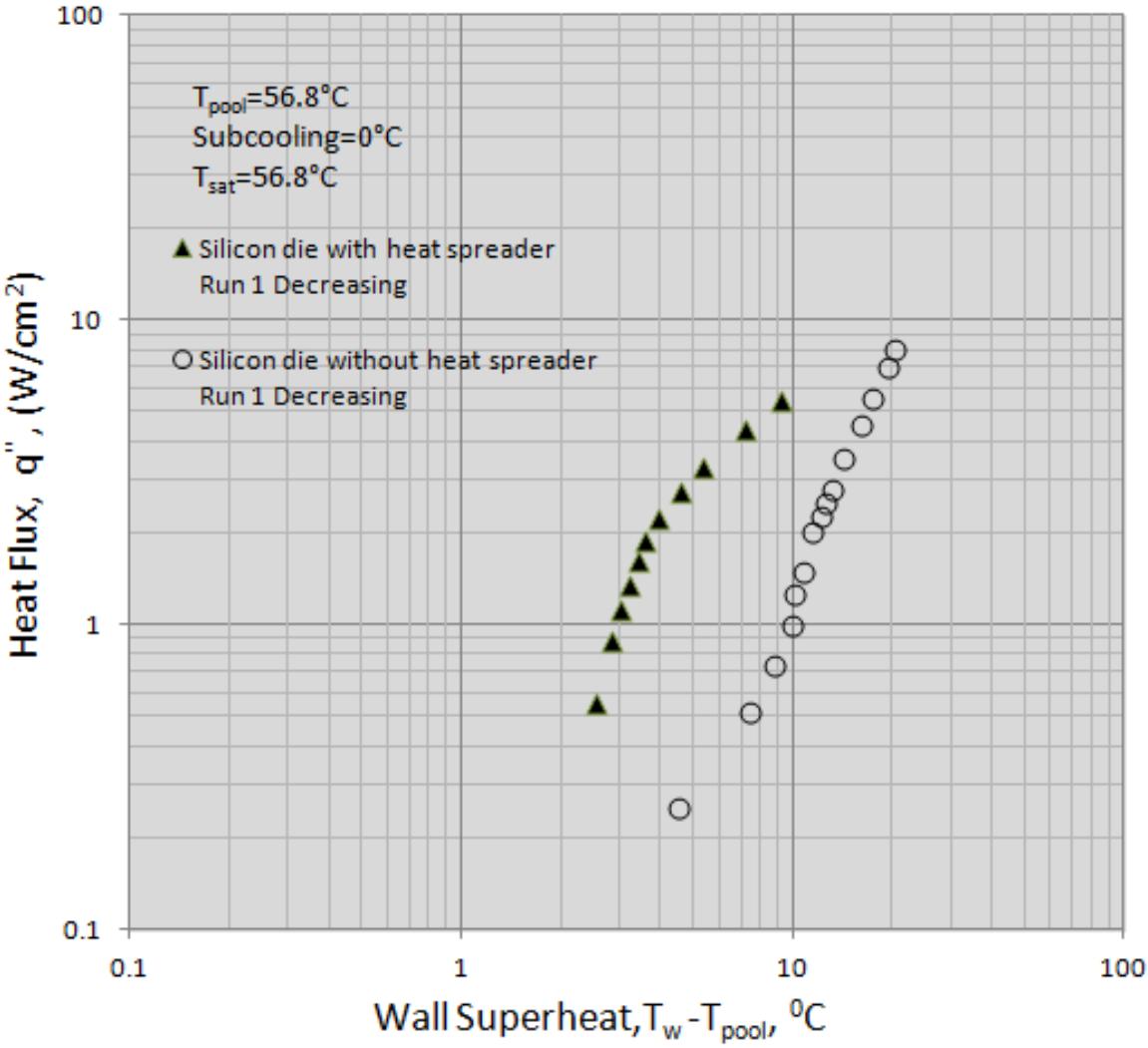


**Figure 34 Performance characteristics of silicon die with or without copper heat**

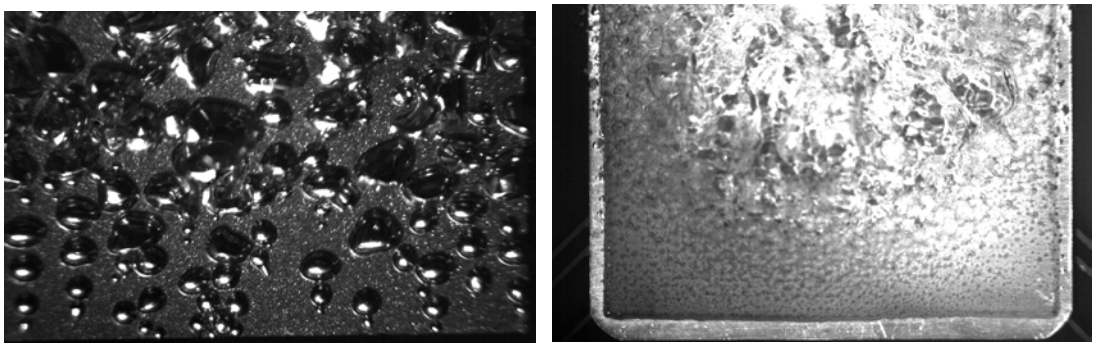

**Figure 35 Screen-captured high-speed images of nucleation activity at 5.5 W/cm$^2$ for (a) bare silicon surface in a saturated pool, and (b) sintered heat spreader in a saturated pool**

temperature sensor forced us not to include it in the data plot. Hence, the maximum point until which there wasn't any fluctuation in the temperature was about 5.5 W/cm$^2$.

It can be seen from Figure 34 that the wall superheat of the die with the microporous copper heat spreader is lower than the wall superheat of the bare die. The reduction in wall superheat for a die with a copper heat spreader attached was about 8°C at a heat flux of about 5.5 W/cm$^2$. In the particle layering technique implemented by You et al [8], it was reported that there was a decrease of 11 °C and 14 °C in the wall superheat for 0.3 and 0.3~3 μm particle layered surfaces as compared to a wall superheat of 30 °C for plain surface. Kim et al [11] conducted pool boiling experiments on sanded and microporous surfaces and found that there was a decrease of 43.4 and 67.3 % in the wall superheat compared to plain surfaces. Other researchers such as Kim et al [11], Li and Peterson [14], Chang and You [10], O'Connor and You [9] have reported reduction in wall superheat due to microporous coating. To ascertain the enhancement in boiling due to microporous coating, a plot comparing the heat transfer coefficients of bare silicon die and die with microporous heat spreader is shown in Figure 36. The surface temperature increases with increase in input power but the microporous show a much higher heat transfer coefficient compared to bare silicon die. However, a decline in heat transfer coefficient was at higher heat fluxes were noted. In microporous heat spreaders, the nucleation sites near the heated surface were activated and start coalescing thereby offering some thermal resistance which decreases the heat transfer coefficient.

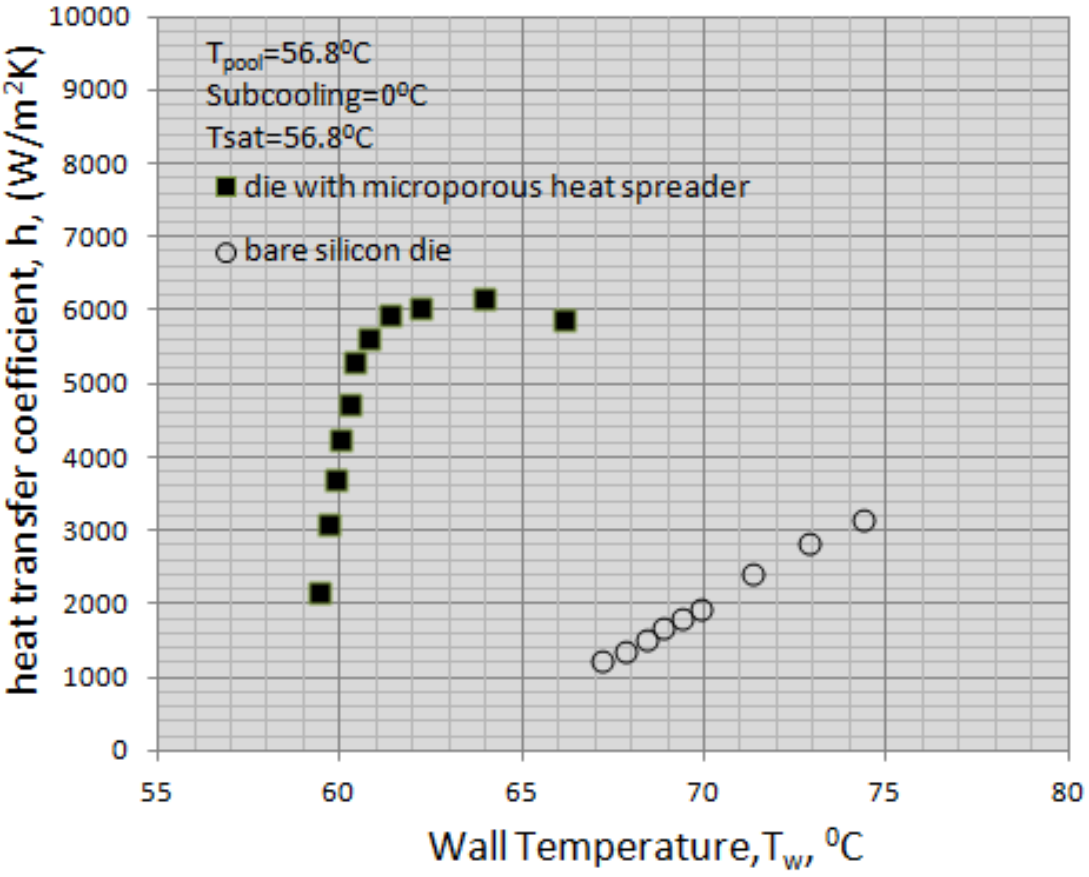


**Figure 36 Comparison of heat transfer coefficients for bare silicon die and die with microporous heat spreaders**

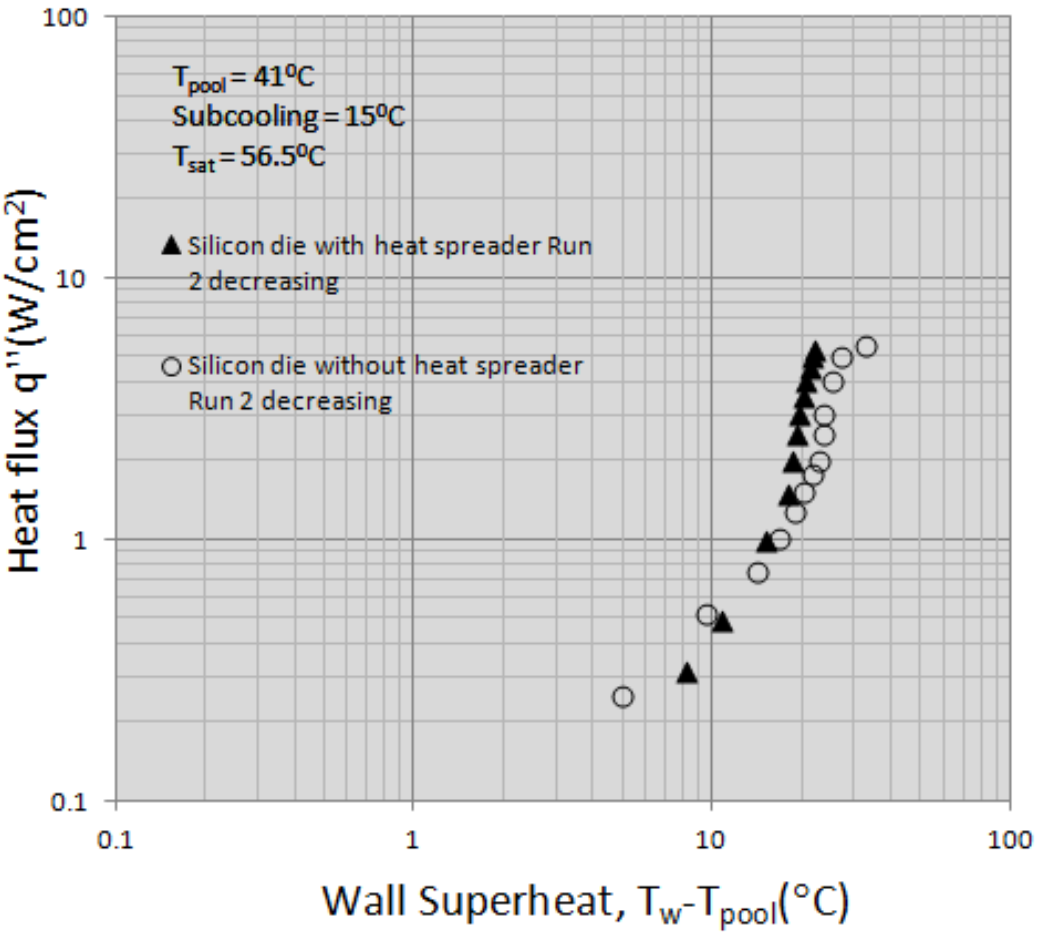


**Figure 37 Performance characteristics of silicon die with and without copper heat spreader in a subcooled pool**

Kim et al [11] reported that the possibility of lower wall superheat for a microporous surface compared to a plain surface is due to the fact that the active site density was higher for the former. Figure 35 shows the high speed images of sintered surface and plain surface taken at 5 W/cm$^2$ in a saturated pool. Both the images show the bottom 2/3$^{rd}$ of the total surface of the chip. It can be noted that the bubble sizes of microporous surface were very small as compared to the plain surface. A visual study of the bubble dynamics was carried out using the high speed images at saturated temperature. The bubbles were measured at 1 W/cm$^2$ and 5 W/cm$^2$. At higher heat fluxes, the bubbles agglomerated forming a vapor blanket which made the measurements of the bubble departure diameter impossible. The departure diameter at 1 W/cm$^2$ and 5 W/cm$^2$ found to be 0.133 mm and 0.2 mm respectively. This shows an increase in the bubble departure diameter with increase in surface heat flux. Similar observations were made for bare silicon chip at 5 W/cm$^2$ and 10 W/cm$^2$ and found to be 0.46 mm and 0.52 mm respectively. Table 5 compares the bubble departure diameter of microporous surface and finned surface. By comparing the bubble departure diameter of the plain surface and the microporous surface at 10 W/cm$^2$, it can be seen that the bubble departure diameter of the microporous surface was half the size of the one departing from plain surface. Also, the bubble site density of the sintered microporous surface is much higher than the plain surface which accounts for the lower wall superheat for the microporous surface.

The microporous surface and plain surface were independently subjected to pool boiling in a subcooled pool. The pool was maintained at 41 °C resulting in a subcooling

of 15 °C. The procedure for running the experiment was similar to the one discussed earlier. The heat flux was increased until a wall superheat of 80 °C and lowered back to zero and was recorded as Run 1. The cycle was repeated for one more cycle denoting it as Run 2. Figure 37 shows a comparison between the pool boiling curves of the sintered microporous die and the bare silicon die in a subcooled pool. The ΔT used for subcooled pool was the difference in temperature between the wall and the pool (41 °C). The figure shows Run 2 decreasing heat flux for better comparison of the data. As discussed earlier in this section, the wall superheat of the die with the microporous copper heat spreader is lower than the wall superheat of the bare die. The reduction in wall superheat for a die with a copper heat spreader attached was about 6°C at a heat flux of about 5 W/cm$^2$.

### 3.3.2 Extended Surfaces

Another important enhancment process that is widely popular in the field of thermal engineering is the addition of fins. Two different fins were analyzed in the present study,namely, pin fins and rectangular fins. Extensive research has been carried out in the boiling of finned array in FC-72. Parameters such as pin spacing and fin length have been studied.

The first type of fins used in the present study were the pin-fins. A rectangular copper bar of dimension 1.8 cm × 1.8 cm is cut into 23 × 23 array of pin-fins with a dimension of 0.387 mm × 0.312 mm and height 1.953 mm using electron beam machining process. The area ratio of the surface with pin-fins to the bare silicon surface was 5.45. A

microscopic view of the pin-fins are shown in Figure 38. Copper pin-fins were indium attached to the silicon chip. The test board is immersed in a saturated pool of FC-72 and heat is supplied to the silicon chip. The heat flux is calculated by taking the base area of the fin and plotted against the wall superheat in a log-log plot to obtain the boiling curve. Figure 39 shows the pool boiling curve for the studded surface in a saturated pool of FC-72. It can be seen that the temperature overshoot in the pin-fin surface is about 3 °C which is very small compared to the temperature overshoot of 10 °C in the bare silicon die. Also, the wall superheat of pin finned surface is much lower than the bare silicon die at lower heat fluxes. However, the lower wall superheat might be due to the increase in area obtained from the pin-fins. In order to understand the enhancement due to pin-fins better, heat flux based on the wetted area was plotted against the wall superheat. Figure 40 compares the pool boiling curve the run 2 decreasing heat flux for die with pin-fins and bare silicon die. It can be seen that the wall superheat for the pin-fins are lower than the wall superheat of bare silicon die. The decrease in wall superheat can be attributed to the enhancement obtained from the structure of the fins in addition to the increase in surface area. A similar experiment was run on the die with rectangular fins as shown in Figure 41.

Gulgliemini et al [17] in their parametric study of finned copper arrays in saturated pool of FC-72 reported that the heat transfer coefficient increases significantlly due to the presence of fins but does not depend on the fin dimensions. However, At higher heat fluxes, there is a significant decrease in the heat transfer coefficient and it was attributed

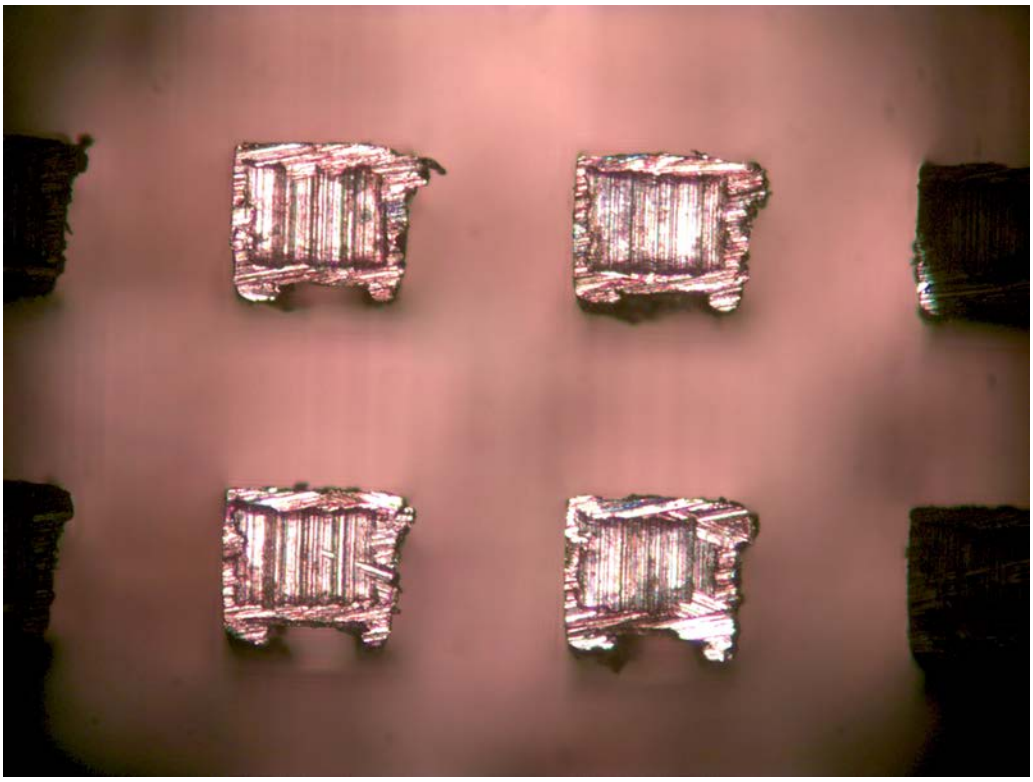

**Figure 38 Microscopic view of the pin fins**

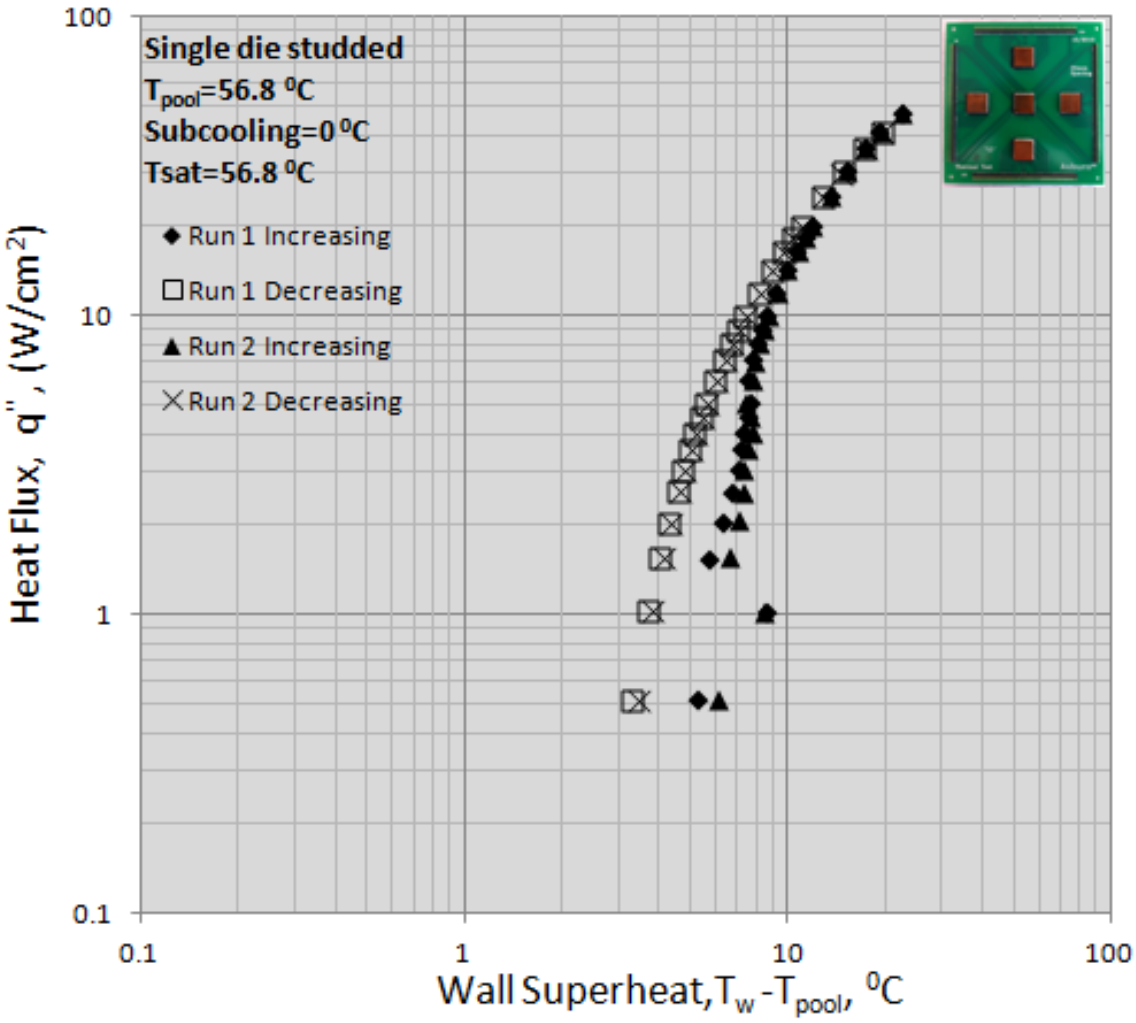


**Figure 39 Boiling curve for the silicon die with pin-fins with the other four die not powered**

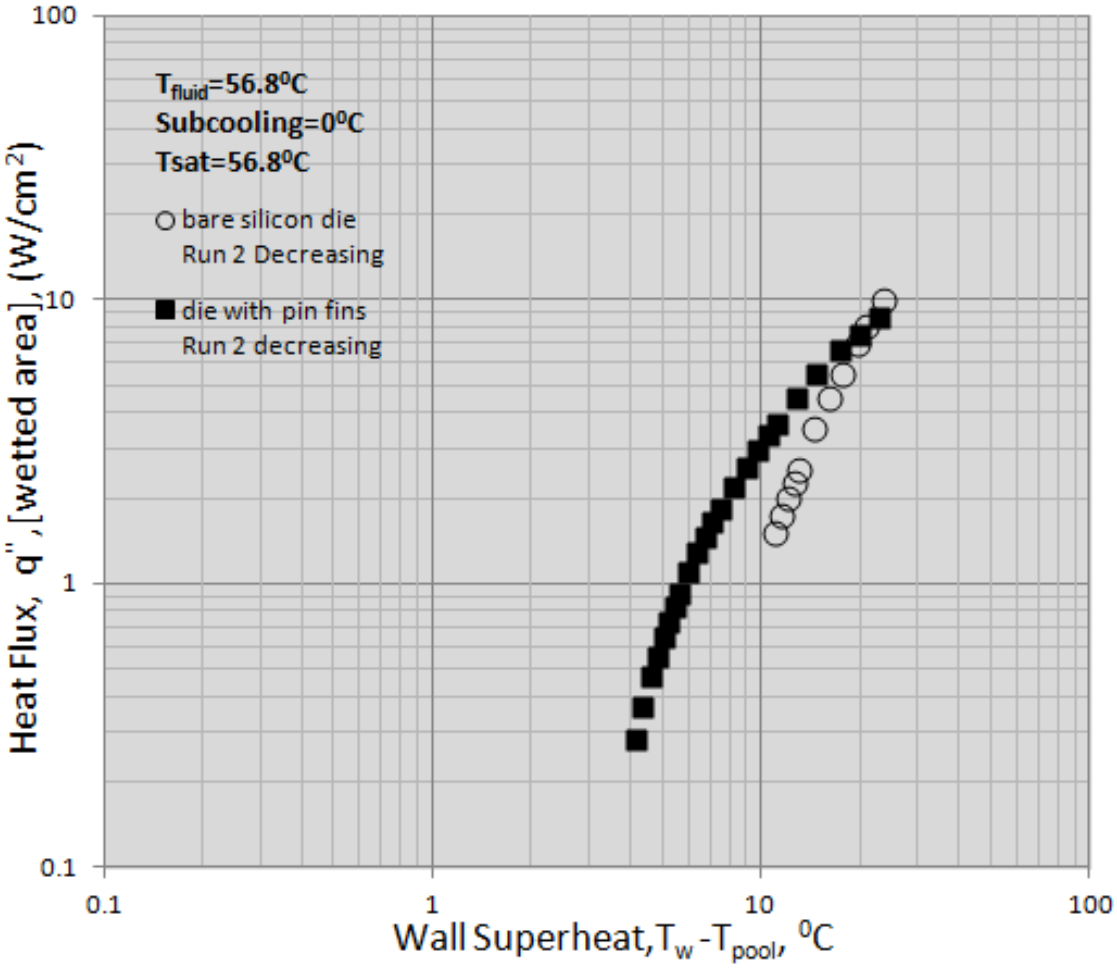


**Figure 40 Performance curve for the die with pin-fins (based on the wetted area) compared to the bare silicon die**

to the fin dimensions. It can be explained that the fin spacing and height determines the bubble growth mechanism and the denser and taller the fins are arranged, it is more difficult for the vapor bubble to grow and depart from the fin surface. Hence, it agglomerates to form a big vapor bubble within the fins thereby decreasing the heat transfer co-efficient. The bubble departure diameter of the pin fins were found out by visual studying the high speed images. Bubble departure diameter at 2 W/cm$^2$ and 5 W/cm$^2$ were studied. The high speed images at higher heat fluxes had big bubble coalsesences which complicated the measurements of bubble departure diameter. It was found that the bubble departure diameter increased from 0.192 mm at 2 W/cm$^2$ to 0.242 mm at 5 W/cm$^2$. Bubble departure diameter increased with increase in heat flux as obtained in the case of plain and microporous die. Bubble departure diameter for all three surfaces are compared in Table 5.

**Table 5 Comparison of bubble departure diameters for all three surfaces**

| **Type of surface** ↓ | **Heat flux** | | | |
|---|---|---|---|---|
| | 1 W/cm$^2$ | 2 W/cm$^2$ | 5 W/cm$^2$ | 10 W/cm$^2$ |
| Microporous surface | **0.133 mm** | **-** | **0.2 mm** | **-** |
| Surface with pin-fins | **-** | **0.192 mm** | **0.252 mm** | **-** |
| Bare silicon surface | **-** | **-** | **0.46 mm** | **0.52 mm** |

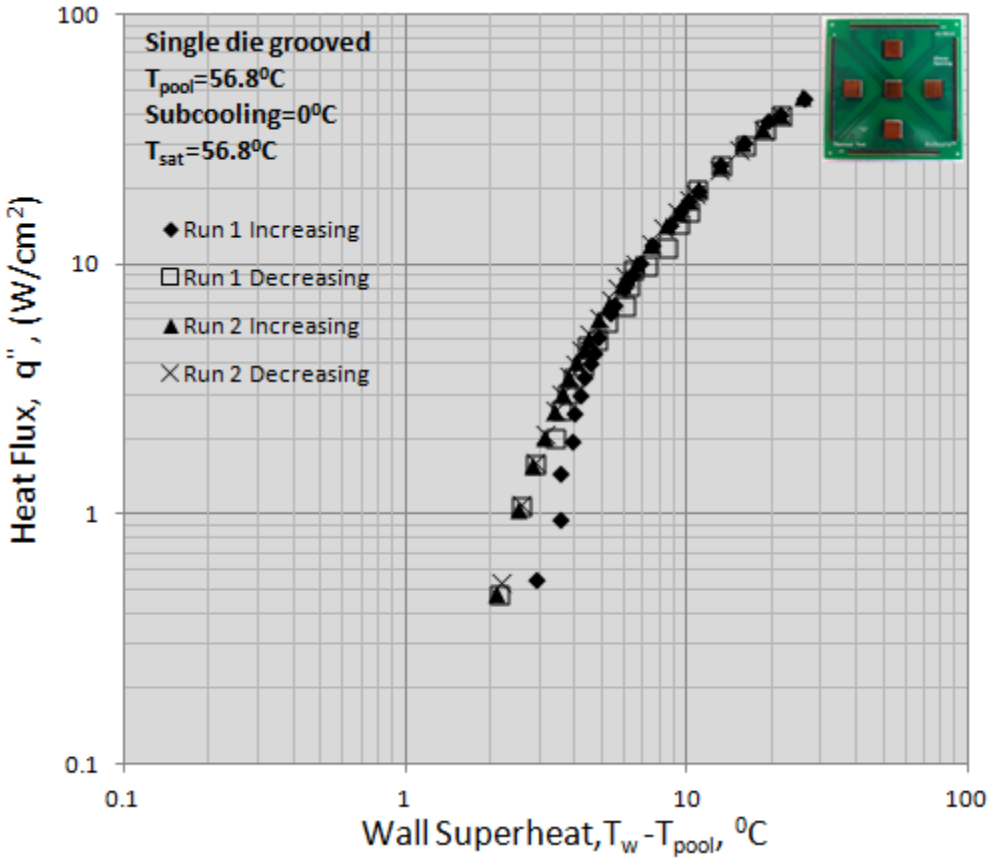


**Figure 41 Boiling curve for the silicon die with rectangular fins with the other four die not powered**

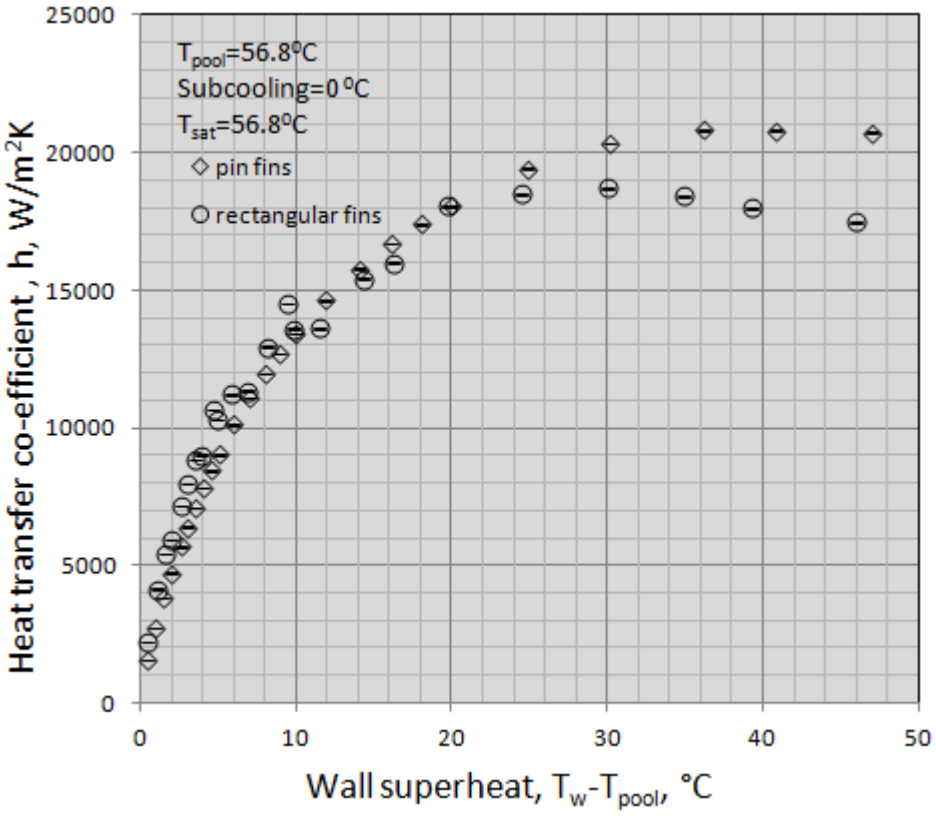


**Figure 42 Comparsion of heat transfer coefficients for pin fins and rectangular fins**

the bubble dynamics depends on the heat flux which inturn depends on heat transfer coefficient of the fluid. The heat transfer coefficients of rectagular fins and pin-fins are plotted against the heat fluxes as shown in Figure 42. The heat transfer cofficient at lower heat fluxes doesn't seem to vary much as it is dominated more by the heat transfer area available than the number of active nucleation sites. However, pin-fins seem to perform much better than the pin-finned surface at higher heat fluxes due to the fact that the number of active nucleation sites is higher than the rectangular finned surface. The vapor bubble generated between the fins in the rectangular finned surface can only travel through one direction unlike pin-finned surface and therfore, the bubble has a longer residence time in the rectangular finned surface therby forming a much bigger vapor blanket which decreases the heat transfer coefficient.

## 3.4 Subcooling Effects

The effects of subcooling were examined by maintaining the pool at a temperature of 41°C, resulting in a subcooling of 15°C since the atmospheric pressure boiling point of FC-72 is 56°C. Subcooling affects nucleate pool boiling in several ways, the most substantive of which is the reduction in the size of the bubble. This happens due to the interaction of the nucleating bubble with a cooler fluid as compared to the effect in a saturated pool. This reduction in size reduces the tendency of bubbles in close proximity to agglomerate, thereby increasing the critical heat flux. Figure 43 (a) & (b) shows a

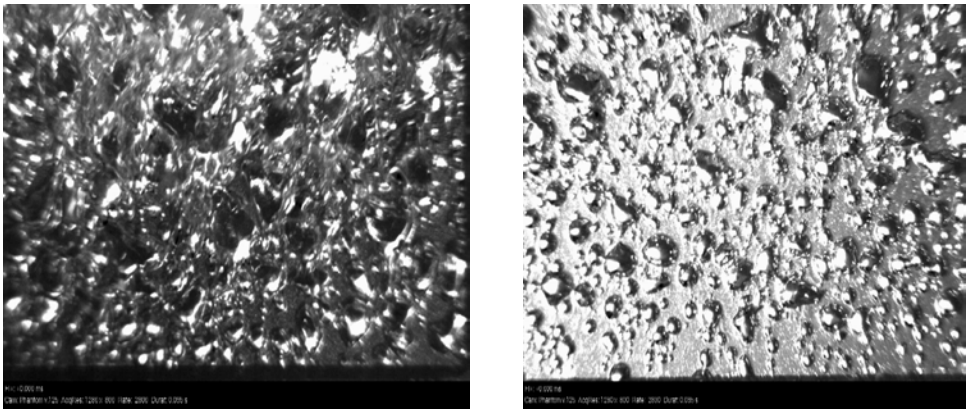

**Figure 43 Screen-captured high-speed images of nucleation activity (a) 10 W/cm$^2$ in a saturated pool, and (b) 12 W/cm$^2$ in a subcooled pool**

heat flux and the bubble departure diameter increased with increase in the heat flux.

**Table 6 Bubble departure diameter for plain silicon die**

| **Pool Condition** ↓ | **Heat Flux** | |
|---|---|---|
| | **5 W/cm$^2$** | **10 W/cm$^2$** |
| **Saturated pool** | **0.46 mm** | **0.52 mm** |
| **Subcooled pool (15 °C)** | **0.22 mm** | **0.24 mm** |

screen-captured high-speed images for saturated pool conditions at 10 W/cm$^2$ and subcooled pool conditions (15°C subcooling) at 12 W/cm$^2$.

The bubble size in Figure 43(b) is smaller compared to that in Figure 43(a) in spite of higher heat flux. A similar observation was made by Medavaram et al. [44] in a study of ebullition characteristics of microstructures in immersion cooling. Also, the bubbles are more distinct indicating that the heat flux can be raised further without reaching CHF. The images were analyzed to measure the bubble departure diameter in order to characterize the nucleation. Actual bubble sizes on the surface are a function of the size of the cavity. The average bubble departure diameter was determined by analyzing the screen-captured images using the chip dimension as a reference scale at different locations and averaging them.There was some naturally occurring variability on the surface of these nominally smooth bare die. Measurements are shown in Table 6 for a center die nucleating in the presence of natural convection plumes from the one below it. Bubble departure diameter is a function of heat flux and pool conditions. The primary

trend indicated is that the bubble departure diameter in a subcooled pool (15°C subcooling) was less than half of the bubble departure diameter of a saturated pool at same

## 3.5 Comparison of CHF

A pool boiling test was run on both saturated and subcooled pool to determine the CHF by increasing the heat flux until a drastic raise in temperature is noted. As the test specimen used in this study is a square surface, the temperature overshoot at CHF is not dramatic as seen on wires or circular tubes, due to spreading effects. The test run was similar as described above except for the fact that the heat flux was increased until a transistion from nucleate boiling to film boiling was encountered. Figure 46 and Figure 47 shows the pool boiling curve with the CHF denoted in it. It was experimentally determined that the CHF for a saturated pool is 16 W/cm$^2$ and subcooled pool is 19.25 W/cm$^2$ (Appendix B for calculations of CHF). The high speed images for CHF and film boiling for a bare silicon chip in a saturated pool is shown in Figure 44 and Figure 45 respectively. From Figure 44, it can be seen that certain spot on the surface was dried out of liquid and is in transition to film boiling. In Figure 45, the entired surface is covered with vapor and this marks the start of film boiling. The heat transport from the chip surface is now due to film boiling. After film boiling was reached, the heat flux was reduced slowly and there is a transition back from film boiling to nucleate boiling. This point is called the Leidenfrost point. However, the transition from film boiling to nucleate boiling occured at a heat flux of 8 W/cm$^2$ in a saturated pool and 6 W/cm$^2$ in a subcooled pool.

**Figure 44 High speed image denoting CHF for pool boiling of bare silicon die in a saturated pool of FC-72**

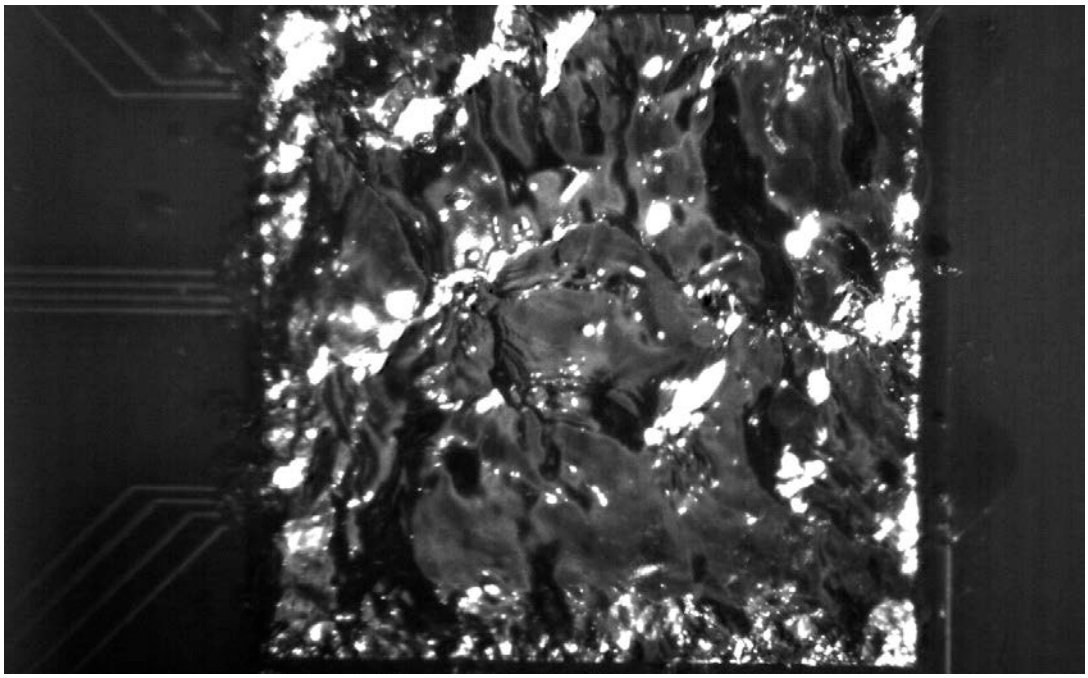

**Figure 45 High speed image denoting film boiling of a bare silicon die in a saturated pool of FC-72**

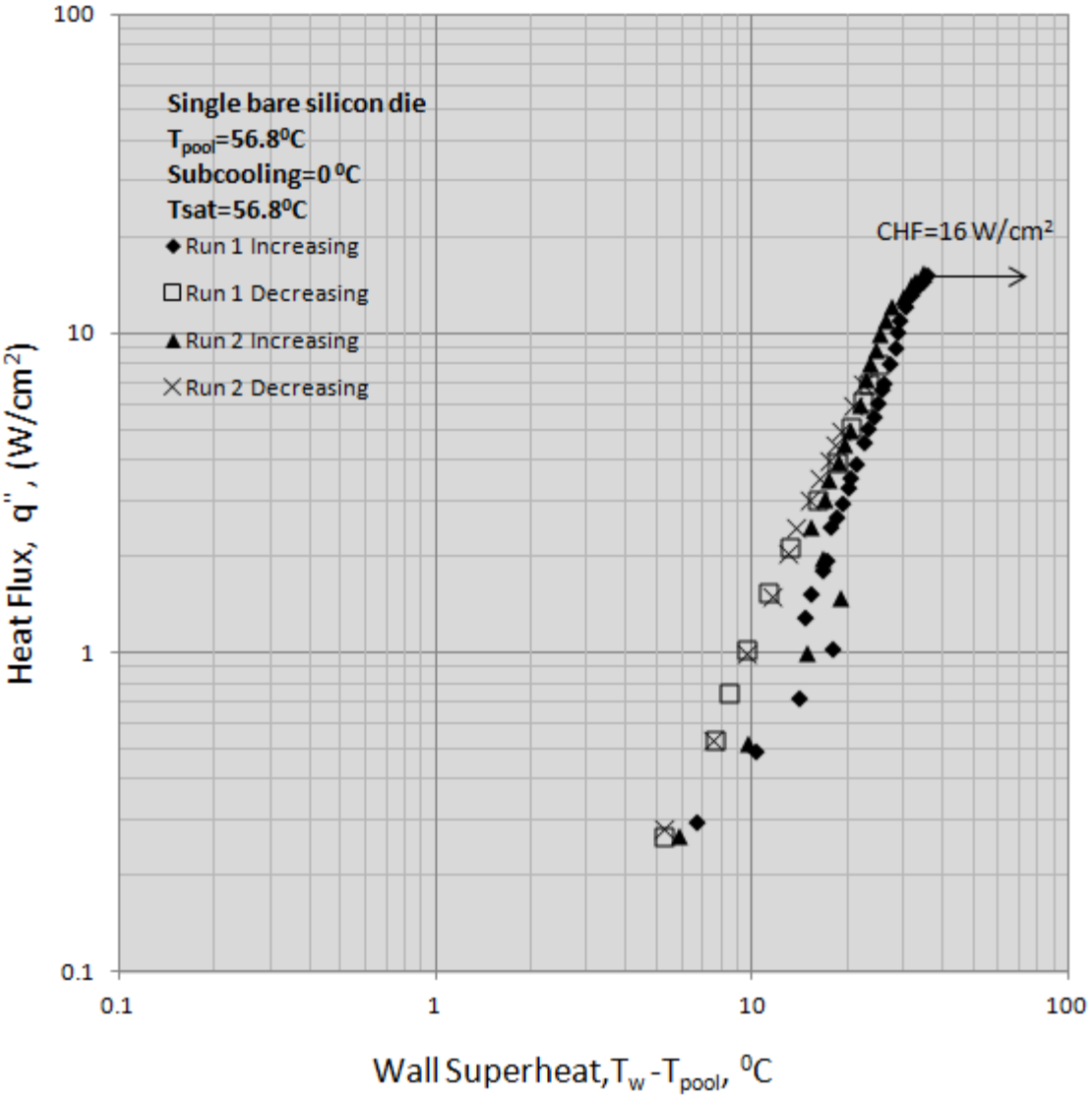


**Figure 46 Pool boiling curve for the bare silicon die with the CHF in a saturated pool**

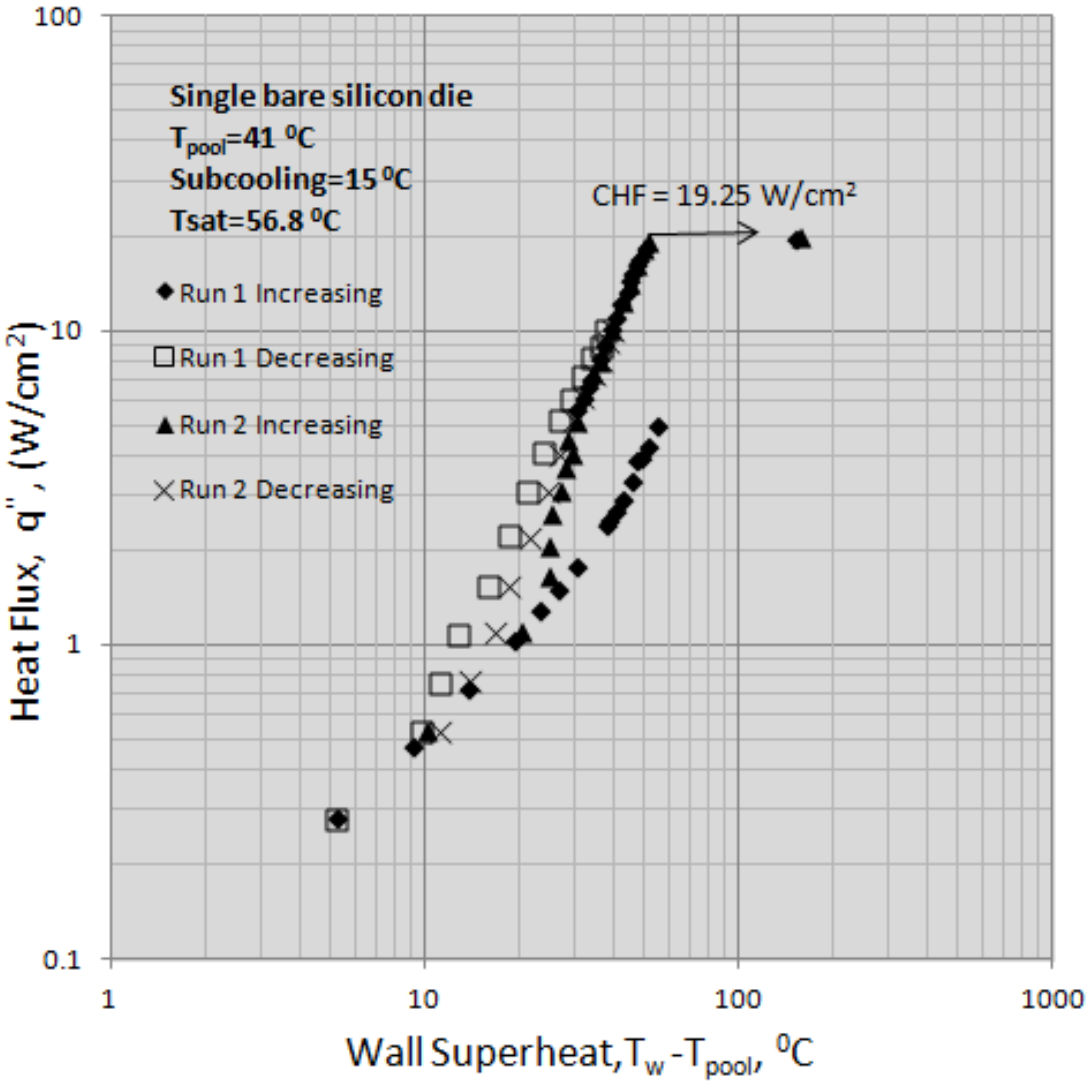


**Figure 47 Pool boiling curve for the bare silicon die with CHF in a subcooled pool**

From Figure 46 and Figure 47, It should be noted that subcooling has increased the CHF of the fluid by 20.3%. The CHF was increased for the subcooled pool because the bubble eminating from the surface encounters a cooler fluid which condenses the vapor bubble therby reducing it's size. This decrease in size delays the CHF for the sucooled pool.

### 3.6 Neighboring Die Effects

In any electronic applications, a circuit board consists more than one number of chips and they do not operate at the same power level. Hotspots are generated due to this difference in power level and hence, it is utmost necessary to address the issue of neighboring die effects on the boiling process. Although, many studies have been conducted on pool boiling in FC-72, very few has addressed the issue of nieghboring die effects. One of the primary objective of this study is about the impact of heat dissipation by a neighboring die operating at different heat levels on the boiling process of the test die.

To understand the effects of neighboring die better, the center die was powered up from 0-10 W/cm2 with other die turned off. The resulting data are shown in Figure 33.

Two different effects were studied. First, the center die was powered up from 0-10 $W/cm^2$ while the die below it was powered to 0.3 $W/cm^2$. A natural convection current generated at the lower die passed over the entire surface of the center die. The resulting data are shown in Figure 48.

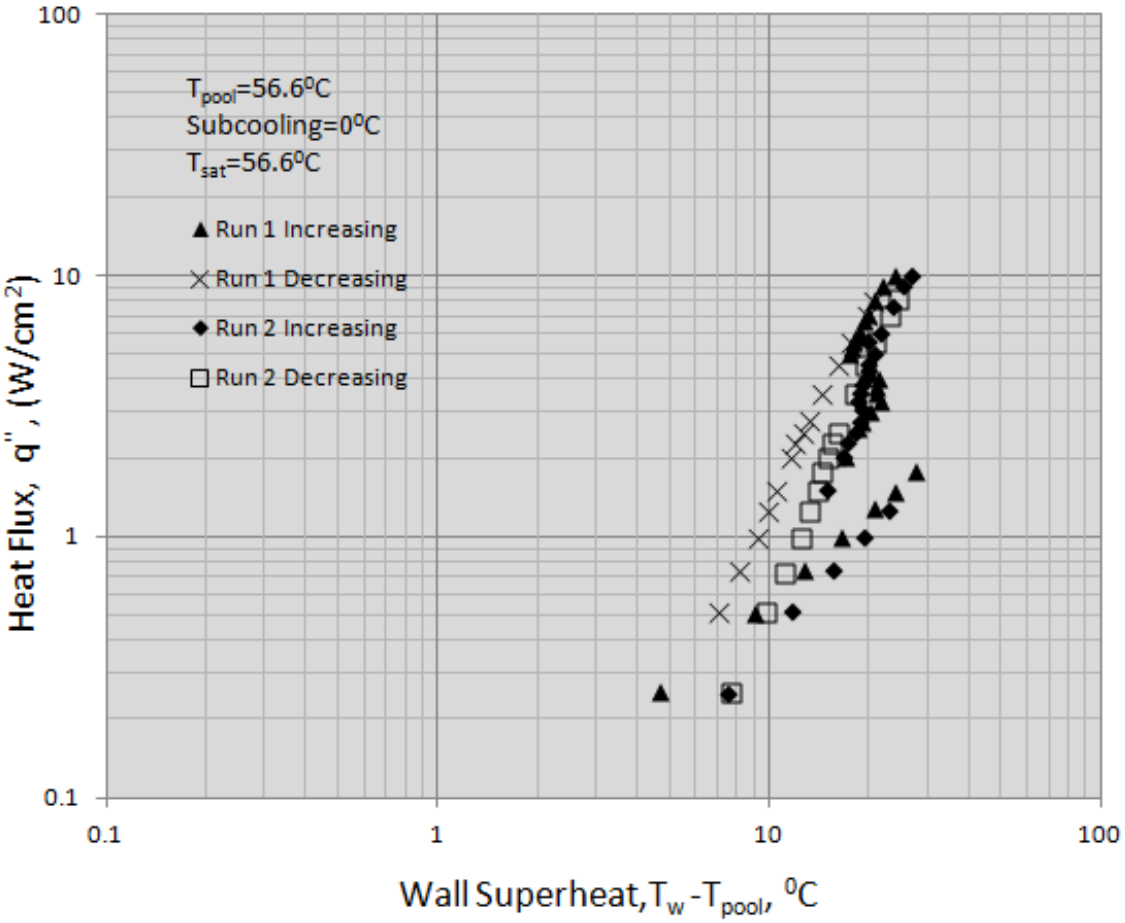


**Figure 48 Boiling curve for the center die with the lower die generating a natural convection plume**

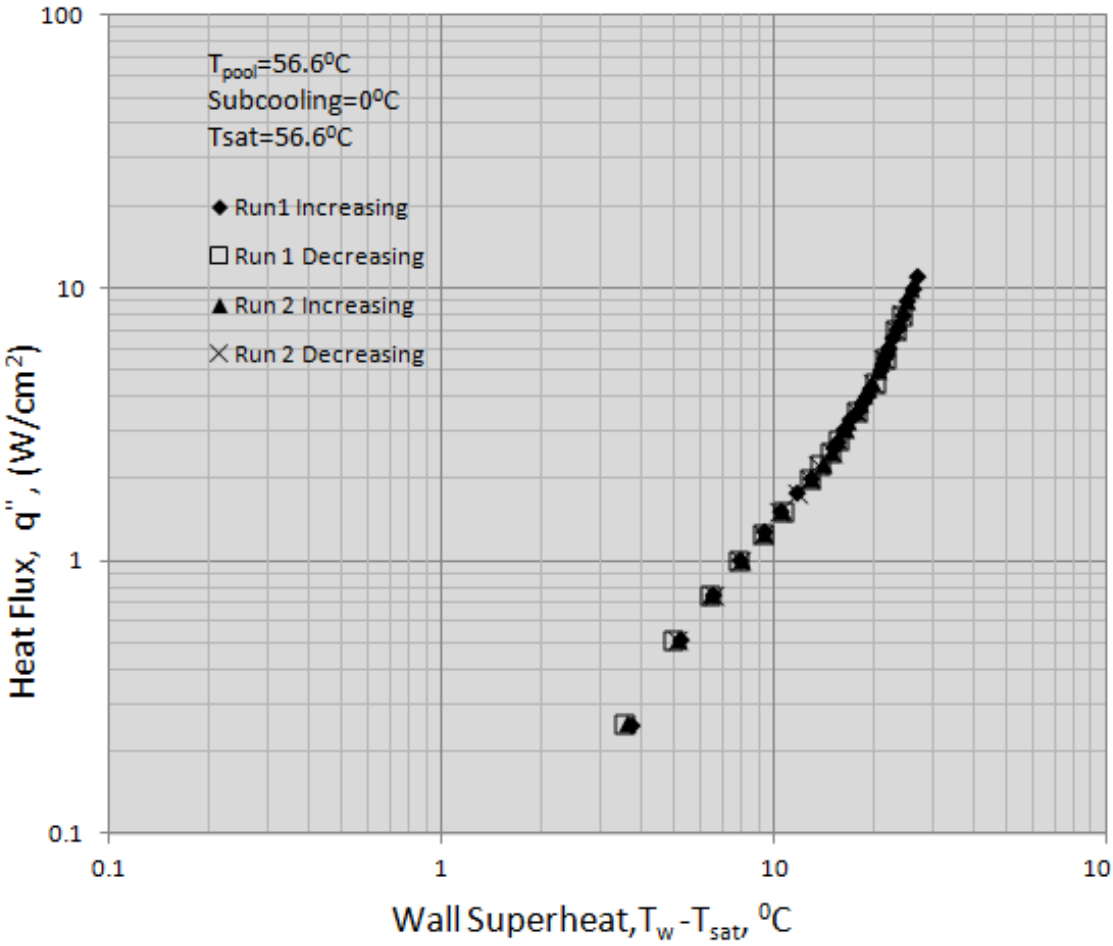


**Figure 49 Boiling curve for the center die in the presence of boiling activity emanating from the lower die**

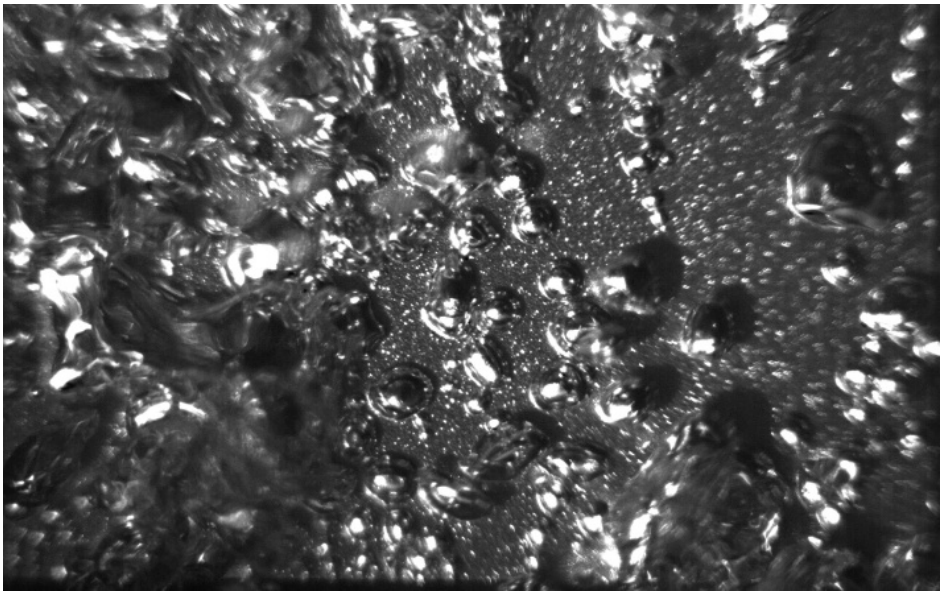

**Figure 50 High speed image of nucleation at the center die at 5 W/cm$^2$ in the presence of boiling eminating from the lower die**

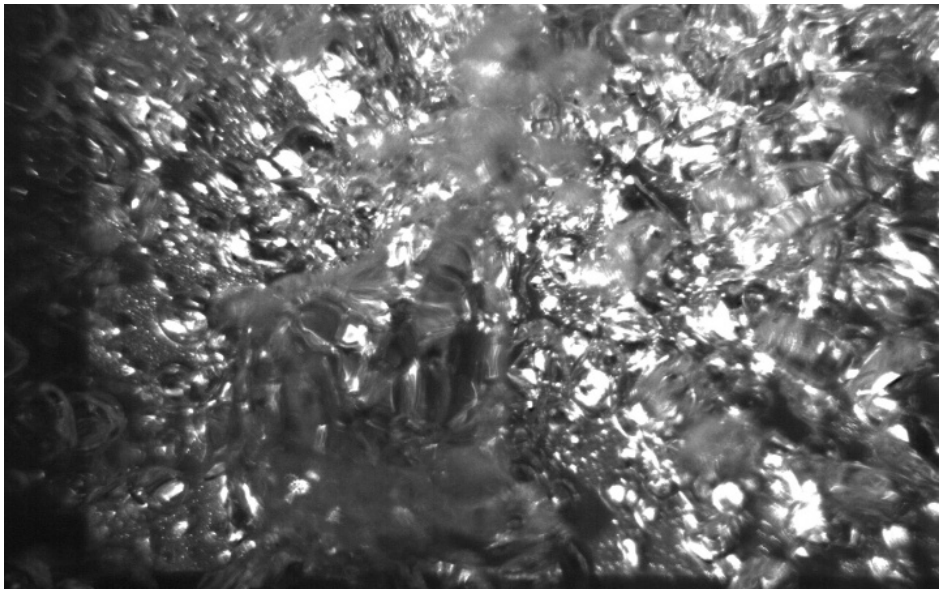

**Figure 51 High speed image of nucleation at the center die at 10 W/cm$^2$ in the presence of boiling eminating from the lower die**

When the boiling curves in Figure 33 and Figure 48 were compared, a few differences in the overshoot characteristics were seen at low heat flux. The temperature overshoot in Figure 48 was lower compared to Figure 33. This is due to the fact that the convection plumes passing over the test die creates a superheated layer on the surface which initiates the boiling process at heat flux lower than the ONB of an isolated die.

A second test was conducted by powering up the center die once again from 0-10W/cm$^2$ while setting the lower die at 6 W/cm$^2$. This heat flux value, based on earlier information gathered, was one that resulted in nucleation on the entire surface. The resulting data are shown in Figure 49.

The nature of the boiling curve changes drastically with overshoot completely eliminated. High speed images of the die at 5 W/cm$^2$ and 10 W/cm$^2$ are shown in Figure 50 and Figure 51, respectively. This phenomenon was observed as in the previously mentioned studies [26, 44]. This is due to the bubble emanating from a chip below, which disrupts the boundary layer of the center chip thereby completely eliminating the overshoot. It is reassuring to note that there is no adverse effect on the surface temperature at the upper end of the heat flux range. This indicates that the configuration can sustain cooling when multiple die are powered.

All five die were powered simultaneously both with and without copper heat spreaders at saturated and subcooled conditions. Only 4 die were powered up for Board C as the top die was above the liquid level due to liquid shortage. The maximum heat

disippation with 25 °C wall superheat was determined. Table 7 shows the highest heat dissipation by all the different surfaces used in this study.

**Table 7 Tabulation for the total power dissipation with all die powered**

| | Saturated pool | Subcooled pool |
|---|---|---|
| Board A (bare silicon die) | 159.468 W | 191.69 W |
| Board B (silicon die with microporous heat spreaders) | 728.681 | 739.412 |
| Board C (silicon die with finned structures) | 568.228 | 570.2 W |

# CHAPTER 5 : CONCLUSION

The study attempts to develop the feasibility of using direct immersion cooling to dissipate heat in high performance server equipment. An experimental study on the pool boiling of a multichip module for saturated and subcooled (15°C subcooling) pool was studied. The performance characteristics of die with and without surface enhancement were obtained for saturated and subcooled conditions. The key results obtained are:

(a) The microporous and finned surfaces were able to maintain lower wall superheat than the plain surface at same heat fluxes which enhanced the boiling process.

(b) The die with micro-porous heat spreaders dissipated significantly higher amounts of heat than the plain die. Due to the microporous coating, bubble departure diameter was smaller than the plain die which triggered the ONB (Onset of Nucleate Boiling) much earlier.

(c) The bubble departure diameter decreased with increase in subcooling. This helped delay the onset of CHF. The bubble departure diameter also increased as a function of heat flux.

(d) The CHF of plain die in saturated conditions and subcooled conditions were found to be 16 and 19.25 $W/cm^2$.

(e) The presence of a neighboring heat source producing convection plumes showed a decrease in the wall superheat as compared to the isolated heat source.

(f) The presence of a nucleating heat source below the test die virtually eliminated the hysteresis at nucleation incipience without any significant increase in the wall superheat even at higher heat fluxes.

(g) The heat transfer coefficient of both the finned structure were almost same at lower heat fluxes but the pin fins performed better than the rectangular fins at higher heat fluxes.

## 5.1 SUGGESTIONS FOR FUTURE STUDY

The current research focuses on studying the primary variables such as wall superheat, bubble dynamics and surface enhancements that can be used to develop a practical dielectric fluid immersion cooling system for server applications.

Current study did not account for the fluid losses due to the Graham condenser which might be a key issue to be noticed while designing an immersion cooled servers. Hence, a robust closed loop system needs to be build that can account for the fluid losses due to condenser.

A typical data center would have racks of processors stacked into one single server. A novel rack structure needs to be designed wherein the processors can be connected to an external heat exchanger and easily replaceable.

The size of the tank used in this study was quite larger than a single processor typically used in a server. Hence, multiple enhancement techniques need to be explored to dissipate same amount of heat in a smaller volume.

## REFERENCES


[1] G. Moore *et al.*, "Cramming more components onto integrated circuits," *Proceedings of the IEEE*, vol. 86, no. 1, pp. 82–85, 1998.

[2] A. Kraus and A. Bar-Cohen, "Thermal analysis and control of electronic equipment," *Washington, DC, Hemisphere Publishing Corp., 1983, 633 p.*, vol. 1, 1983.

[3] J. Koomey, "Growth in data center electricity use 2005 to 2010," *Retrieved October*, vol. 9, p. 2011, 2011.

[4] US EPA, 2007, "Report to Congress on Server and Data Center Energy Efficiency, Public Law 109-431," Prepared for the U.S. Environmental Protection Agency, ENERGY STAR Program, by Lawrence Berkeley National Laboratory. LBNL-363E. August 2

[5] M. Salim and R. Tozer, "Or-10-013 data centers' energy auditing and benchmarking-progress update," *ASHRAE Transactions*, vol. 116, no. 1, p. 109, 2010.

[6] Y. Lui, "Waterside and airside economizers design considerations for data center facilities," *ASHRAE Transactions*, vol. 116, no. 1, p. 98, 2010.

[7] M. Iyengar, R. Schmidt, and J. Caricari, "Reducing energy usage in data centers through control of room air conditioning units," in *Thermal and Thermomechanical*

*Phenomena in Electronic Systems (ITherm), 2010 12th IEEE Intersociety Conference on*. IEEE, 2010, pp. 1–11.

[8] S. You, T. Simon, and A. Bar-Cohen, "A technique for enhancing boiling heat transfer with application to cooling of electronic equipment," *Components, Hybrids, and Manufacturing Technology, IEEE Transactions on*, vol. 15, no. 5, pp. 823–831, 1992.

[9] J. O'Connor and S. You, "A painting technique to enhance pool boiling heat transfer in saturated fc-72," *Journal of heat transfer*, vol. 117, p. 387, 1995.

[10] J. Chang and S. You, "Boiling heat transfer phenomena from microporous and porous surfaces in saturated fc-72," *International Journal of Heat and Mass Transfer*, vol. 40, no. 18, pp. 4437–4447, 1997.

[11] J. Kim, K. Rainey, S. You, and J. Pak, "Mechanism of nucleate boiling heat transfer enhancement from microporous surfaces in saturated fc-72," *Journal of heat transfer*, vol. 124, p. 500, 2002.

[12] H. Honda, H. Takamastu, and J. Wei, "Enhanced boiling of fc-72 on silicon chips with micro-pin-fins and submicron-scale roughness," *Journal of heat transfer*, vol. 124, p. 383, 2002.

[13] J. Parker and M. El-Genk, "Enhanced saturation and subcooled boiling of FC-72 dielectric liquid," *International journal of heat and mass transfer*, vol. 48, no. 18, pp. 3736–3752, 2005.

[14] C. Li and G. Peterson, “Parametric study of pool boiling on horizontal highly conductive microporous coated surfaces,” *Journal of Heat Transfer*, vol. 129, p. 1465, 2007.

[15] S. Vemuri and K. Kim, “Pool boiling of saturated fc-72 on nano-porous surface,” *International communications in heat and mass transfer*, vol. 32, no. 1-2, pp. 27–31, 2005.

[16] A. Ali and M. El-Genk, “Spreaders for immersion nucleate boiling cooling of a computer chip with a central hot spot,” *Energy Conversion and Management*, vol. 53, no. 1, pp. 259–267, 2012.

[17] G. Guglielmini, M. Misale, and C. Schenone, “Experiments on pool boiling of a dielectric fluid on extended surfaces,” *International communications in heat and mass transfer*, vol. 23, no. 4, pp. 451–462, 1996.

[18] J. Wei and H. Honda, “Effects of fin geometry on boiling heat transfer from silicon chips with micro-pin-fins immersed in fc-72,” *International journal of heat and mass transfer*, vol. 46, no. 21, pp. 4059–4070, 2003.

[19] C. Yu and D. Lu, “Pool boiling heat transfer on horizontal rectangular fin array in saturated fc-72,” *International journal of heat and mass transfer*, vol. 50, no. 17, pp. 3624–3637, 2007.

[20] C. Ghiu and Y. Joshi, “Boiling performance of single-layered enhanced structures,” *Journal of heat transfer*, vol. 127, p. 675, 2005.

[21] D. Cooke and S. Kandlikar, “Pool boiling heat transfer and bubble dynamics over plain and enhanced microchannels,” *Journal of Heat Transfer*, vol. 133, no. 5, p. 52902, 2011.

[22] T. Willingham and I. Mudawar, “Forced-convection boiling and critical heat flux from a linear array of discrete heat sources,” *International journal of heat and mass transfer*, vol. 35, no. 11, pp. 2879–2890, 1992.

[23] S. You, T. Simon, and A. Bar-Cohen, “Reduced incipient superheats in boiling of fluids which hold dissolved gas,” *ASME Publication, HTD*, vol. 159, pp. 109–117, 1991.

[24] S. Bhavnani, S. Balch, and R. Jaeger, “Control of incipience hysteresis effects in liquid cooled electronics heat sinks,” *Journal of Electronics Manufacturing*, vol. 9, no. 2, pp. 179–190, 1999.

[25] A. Bergles and C. Kim, “A method to reduce temperature overshoots in immersion cooling of microelectronic devices,” in *Thermal Phenomena in the Fabrication and Operation of Electronic Components: I-THERM’88, InterSociety Conference on*. IEEE, 1988, pp. 100–105.

[26] M. Jensen and G. Memmel, “Evaluation of bubble departure diameter correlations,” in *Proceedings of the Eighth International Heat Transfer Conference*, vol. 4, 1986, pp. 1907–1912.

[27] S. Kutateladze and I. Gogonin, “Growth rate and detachment diameter of a vapor bubble in free convection boiling of a saturated liquid,” *Teplofizika Vysokikh Temperatur*, vol. 17, pp. 792–797, 1980.

[28] R. Cole and H. Shulman, “Bubble departure diameters at subatmospheric pressures,” in *Chemical Engineers Progress Symposium Series*, vol. 62, no. 64, 1966, pp. 6–16.

[29] K. e. a. Nishikawa, *Japan Soc. Mech. Engrs.,*, vol. 2B79, pp. 42–361, 1976.

[30] M. Jakob, *Heat Transfer, John Wiley,New York*, vol. 1, 1958.

[31] F. Peebles and H. Garber, “Studies on the motion of gas bubbles in liquids,” *Chem. Eng. Prog*, vol. 49, no. 2, pp. 88–97, 1953.

[32] N. Zuber, “Hydrodynamic aspects of boiling heat transfer (thesis),” California. Univ., Los Angeles; and Ramo-Wooldridge Corp., Los Angeles, Tech. Rep., 1959.

[33] P. McFadden and P. Grassmann, “The relation between bubble frequency and diameter during nucleate pool boiling,” *International Journal of Heat and Mass Transfer*, vol. 5, no. 3, pp. 169–173, 1962.

[34] H. Ivey, “Relationships between bubble frequency, departure diameter and rise velocity in nucleate boiling,” *International Journal of Heat and Mass Transfer*, vol. 10, no. 8, pp. 1023–1040, 1967.

[35] C. Pascual, S. Jeter, and S. Abdel-Khalik, “Visualization of boiling bubble dynamics using a flat uniformly heated transparent surface,” *International journal of heat and mass transfer*, vol. 45, no. 3, pp. 691–696, 2002.

[36] S. Chatpun, M. Watanabe, and M. Shoji, “Experimental study on characteristics of nucleate pool boiling by the effects of cavity arrangement,” *Experimental thermal and fluid science*, vol. 29, no. 1, pp. 33–40, 2004.

[37] C. Ramaswamy, Y. Joshi, W. Nakayama, and W. Johnson, “High-speed visualization of boiling from an enhanced structure,” *International journal of heat and mass transfer*, vol. 45, no. 24, pp. 4761–4771, 2002.

[38] N. Nimkar, S. Bhavnani, and R. Jaeger, “Effect of nucleation site spacing on the pool boiling characteristics of a structured surface,” *International journal of heat and mass transfer*, vol. 49, no. 17, pp. 2829–2839, 2006.

[39] Y. Kim, K. Lee, and D. Han, “Pool boiling enhancement with surface treatments,” *Heat and Mass Transfer*, vol. 45, no. 1, pp. 55–60, 2008.

[40] C. Hutter, D. Kenning, K. Sefiane, T. Karayiannis, H. Lin, G. Cummins, and A. Walton, “Experimental pool boiling investigations of fc-72 on silicon with artificial cavities and integrated temperature microsensors,” *Experimental Thermal and Fluid Science*, vol. 34, no. 4, pp. 422–433, 2010.

[41] J. McHale and S. Garimella, “Bubble nucleation characteristics in pool boiling of a wetting liquid on smooth and rough surfaces,” *International Journal of Multiphase Flow*, vol. 36, no. 4, pp. 249–260, 2010.

[42] V. P. Carey, *Liquid-Vapor Phase-Change Phenomena: An Introduction to the Thermophysics of Vaporization and Condensation Processes in Heat Transfer Equipment*, 2007.

[43] S. You, A. Bar-Cohen, and T. Simon, "Boiling incipience and nucleate boiling heat transfer of highly wetting dielectric fluids from electronic materials," *Components, Hybrids, and Manufacturing Technology, IEEE Transactions on*, vol. 13, no. 4, pp. 1032–1039, 1990.

[44] G. Medavaram, S. Bhavnani, and R. Jaeger, "Ebullition characteristics of an isolated surface microstructure for immersion cooled heat sinks," in *Thermal and Thermomechanical Phenomena in Electronic Systems, 2004. ITHERM'04. The Ninth Intersociety Conference on*, vol. 2. IEEE, 2004, pp. 1–10.

[45] S. Kline and F. McClintock, "Describing uncertainties in single-sample experiments," *Mechanical engineering*, vol. 75, no. 1, pp. 3–8, 1953.

# APPENDIX A – CALIBRATION CURVES AND VI DESIGN

## Calibration Curves

Calibration for the temperature sensors were carried out as explained in chapter 2. After the calibration was done, the resulting data for the temperature values were in voltages. 1000 voltage values were recorded and averaged for each data point. All the data points were tabulated in an Excel sheet. Voltages were plotted against the temperature obtained from the thermister reading. Figure A 1 shows five sample curves for the center sensor in each of five chips. An equation for temperature as a function of voltage was obtained from the curve. The equation was then incorporated into the LabView. LabView consists of two panels i.e., front panel and block diagram. Front panel typically consists of five charts, one each for the center diodes of the test chips. The chart displays the temperature of the sensors in °C. The panel contains four indicators displaying the current flowing through the heater circuit. Sample image of the front panel is shown in Figure A2.

In the block diagram panel (Figure A3) , DAQ assistant was added wherein the details about the quantity (i.e., voltage and current) being measured were entered. The DAQ assistant was connected to signal splitter which separates each voltage input and current input. The equation obtained from the calibration curve was entered using the objects available in LabView. Various are connected through wires which carries the signal. The data was stored in a file using the function “Write To Measurement File”. The temperature obtained from the equation was connected to waveform chart to display the temperature readings live on the VI.

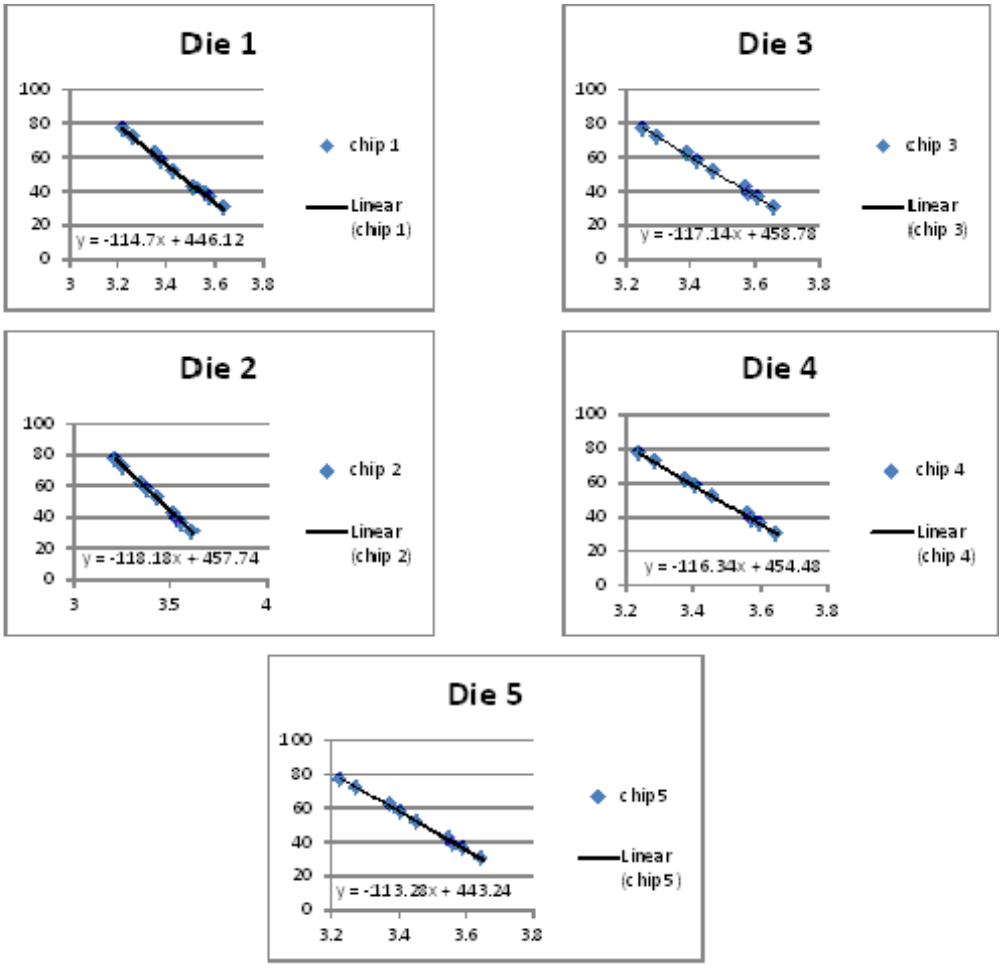


**Figure A 1 Sample calibration curves**

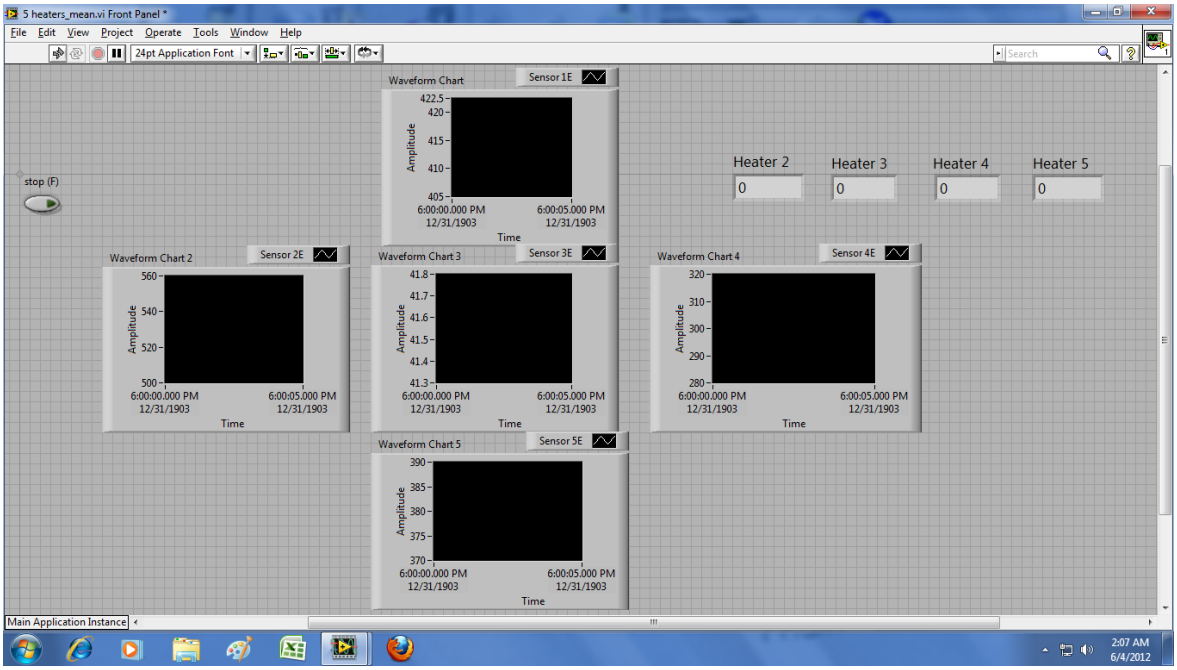


**Figure A2 Front panel**

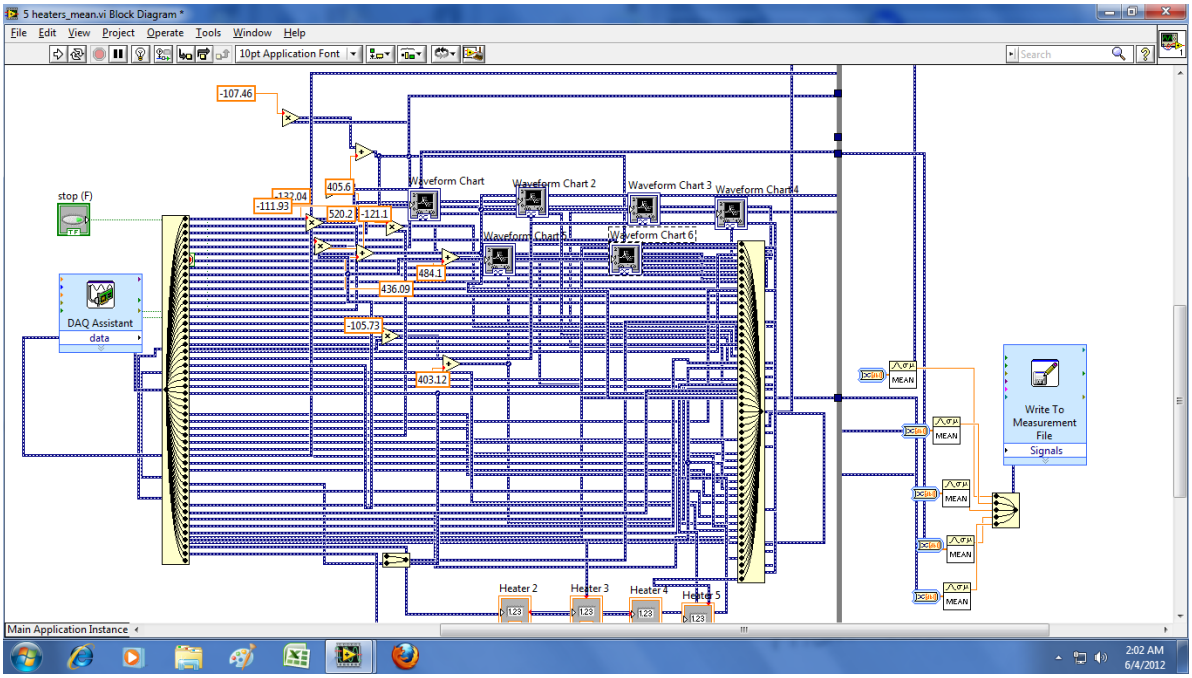


**Figure A3 Block diagram**

## APPENDIX B – SAMPLE CALCULATIONS

### Coil Condenser Design

In the present study, the amount of heat dissipated by the test chips was about 750 W. As the test chamber used was small, an external condenser was needed in addition to the graham condenser. An external coil condenser was designed and the dimensions were calculated theoretically. Properties of FC-72 at atmospheric pressure were taken and the CHF was determined using the Zuber Correlation given in Carey [41]. Using the CHF value, the maximum power dissipation was calculated. Using the equation for film condensation on cylinder, the Nusselt number was found out thereby determining the heat transfer coefficient. By using Newton's law of cooling, the surface area of the condenser is calculated. Using the value of the diameter of the tube, and surface area of the tube, the number of turns of the coil was determined. The sample calculation for the coil condenser is shown below:

Properties of FC-72 at 1 atm :

$T_{sat}$ = 56.6 ℃, $C_p$ = 1098.41 J/kgK, $h_{lv}$ = 84510.9 K/kg, k = 5.216*$10^{-2}$ W/mK, μ = 4.537*$10^{-4}$ Ns/$m^2$, Pr=9.555, $\rho_l$ = 1619.73 kg/$m^3$, $\rho_v$ = 13.396 kg/$m^3$, σ = 0.8273*$10^{-2}$ N/m.

From Zuber Correlation,

$$q''_{max,Z} = 0.149\ \rho_v\ h_{lv}\ \left[\frac{\sigma(\rho_l - \rho_v)}{\rho_v^2}\right]^{\frac{1}{4}}$$

$$q''_{max,Z} = 0.149 * 13.396 * 84510.9 \left[\frac{0.008273(1619.73 - 13.396)}{13.396^2}\right]^{\frac{1}{4}} = 15.5739 \frac{W}{cm^2}$$

$$L_b = \sqrt{\frac{\sigma}{g(\rho_l - \rho_v)}} = 0.000725\ m$$

$$\frac{L}{L_b} = \frac{0.000725}{0.018} = 0.0402$$

As the ratio is very small, the correction factor for CHF is 1.

$$\text{Hence,}\quad q''_{max} = 15.5739 \frac{W}{cm^2}$$

For film condensation on cylinder,

$$\overline{Nu_D} = \frac{\bar{h}D}{k_l} = 0.728 \left[\frac{g\ (\rho_l - \rho_v)\rho_l D^3 h_{lv}}{\mu_l k_l\ (T_{sat} - T_w)}\right]^{\frac{1}{4}}$$

The diameter of the pipe is taken to be 12.7 mm which is a standard pipe available in the market.

$$\overline{Nu_D} = \frac{\bar{h}D}{k_l} = 0.728 \left[\frac{9.81 \times (1619.73 - 13.396) \times 1619.73 \times (12.7 \times 10^{-3})^3 \times 84510.9}{4.537 \times 10^{-4} \times 5.216 \times 10^{-2} \times (56.6 - 15)}\right]^{\frac{1}{4}}$$

$$\overline{Nu_D} = 106.47$$

$$\bar{h} = \frac{106.47 \times 5.233 \times 10^{-2}}{12.7 \times 10^{-3}} = 438.71 \frac{W}{m^2 K}$$

$$q'' = \bar{h}(T_{sat} - T_w) = 438.71\ (56.6 - 15) = 18250.4 \frac{W}{m^2}$$

$$q_{max} = \bar{h}(T_{sat} - T_w) \times Surface\ area\ of\ the\ condenser$$

$$1.69\ kW = 18250.4 \times Surface\ area$$

$$Surface\ area = 0.0926\ m^2$$

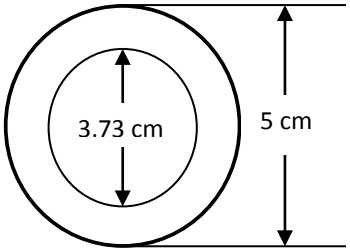


If the pipe is bend into circular coil of radius 5 cm, we get,

$$Area\ of\ circular\ coil = \frac{\pi}{4}((5 \times 10^{-2})^2 - (3.73 \times 10^{-2})^2) = 9.974 \times 10^{-3} m^2$$

$$\therefore No.of\ turns = \frac{0.05307}{9.974 \times 10^{-3}} = 9.284 \cong 10\ turns$$

**Theoretical nucleate boiling regime and CHF calculation**

The nucleate boiling region and the CHF are theoretically calculated using the rohsenow correlation and zuber correlation respectively.

**Rohsenow Correlation:**

Wall superheat for the nucleate boiling regime is calculated using the rohsenow correlation. It can be shown as :

$$\frac{q''_{snb}}{\mu_l h_{lv}}\left[\frac{\sigma}{g(\rho_l - \rho_v)}\right]^{\frac{1}{2}} = \left(\frac{1}{C_{sf}}\right)^{\frac{1}{r}} (Pr_l)^{-\frac{s}{r}} \left(\frac{c_{pl}(T_w - T_{sat})}{h_{lv}}\right)^{\frac{1}{r}}$$

The fluid properties and the heat flux values in the nucleate boiling regime are substituted in the rohsenow correlation and the wall temperature is found out. Constants, $C_{sf}$ = 0.0058, r = 1.7 and s = 0.04 are taken from You et al. [43].

**CHF Calculation**

**Saturated CHF**

Properties of FC-72 at 1 atm :

$T_{sat}$ = 56.6 ℃, $C_p$ = 1098.41 J/kgK, $h_{lv}$ = 84510.9 K/kg, k = 5.216*$10^{-2}$ W/mK, μ = 4.537*$10^{-4}$ Ns/$m^2$, Pr=9.555, $\rho_l$ = 1619.73 kg/$m^3$, $\rho_v$ = 13.396 kg/$m^3$, σ = 0.8273*$10^{-2}$ N/m.

From Zuber Correlation,

$$q''_{max,Z} = 0.149\ \rho_v\ h_{lv}\ \left[\frac{\sigma(\rho_l - \rho_v)}{\rho_v^2}\right]^{\frac{1}{4}}$$

$$q''_{max,Z} = 0.149 * 13.396 * 84510.9\ \left[\frac{0.008273(1619.73 - 13.396)}{13.396^2}\right]^{\frac{1}{4}} = 15.5739\frac{W}{cm^2}$$

$$L_b = \sqrt{\frac{\sigma}{g(\rho_l - \rho_v)}} = 0.000725\ m$$

$$\frac{L}{L_b} = \frac{0.000725}{0.018} = 0.0402$$

As the ratio is very small, the correction factor for CHF is 1.

Hence, $q''_{max} = 15.5739\frac{W}{cm^2}$

**Subcooled CHF**

Properties of FC-72 at 1 atm, $T_l$ = 41°C :

$T_{sat}$ = 56.6 ℃, $C_p$ = 1074.55 J/kgK, $h_{lv}$ = 88985.35 K/kg, k = 5.399*$10^{-2}$ W/mK, μ = 5.22*$10^{-4}$ Ns/$m^2$, Pr=10.47, $\rho_l$ = 1647.53 kg/$m^3$, $\rho_v$ = 6.986 kg/$m^3$, σ = 0.9594*$10^{-2}$ N/m.

Kutateladze correlation for subcooled CHF,

$$q''_{max} = 0.16\,\rho_v\,h_{lv}\left[\frac{\sigma(\rho_l-\rho_v)}{\rho_v^2}\right]^{\frac{1}{4}}\left[1+C_0\left(\frac{\rho_l}{\rho_v}\right)^m\left(\frac{c_{pl}(T_{sat}-T_l)}{h_{lv}}\right)\right]$$

Where, m = 0.8 and $C_0$ = 0.065,

$$Therefore, q''_{max} = 26\,\frac{W}{cm^2}$$

## APPENDIX C – DATA REDUCTION PROCEDURE

Due to the geographic location and change in weather condition, the ambient pressure might not be 1 atm. Hence, before the start of the experiment, the ambient pressure was noted down and the saturation temperature of the fluid was calculated. The heat flux was calculated as a function of the current supplied and the voltage measured.

Bubble departure diameter was calculated using PCC 1.2 software provided by the high speed camera manufacturers (Phantom). The departure diameter was measured by specifying the scale for a known dimension in the diagram. For example, in a plain silicon chip experiment, the size of the silicon chip was known. Hence, the size of the silicon chip was specified for the purpose of scaling and the bubble departure diameter was measured. As the bubble departure diameter was measured with the naked eye, multiple bubbles from single site were measured and an average was taken.

Sample data for single heater bare silicon die experiment is shown in Table C1:

**Table C1 Sample pool boiling data**

| **Atmospheric Pressure** | | | heat flux full surface covered | | | | | |
|---|---|---|---|---|---|---|---|---|
| **28.96** | | | 5.75266 | | | | | |
| **Tsat** | | | | | | | | |
| 56.536 | | | | | | | | |
| **S. No** | **Tsat** | **Tw** | **Voltage** | **Current** | **Power** | **Area** | **Heat Flux** | **Comments** |
| **First Run** | | | | | | | | **Tw-Tsat** |
| **1** | 56.536 | **61** | **3.927** | **0.231** | **0.907137** | **3.24** | **0.279981** | **4.464** |
| **2** | 56.536 | **61.172** | **5.304** | **0.312** | **1.654848** | **3.24** | **0.510756** | **4.636** |

| **Atmospheric Pressure** | | | heat flux full surface covered | | | | | |
|---|---|---|---|---|---|---|---|---|
| **28.96** | | | 5.75266 | | | | | |
| **Tsat** | | | | | | | | |
| 56.536 | | | | | | | | |
| **S. No** | **Tsat** | **Tw** | **Voltage** | **Current** | **Power** | **Area** | **Heat Flux** | **Comments** |
| **First Run** | | | | | | | | **Tw-Tsat** |
| **3** | 56.536 | **64.948** | **6.386** | **0.376** | **2.401136** | **3.24** | **0.741091** | **8.412** |
| **4** | 56.536 | **65.237** | **7.385** | **0.435** | **3.212475** | **3.24** | **0.991505** | **8.701** |
| **5** | 56.536 | **65.683** | **8.394** | **0.494** | **4.146636** | **3.24** | **1.279826** | **9.147** |
| **6** | 56.536 | **66.742** | **9.088** | **0.535** | **4.86208** | **3.24** | **1.500642** | **10.206** |
| **7** | 56.536 | **67.14** | **9.821** | **0.578** | **5.676538** | **3.24** | **1.752018** | **10.604** |
| **8** | 56.536 | **67.317** | **10.501** | **0.617** | **6.479117** | **3.24** | **1.999727** | **10.781** |
| **9** | 56.536 | **68.083** | **11.915** | **0.7** | **8.3405** | **3.24** | **2.574228** | **11.547** |
| **10** | 56.536 | **68.884** | **12.333** | **0.725** | **8.941425** | **3.24** | **2.759699** | **12.348** |
| **11** | 56.536 | **69.289** | **12.928** | **0.759** | **9.812352** | **3.24** | **3.028504** | **12.753** |
| **12** | 56.536 | **69.711** | **13.525** | **0.794** | **10.73885** | **3.24** | **3.31446** | **13.175** |
| **13** | 56.536 | **70.401** | **13.9** | **0.816** | **11.3424** | **3.24** | **3.500741** | **13.865** |
| **14** | 56.536 | **70.63** | **14.396** | **0.845** | **12.16462** | **3.24** | **3.754512** | **14.094** |
| **15** | 56.536 | **71.459** | **14.862** | **0.872** | **12.95966** | **3.24** | **3.999896** | **14.923** |
| **16** | 56.536 | **71.585** | **15.352** | **0.9** | **13.8168** | **3.24** | **4.264444** | **15.049** |
| **17** | 56.536 | **71.956** | **16.593** | **0.972** | **16.1284** | **3.24** | **4.9779** | **15.42** |
| **18** | 56.536 | **73.318** | **17.038** | **0.998** | **17.00392** | **3.24** | **5.248125** | **16.782** |
| **19** | 56.536 | **73.634** | **17.449** | **1.022** | **17.83288** | **3.24** | **5.503975** | **17.098** |
| **20** | 56.536 | **74.038** | **17.836** | **1.045** | **18.63862** | **3.24** | **5.75266** | **17.502** |
| **21** | 56.536 | **74.442** | **18.217** | **1.067** | **19.43754** | **3.24** | **5.99924** | **17.906** |
| **22** | 56.536 | **75.261** | **19.154** | **1.121** | **21.47163** | **3.24** | **6.627048** | **18.725** |
| **23** | 56.536 | **75.865** | **19.676** | **1.151** | **22.64708** | **3.24** | **6.989838** | **19.329** |
| **24** | 56.536 | **77.024** | **21.044** | **1.23** | **25.88412** | **3.24** | **7.988926** | **20.488** |
| **25** | 56.536 | **78.273** | **22.306** | **1.303** | **29.06472** | **3.24** | **8.970592** | **21.737** |
| **26** | 56.536 | **79.983** | **23.522** | **1.372** | **32.27218** | **3.24** | **9.960551** | **23.447** |
| **27** | 56.536 | **76.972** | **20.971** | **1.226** | **25.71045** | **3.24** | **7.935323** | **20.436** |
| **28** | 56.536 | **75.851** | **19.676** | **1.151** | **22.64708** | **3.24** | **6.989838** | **19.315** |
| **29** | 56.536 | **73.981** | **17.45** | **1.022** | **17.8339** | **3.24** | **5.50429** | **17.445** |
| **30** | 56.536 | **72.711** | **15.808** | **0.927** | **14.65402** | **3.24** | **4.522844** | **16.175** |

| **Atmospheric Pressure** | | | heat flux full surface covered | | | | | |
|---|---|---|---|---|---|---|---|---|
| **28.96** | | | 5.75266 | | | | | |
| **Tsat** | | | | | | | | |
| 56.536 | | | | | | | | |
| **S. No** | **Tsat** | **Tw** | **Voltage** | **Current** | **Power** | **Area** | **Heat Flux** | **Comments** |
| **First Run** | | | | | | | | **Tw-Tsat** |
| **31** | 56.536 | **70.862** | **13.9** | **0.816** | **11.3424** | **3.24** | **3.500741** | **14.326** |
| **32** | 56.536 | **69.621** | **12.333** | **0.724** | **8.929092** | **3.24** | **2.755893** | **13.085** |
| **33** | 56.536 | **69.132** | **11.76** | **0.691** | **8.12616** | **3.24** | **2.508074** | **12.596** |
| **34** | 56.536 | **68.704** | **11.157** | **0.656** | **7.318992** | **3.24** | **2.258948** | **12.168** |
| **35** | 56.536 | **68.013** | **10.501** | **0.617** | **6.479117** | **3.24** | **1.999727** | **11.477** |
| **36** | 56.536 | **67.307** | **9.088** | **0.535** | **4.86208** | **3.24** | **1.500642** | **10.771** |
| **37** | 56.536 | **66.608** | **8.32** | **0.489** | **4.06848** | **3.24** | **1.255704** | **10.072** |
| **38** | 56.536 | **66.526** | **7.385** | **0.434** | **3.20509** | **3.24** | **0.989225** | **9.99** |
| **39** | 56.536 | **65.396** | **6.37** | **0.375** | **2.38875** | **3.24** | **0.737269** | **8.86** |
| **40** | 56.536 | **63.996** | **5.333** | **0.314** | **1.674562** | **3.24** | **0.51684** | **7.46** |
| **41** | 56.536 | **61.065** | **3.708** | **0.218** | **0.808344** | **3.24** | **0.249489** | **4.529** |
| **Run 2** | 56.536 | | | | | | | |
| **1** | 56.536 | **61.284** | **3.7088** | **0.218** | **0.808518** | **3.24** | **0.249543** | **4.748** |
| **2** | 56.536 | **65.965** | **5.306** | **0.312** | **1.655472** | **3.24** | **0.510948** | **9.429** |
| **3** | 56.536 | **69.816** | **6.395** | **0.375** | **2.398125** | **3.24** | **0.740162** | **13.28** |
| **4** | 56.536 | **73.354** | **7.385** | **0.432** | **3.19032** | **3.24** | **0.984667** | **16.818** |
| **5** | 56.536 | **76.835** | **8.32** | **0.486** | **4.04352** | **3.24** | **1.248** | **20.299** |
| **6** | 56.536 | **67.189** | **9.088** | **0.531** | **4.825728** | **3.24** | **1.489422** | **10.653** |
| **7** | 56.536 | **68.3** | **10.501** | **0.617** | **6.479117** | **3.24** | **1.999727** | **11.764** |
| **8** | 56.536 | **68.764** | **11.157** | **0.655** | **7.307835** | **3.24** | **2.255505** | **12.228** |
| **9** | 56.536 | **69.225** | **11.75** | **0.69** | **8.1075** | **3.24** | **2.502315** | **12.689** |
| **10** | 56.536 | **69.708** | **12.33** | **0.724** | **8.92692** | **3.24** | **2.755222** | **13.172** |
| **11** | 56.536 | **70.23** | **12.928** | **0.759** | **9.812352** | **3.24** | **3.028504** | **13.694** |
| **12** | 56.536 | **70.784** | **13.511** | **0.793** | **10.71422** | **3.24** | **3.306859** | **14.248** |
| **13** | 56.536 | **71.062** | **13.9** | **0.816** | **11.3424** | **3.24** | **3.500741** | **14.526** |
| **14** | 56.536 | **71.389** | **14.403** | **0.845** | **12.17054** | **3.24** | **3.756338** | **14.853** |
| **15** | 56.536 | **71.768** | **14.862** | **0.872** | **12.95966** | **3.24** | **3.999896** | **15.232** |
| **16** | 56.536 | **72.332** | **15.352** | **0.9** | **13.8168** | **3.24** | **4.264444** | **15.796** |

| **Atmospheric Pressure** | | | heat flux full surface covered | | | | | |
|---|---|---|---|---|---|---|---|---|
| **28.96** | | | 5.75266 | | | | | |
| **Tsat** | | | | | | | | |
| 56.536 | | | | | | | | |
| **S. No** | **Tsat** | **Tw** | **Voltage** | **Current** | **Power** | **Area** | **Heat Flux** | **Comments** |
| **First Run** | | | | | | | | **Tw-Tsat** |
| **17** | 56.536 | **72.7** | **15.8** | **0.927** | **14.6466** | **3.24** | **4.520556** | **16.164** |
| **18** | 56.536 | **73.379** | **16.593** | **0.972** | **16.1284** | **3.24** | **4.9779** | **16.843** |
| **19** | 56.536 | **74.254** | **17.449** | **1.022** | **17.83288** | **3.24** | **5.503975** | **17.718** |
| **20** | 56.536 | **74.946** | **18.217** | **1.066** | **19.41932** | **3.24** | **5.993618** | **18.41** |
| **21** | 56.536 | **76.62** | **20.376** | **1.191** | **24.26782** | **3.24** | **7.490067** | **20.084** |
| **22** | 56.536 | **78.607** | **22.31** | **1.303** | **29.06993** | **3.24** | **8.972201** | **22.071** |
| **23** | 56.536 | **80.28** | **23.522** | **1.372** | **32.27218** | **3.24** | **9.960551** | **23.744** |
| **24** | 56.536 | **77.313** | **21.044** | **1.23** | **25.88412** | **3.24** | **7.988926** | **20.777** |
| **25** | 56.536 | **76.083** | **19.676** | **1.151** | **22.64708** | **3.24** | **6.989838** | **19.547** |
| **26** | 56.536 | **74.09** | **17.455** | **1.022** | **17.83901** | **3.24** | **5.505867** | **17.554** |
| **27** | 56.536 | **72.605** | **15.808** | **0.927** | **14.65402** | **3.24** | **4.522844** | **16.069** |
| **28** | 56.536 | **71.014** | **13.9** | **0.816** | **11.3424** | **3.24** | **3.500741** | **14.478** |
| **29** | 56.536 | **69.596** | **11.765** | **0.691** | **8.129615** | **3.24** | **2.50914** | **13.06** |
| **30** | 56.536 | **69.088** | **11.157** | **0.655** | **7.307835** | **3.24** | **2.255505** | **12.552** |
| **31** | 56.536 | **68.56** | **10.5** | **0.617** | **6.4785** | **3.24** | **1.999537** | **12.024** |
| **32** | 56.536 | **68.106** | **9.82** | **0.577** | **5.66614** | **3.24** | **1.748809** | **11.57** |
| **33** | 56.536 | **67.563** | **9.088** | **0.534** | **4.852992** | **3.24** | **1.497837** | **11.027** |
| **34** | 56.536 | **66.901** | **8.32** | **0.489** | **4.06848** | **3.24** | **1.255704** | **10.365** |
| **35** | 56.536 | **66.415** | **7.384** | **0.434** | **3.204656** | **3.24** | **0.989091** | **9.879** |
| **36** | 56.536 | **66.032** | **6.34** | **0.373** | **2.36482** | **3.24** | **0.729883** | **9.496** |
| **37** | 56.536 | **64.204** | **5.332** | **0.314** | **1.674248** | **3.24** | **0.516743** | **7.668** |
| **38** | 56.536 | **61.324** | **3.708** | **0.218** | **0.808344** | **3.24** | **0.249489** | **4.788** |

## APPENDIX D – MICROPOROUS SURFACES

The microporous surface used in this study was made with a material called L-20227 developed by 3M Corporation. It composes copper particles fused to copper surface at elevated temperature. The coating was prepared by screen printing a mixture of L-20227 particles and Dow 704 silicone diffusion pump oil. The microporous coating can be used for any application as it is insensitive with most of the engineered fluids available for immersion cooling. Microporous particle is sub 20 µm in size. SEM image of the microporous coating is shown in Figure D1.

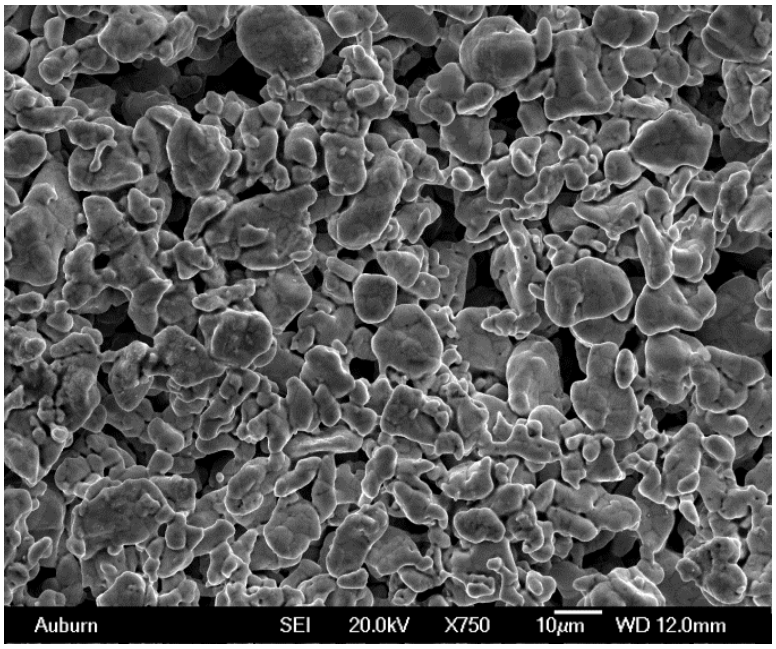


**Figure D1 SEM image of the microporous coating**

## APPENDIX E : UNCERTAINTY ANALYSIS

Any data obtained experimentally cannot be one hundred percent accurate. Some discrepancy in the data will always exist in spite of careful experimentation. Hence, it is very important to calculate the uncertainty in the data that is obtained.

Uncertainty analysis was done using the method proposed by Kline and McClintock [44]. The equation for uncertainty of the quantity measured is given by,

$$U_R = \sqrt{\left(\left(\frac{\partial R}{\partial V_1}\right).U_{V_1}\right)^2 + \left(\left(\frac{\partial R}{\partial V_2}\right).U_{V_2}\right)^2 + \left(\left(\frac{\partial R}{\partial V_3}\right).U_{V_3}\right)^2 + \left(\left(\frac{\partial R}{\partial V_4}\right).U_{V_4}\right)^2 + \cdots + \left(\left(\frac{\partial R}{\partial V_n}\right).U_n\right)^2}$$

Where,

$U_R$ is the uncertainty

R is the quantity for which the uncertainty is calculated

$V_1$, $V_2$, $V_3$, $V_4 \ldots V_n$ are individual components that R is a function of.

The uncertainties of individual variables are found from the user manuals provided by the equipment manufacturers.

### Uncertainty in Heat Flux

Heat Flux, q" = V.I/A

$$\frac{U_{q"}}{q"} = \sqrt{\left(\frac{U_V}{V}\right)^2 + \left(\frac{U_I}{I}\right)^2 + \left(\frac{U_A}{A}\right)^2}$$

Voltage is supplied by the power supply using the power supply and measured using the multimeter. Hence, there are two components involved in the process of finding the uncertainty of voltage. From the user manuals of the equipment manufacturers, we get,

Uncertainty of power supply = ±2 mV

Uncertainty of multimeter = ±3 mV

$$U_V = \sqrt{2^2 + 3^2} = \pm 3.605\ mV$$

Current is supplied by the power supply and measured using the NI DAQ 5227 module. The specifications are found to be

Uncertainty of power supply = ±18 mA

Uncertainty of NI module = ±15 mA

$$U_I = \sqrt{(0.018)^2 + (0.015)^2} = \pm 0.023\ A$$

A sample value for current and voltage is taken from Table C1, Page 113. The uncertainty in heat flux for this data point is calculated below:

$$U_{q"} = q" \times \sqrt{\left(\frac{0.03605}{3.927}\right)^2 + \left(\frac{0.023}{0.231}\right)^2} = \pm 0.028\ \frac{W}{cm^2}$$